AD-A019 240

REMOTE ASSESSMENT OF GASES

Leona Marshall Libby

R and D. Associates

Prepared for:

Defense Supply Service
Defense Advanced Research Projects Agency

September 1975

RDA-TR-4302-001

REMOTE ASSESSMENT OF GASES

SEPTEMBER 1975

By:
LEONA MARSHALL LIBBY

Sponsored By:
DEFENSE ADVANCED RESEARCH PROJECTS AGENCY
1400 Wilson Boulevard
Arlington, Virginia 22209

R & D ASSOCIATES
Post Office Box 9695
Marina del Rey,
California 90291

4640 ADMIRALTY WAY • MARINA DEL REY • TELEPHONE: (213) 822-1715

UNCLASSIFIED

SECURITY CLASSIFICATION OF THIS PAGE (When Data Entered)

REPORT DOCUMENTATION PAGE	READ INSTRUCTIONS BEFORE COMPLETING FORM
1. REPORT NUMBER: RDA-TR-4302-001	2. GOVT ACCESSION NO. / 3. RECIPIENT'S CATALOG NUMBER
4. TITLE (and Subtitle): REMOTE ASSESSMENT OF GASES	5. TYPE OF REPORT & PERIOD COVERED: Final Technical Report
	6. PERFORMING ORG. REPORT NUMBER
7. AUTHOR(s): Leona Marshall Libby	8. CONTRACT OR GRANT NUMBER(s): MDA903-74-C-0090
9. PERFORMING ORGANIZATION NAME AND ADDRESS: R & D Associates Post Office Box 9695 Marina del Rey, California 90291	10. PROGRAM ELEMENT, PROJECT, TASK AREA & WORK UNIT NUMBERS: ARPA Order No. 2558 Program Code 6G10
11. CONTROLLING OFFICE NAME AND ADDRESS: Defense Advanced Research Projects Agency 1400 Wilson Boulevard Arlington, Virginia 22209	12. REPORT DATE: September 1975 13. NUMBER OF PAGES: 197
14. MONITORING AGENCY NAME & ADDRESS (if different from Controlling Office): Defense Supply Service-Washington Room 1D 245, The Pentagon Washington, D.C. 20310	15. SECURITY CLASS (of this report): Unclassified 15a. DECLASSIFICATION/DOWNGRADING SCHEDULE
16. DISTRIBUTION STATEMENT (of this Report): ~~NONE~~ DISTRIBUTION STATEMENT A Approved for public release; Distribution Unlimited	
17. DISTRIBUTION STATEMENT (of the abstract entered in Block 20, if different from Report)	
18. SUPPLEMENTARY NOTES	
19. KEY WORDS (Continue on reverse side if necessary and identify by block number)	

20. ABSTRACT (Continue on reverse side if necessary and identify by block number)

Remote assessment of gases by ectroscopic means is surveyed. The "windows" of the atmosphere a[re] described. Electromagnetic signatures of gaseous molecul[es] from 1 Mc to 4000 Å are computed and the methods to compute are explained. Passive and active methods which have been successful are described. Lasers and solid state detectors which might be useful are surveyed.

DD FORM 1 JAN 73 1473 EDITION OF 1 NOV 55 IS OBSOLETE

UNCLASSIFIED

SECURITY CLASSIFICATION OF THIS PAGE (When Data Entered)

TABLE OF CONTENTS

	Page
1. Introduction	1-1
References to Section 1	1-21
2. The Electromagnetic Signatures	2-1
2.1 Magnetic Spin Flip in the Earth's Magnetic Field 1-10 Mc; Magnetic Moments of Gases	2-1
2.2 Rotational Frequencies, 1-100 cm^{-1}, Microwave, λ = 1-0.01 cm	2-6
2.3 Vibrational Frequencies, 10^2 - 10^4 cm^{-1}, Infrared, λ = 1-100μ	2-12
2.4 Raman - Infrared	2-30
2.5 Electronic Transitions, >10^4 cm^{-1}, Near Ultraviolet and Visible λ < 10,000 Å	2-32
References to Section 2	2-47
3. Methods of Assessment by Passive Methods: Successful Experiments	3-1
3.1 Excitation by Decametric Radiation from Ground-Based and Satellite Transmitters Followed by Emission and Detection of Magnetic Spin Flip Radiation	3-1
3.2 Remote Detection of Emission and Absorption in the Infrared and Visible Using Passive Sensing	3-9
3.2.1 Experiment No. 1a	3-9
3.2.2 Experiment No. 1b	3-13
3.2.3 Experiment No. 2	3-18
3.2.4 Experiment No. 3	3-18
3.2.5 Experiment No. 4	3-27
3.2.6 Experiment No. 5	3-27
3.2.7 Experiment No. 6	3-31
3.2.8 Experiment No. 7	3-41
3.2.9 Experiment No. 8	3-46
3.2.10 Experiment No. 9	3-53
3.2.11 Experiment No. 10	3-53
3.2.12 Experiment No. 11	3-55
3.2.13 Experiment No. 12	3-60
3.2.14 Experiment No. 13	3-64
3.2.15 Conclusions	3-6[illegible]

TABLE OF CONTENTS (Cont.)

	Page
3.3 Excitation of Visible and Infrared Emission and Absorption by Ground-Based Sources such as Fire, Lightning, Artificial Electric Light, and Sun Glitter on Oceans, Lakes, Rivers and Harbors	3-67
3.4 Excitation by Tropospheric Lightning	3-69
3.4.1 Experiment No. 14	3-69
3.4.2 Experiment No. 15	3-69
3.4.3 Experiment No. 16	3-74
3.4.4 Summary	3-74
References to Section 3	3-77
4. Methods of Assessment by Active Methods: Successful Experiments	4-1
4.1 Active Probing at Airplane and Satellite Altitudes	4-1
4.1.1 Experiment No. 1	4-1
4.1.2 Experiment No. 2	4-1
4.1.3 Experiment No. 3	4-1
4.1.4 Experiment No. 4	4-1
4.1.5 Experiment No. 5	4-2
4.1.6 Experiment No. 6	4-2
4.1.7 Experiment No. 7	4-2
4.1.8 Experiment No. 8	4-2
4.1.9 Experiment No. 9	4-3
4.1.10 Experiment No. 10	4-3
4.1.11 Experiment No. 11	4-5
4.1.12 Experiment No. 12	4-5
4.1.13 Experiment No. 13	4-9
4.1.14 Experiment No. 14	4-9
4.1.15 Experiment No. 15	4-11
4.1.16 Experiment No. 16	4-11
4.1.17 Experiment No. 17	4-11
4.2 Safety Aspects of Laser Probe from a Satellite	4-12
4.3 Recent Developments in Laser Technology	4-15
4.4 Present Capabilities of Bolometric Sensors and Theoretical Limits to Sensitivities	4-15
References to Section 4	4-23
5. Summary and Recommendations	5-1
Appendix A	A-1

LIST OF FIGURES

Figure		Page
Introduction		
1-1	Terminology, Frequency Wave Length, and Equivalent Temperatures of the Electromagnetic Spectrum	1-2
1-2	Illustrating the Obstruction by the Atmosphere to Electromagnetic Waves and the Optical and Radio "Windows"	1-3
1-3	One-Way Attenuation Through the Standard Summer Atmosphere Due to Oxygen and Water Vapor	1-3
1-4a	Transparent Windows in the Infrared Spectrum of the Earth's Atmcsphere; Sensitivity vs Infrared Wavelength for Some Solid State Detectors	1-4
1-4b	Parts of the Observed Infrared Absorption Spectrum of CO_2 Under Low Dispersion	1-5
1-4c	Overview of Atmospheric and Pollutant Absorption Bands	1-6
1-4d	(a) Blackbody emission for 6000° K and 245° K, being approximate emissions spectra...	1-7
1-5	Typical Remote Sensing Geometry	1-8
1-6	Transmission Spectra for a Path from a Typical Satellite Altitude to the Earth	1-9
1-7	Transmission vs Wavelength Due to Haze Extinction	1-10
1-8	Comparison of Calculated Spectral Radiance with Measurements for a Clear Atmosphere	1-11
1-9	The Effect of Temperature Distribution on Radiance	1-12
1-10	The Effect of Surface Temperature on Radiance	1-13
1-11	The Effect of Water Vapor on Radiance	1-14
1-12	Radiance for Three Nadir Angles	1-15
1-13	Energy Available for Remote Sensing	1-16
1-14	Galactic Noise Temperature	1-17
1-15	Sky Noise Temperature Due to Oxygen and Water Vapor at Various Zenith Angles, (θ)	1-17
1-16	Comparison of UVDM Solar Spectrum (Solid Line) with Perkin-Elmer Spectrum (Dashed Line) of Thekaekara (1970)	1-18

LIST OF FIGURES (Cont.)

Figure		Page
The Electromagnetic Signatures		
2-1	Lande´ g Values for Atomic and Molecular Species Observed in Earth's Ionosphere Over Antarctica Compared with Calculated Values .	2-3
2-2a	The Allowed Rotational Energy Levels of a Rigid Diatomic Molecule	2-7
2-2b	Allowed Transitions Between the Energy Levels of a Rigid Diatomic Molecule and the Spectrum which Arises from Them	2-7
2-3	The Allowed Vibrational Energy Levels and Some Transitions Between Them for a Diatomic Molecule Undergoing Anharmonic Oscillations	2-13
2-4	The Fundamental Absorption (Centered at about 2143 cm^{-1}) and the First Overtone...	2-14
2-5	The Center of the Fundamental Band of Carbon Monoxide Under Higher Resolution...	2-16
2-6	The Fundamental Band of Figure 2-5 Under Very Low Resolution; All Rotational... . . .	2-17
2-7a	The Rotational Energy Levels for Two Vibrational States Showing...	2-18
2-7b	Spectrum of the Bending Mode of the HCN Molecule Showing the PQR Structure... . . .	2-19
2-7c	The Contour of a PQR Band Under Low Resolution	2-20
2-7d	The Spectrum of a Bending Mode of Acetylene, HC = CH, Showing the Strong, Weak,... . . .	2-21
2-7e	The Parallel Stretching Vibration, Centered at 1251 cm^{-1}, of the Symmetric...	2-22
2-8	The Rotation Energy Levels of a Diatomic Molecule and the Rotational...	2-31
2-9	The Pure Rotation and the Rotation-Vibration Spectrum of a Diatomic Molecule...	2-33
2-10	Raman Spectra of CCl_4 and $CHCl_2BR$ Showing Anti-Stokes' Lines after Glocker...	2-36
Methods of Assessment by Passive Methods: Successful Experiments		
3-1	Radio Spectrum as Depicted by the International Telecommunications System	3-8
3-2	Schematic Signals Received in a Correlation Spectrometer	3-11

LIST OF FIGURES (Cont.)

Figure		Page
3-3	Dispersive System for Vapor Detection Using Spectrum Correlation Filter	3-12
3-4	Attenuation and Dilution	3-14
3-5	Balloon Flight SO2 Profile: Chicago Area, September 3, 1969	3-15
3-6	Balloon Flight NO2 Profile: Chicago Area, September 3, 1969	3-16
3-7	Sulfur Dioxide Concentration--Total Vertical Burden Toronto, November 15, 1967	3-19
3-8	SO_2 Profile Over Lake Ontario	3-20
3-9	SO_2 Mass Balance--Washington, D.C.	3-21
3-10	NO_2 Profile--Toronto, March 7, 1968	3-22
3-11	Artist's Impression of a Nimbus Satellite in Orbit Carrying Two Correlation Spectrometers for Remote Sensing of Pollutant Gases	3-23
3-12	Fish and Mineral Oil Spectral Signatures	3-26
3-13	Mean Reflectance of Three Lavic Phases of Pisgah Crater Basalts	3-28
3-14	Temperature Map of the Caspian Sea, Obtained from Infrared and Microwave Radiometer Data λ = 3-10 cm, Microwave and Infrared, Passive	3-30
3-15a	Typical Spectral Atmospheric Radiance Measured 10 December 1969 at Altitudes of 3.4, 10.0, 20.1, and 24.7 km	3-32
3-15b	Atmospheric Transmittance vs Wavenumber from Consecutive Records at Various Altitudes for the 2125-2175 cm^{-1} Region	3-32
3-16a	Samples of the Reduced Data Obtained 22 February 1971 at Alamogordo,...	3-33
3-16b	Comparison of Calculated and Measured Emission Spectra in the 20-30μ Region...	3-34
3-17	Atmospheric Transmittance vs Wavenumber at Various Altitudes for the 2175-2250 cm^{-1} Region, Records 23-26	3-35
3-18	Atmospheric Transmittance vs Wavenumber at Various Altitudes for the 2175-2250 cm^{-1} Region, Records 43-46	3-36
3-19	Solar Absorption in the CO Fundamental Region, and Its Interpretation as Solar CO at 4500° K	3-37
3-20	Concentrations of Atmospheric Pollutants, Both Measured and Computed, vs Altitude	3-38

LIST OF FIGURES (Cont.)

Figure		Page
3-21a	COPE Correlation and Interferometer	3-39
3-21b	Interferogram and Spectrum of CO	3-39
3-22a	CO Effect on Interferogram	3-44
3-22b	NO Effect on Interferogram	3-44
3-22c	Methane Effect on Interferogram	3-45
3-22d	SO_2 Effect on Interferogram	3-45
3-23a	Weighting Functions of the Nimbus IV SCR	3-47
3-23b	Orbit Plot Overlay	3-47
3-24	Typical Temperature vs Altitude and Latitude Plots Deduced from Nimbus Measurements	3-48
3-25	Comparison Between Temperature Profile Deduced from the Radiances...	3-49
3-26a	Millimeter Spectral Lines Observed for Several Molecular Transitions in...	3-51
3-26b	Methyl Cyanide Emission from Sgr B2 (OH) in the J = 6_K Transition...	3-52
3-27	Observed Spectral Transmittance at Various Altitudes and Solar Zenith Angles...	3-54
3-28a	Heterodyne Detection of N_2O Absorption...	3-57
3-28b	Spectrometer (8.5 μm) Optical System	3-58
3-28c	Heterodyne Signals at 8.5 μm from the Moon and Mars...	3-59
3-29	The Average of Two Spectra at a Resolution of 0.067 cm^{-2}	3-61
3-30	Spectrum Observed at Various Altitudes	3-65
3-31	Spectra Observed with Spectograph Slit Laid Across Sun's Glitter into Regions of Little Reflection from Earth's Surface	3-68
3-32a	Region of H-Alpha--Enlargement of a Negative from 0.6 Meter Spectrograph	3-71
3-32b	Region of 7423 A to 7774 A--Broadened NI and OI Lines	3-71
3-32c	Absorption Bands Due to O_2 in Air-Path	3-72
3-32d	NI and IO Multiplets, from 7947 A to Region of 8683 A	3-72
3-32e	A Slitless Spectrum of Lightning in Near Infrared	3-72
3-33a	Absorption Bands Due to O_2 in Air Path	3-73
3-33b	Isodensity Tracing of H-Alpha	3-73
3-34a	High-Speed, Time-Resolved Spectrum of a Lightning Stroke (b) The Same...	3-75
3-34b	High-Speed, Time-Resolved Spectrum of a Lightning Stroke (a) A 10-m...	3-75

LIST OF FIGURES (Cont.)

Figure		Page
Methods of Assessment by Active Methods: Successful Experiments		
4-1	Major Atmospheric Absorption Lines from 6940 Å to 6946 Å	4-4
4-2	Schematic Timing Diagram Showing Laser Pulse and Various Return Signals	4-6
4-3	Fluorescent Spectra of Various Species of Algae	4-7
4-4	Excitation and Absorption Spectra for Various Algae Species	4-8
4-5	Spectrum of the Scattered Light Excited in Air by the Incident Radiation	4-10
4-6	Characteristic Responses of Various Infrared Detectors	4-21
4-7	Present and Projected Radiometric Sensitivities	4-22

LIST OF TABLES

Table		Page
Introduction		
-1	Atmospheric Trace Gases: Candidates for Assessment	1-20
The Electromagnetic Signatures		
2-1	Values of g for Expected Electron Spin Resonance Signals from Possible Molecular Species in the Jovian Atmosphere	2-4
2-2	Rotational Absorption and Emission Frequencies of Diatomic Gases at 300^0K	2-9
2-3	Vibrational Frequencies for Diatomic Molecules and Bandwidth $\Delta\nu$ in Units of cm^{-1}	2-23
2-4	Infrared Vibrational Frequencies for Polyatomic Molecules	2-25
2-5	Vibrational Frequencies of Various Groups	2-29
2-6a	Infrared and Raman Bands of Sulphur Dioxide	2-34
2-6b	Infrared and Raman Spectra of Nitrous Oxide	2-34
2-7	Activities of Vibrations of Planar and Pyramidal AB_3 Molecules	2-35
2-8	A Summary of Characteristic Raman Frequencies	2-37
2-9	Characteristic Frequencies for Visible and Ultraviolet Electronic Transitions of Various Groups of Atoms Bound in Hydrocarbon Molecules	2-43
2-10	Some Vapors and Gases Having Electronic Transitions in the Visible and Near Ultraviolet	2-45
Methods of Assessment by Passive Methods: Successful Experiments		
3-1	A Summary of the U.S. Amateur Bands	3-6
3-2	SO_2 Determinations	3-24
3-3	Summary of Airborne Results	3-25
3-4	Average Reflectance (Relative to MgO) of Typical Spectra of Various Minerals and Vegetation	3-29
3-5	Spectra Used for Interferogram	3-40
3-6	Estimated Detection Sensitivities Relative to CO (Assuming Source Intensity to be Independent of Wavelength)	3-43

LIST OF TABLES (Cont.)

Table		Page
3-7	Molecules Observed in the Interstellar Medium	3-50
3-8	Experimental Sensitivities to Pollutant Gases	3-56
3-9	Partial List of Spectral Line Assignments	3-62
3-10	Experimentally Measured Mixing Ratios	3-63
3-11	Lines Identified in the Slitless Spectrum of Lightning from 6563 to 8820 A	3-70
	Methods of Assessment by Active Methods: Successful Experiments	
4-1	Raman-Scattering Cross Section	4-14
4-2	Characteristics of High-Intensity Lasers	4-16
4-3	Operating Characteristics of Double-Pulsed Metallic Vapor Lasers	4-17
4-4	Blue-Green Laser State-of-the-Art	4-18
4-5	Blue-Green Laser Potential	4-19
4-6	Laser Transmitter and Receiver Sizes	4-20

SECTION 1. INTRODUCTION

The problem of detecting trace gases in the lower troposphere by electromagnetic radiations and absorptions measured above the atmosphere can be treated in two parts. The first is computation and listing the electromagnetic frequencies which characterize those molecules which are gases at temperatures ambient on the earth's surface; namely, about 300° K. These frequencies in increasing magnitude are caused by (we ignore nuclear spin flip):

1. Electron spin flip between hyperfine energy levels split by the earth's magnetic field (decametric and microwave)
2. Rotation (microwave and infrared)
3. Vibration (infrared)
4. Electronic excitations (visible and ultraviolet).

The corresponding blackbody temperatures are shown in Figure 1-1.

The second part, for those frequencies which may possibly be detected through the blanket of the earth's atmosphere either in absorption or emission, comprises examination of methods of their detection. The electromagnetic "windows" in the atmosphere are shown in Figure 1-2. Besides the rather narrow windows in the visible and in the near infrared, there is the broad radio window extending from about 2 Mc to about 2 kMc (see Figure 1-3). Transmission in the far infrared and microwave regions is blocked by absorption of water vapor, CO_2 and ozone. The atmospheric transmission in the visible and infrared is shown in more detail in Figure 1-4.

Remote sensing geometry is shown in Figure 1-5. Transmission spectra of the earth as seen from satellite altitude are shown in Figures 1-7 through 1-13. The noise spectrum of the sky with equivalent temperatures is shown in Figures 1-14 and 1-16.

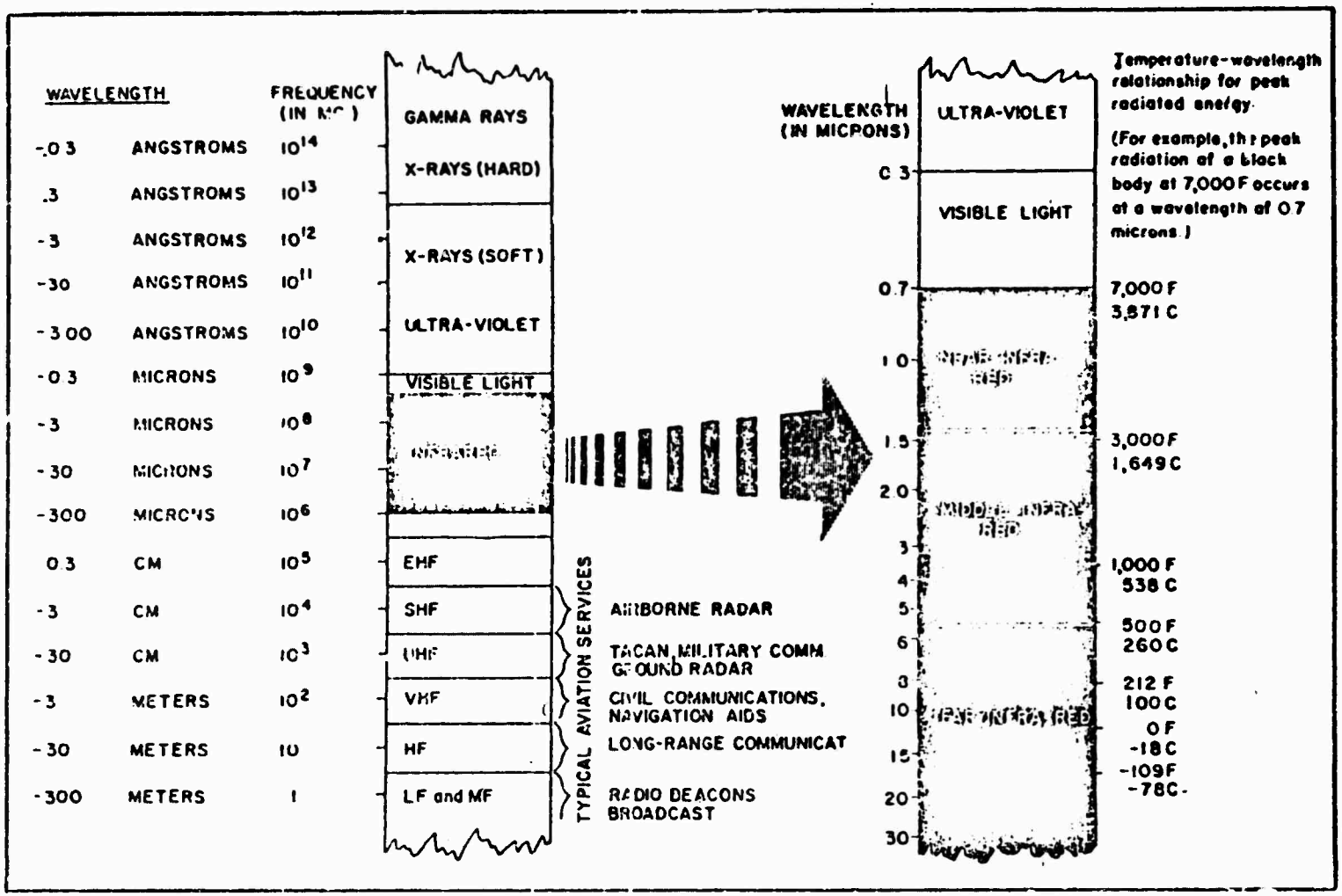

Figure 1-1. Terminology, Frequency Wave Length, and Equivalent Temperatures of the Electromagnetic Spectrum

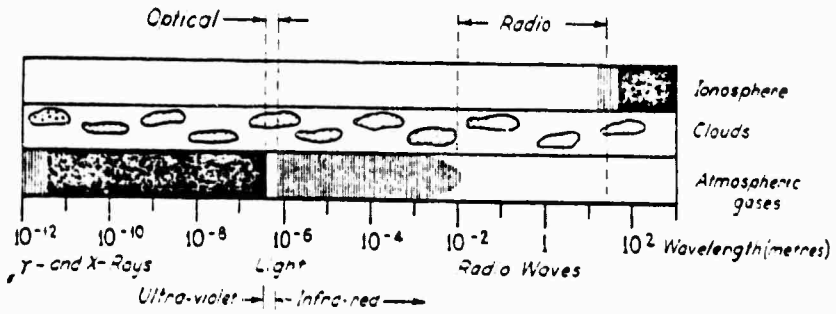

Figure 1-2. Illustrating the Obstruction by the Atmosphere to Electro-Magnetic Waves and the Optical and Radio "Windows" [Ref. 1-1]

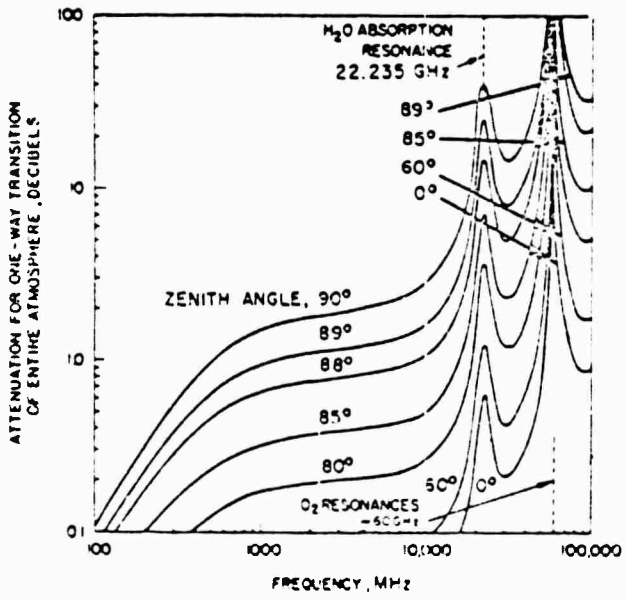

Figure 1-3. One-Way Attenuation Through the Standard Summer Atmosphere Due to Oxygen and Water Vapor [Ref. 1-2]

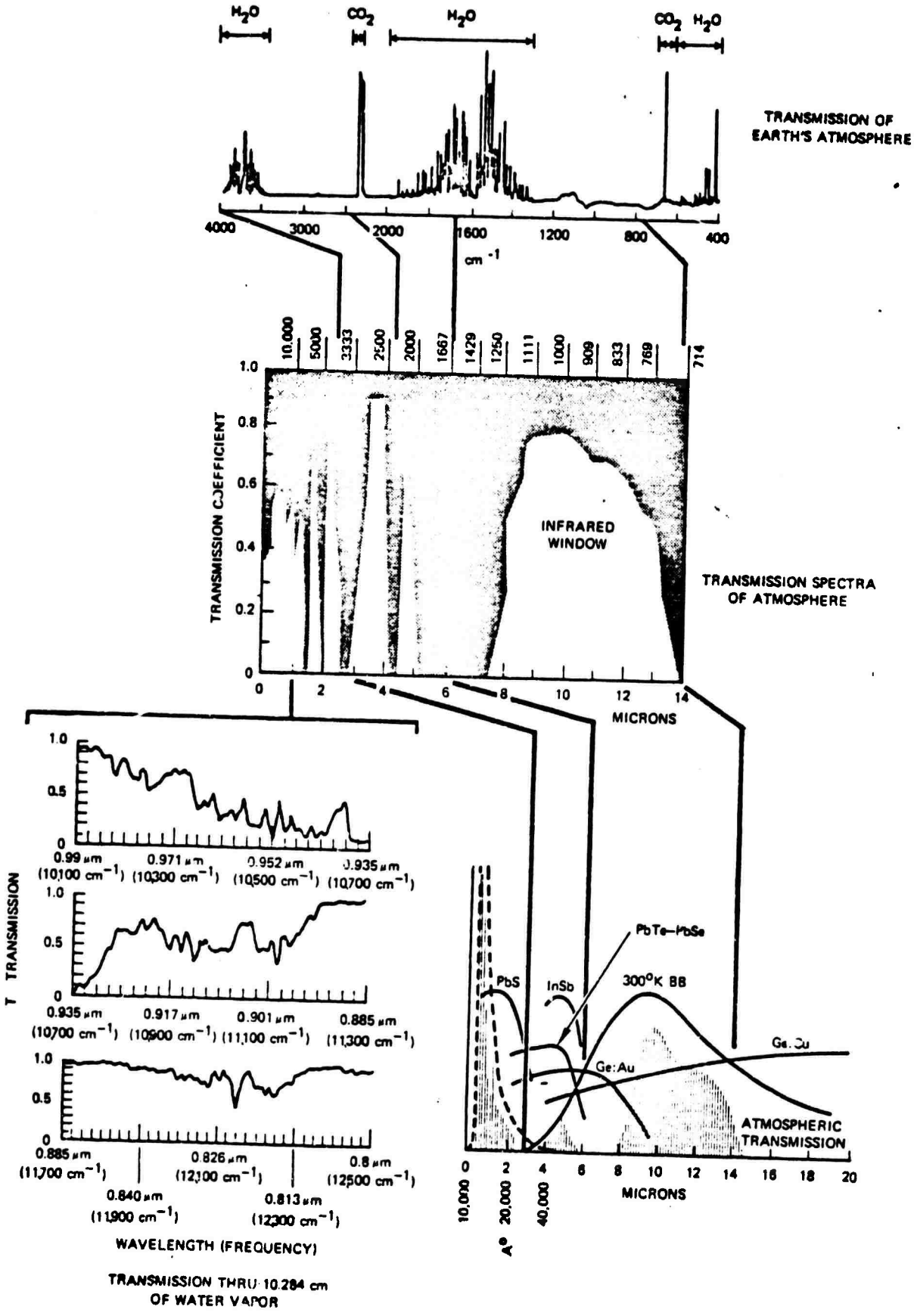

Figure 1-4a. Transparent Windows in the Infrared Spectrum of the Earth's Atmosphere; Sensitivity vs Infrared Wavelength for Some Solid State Detectors

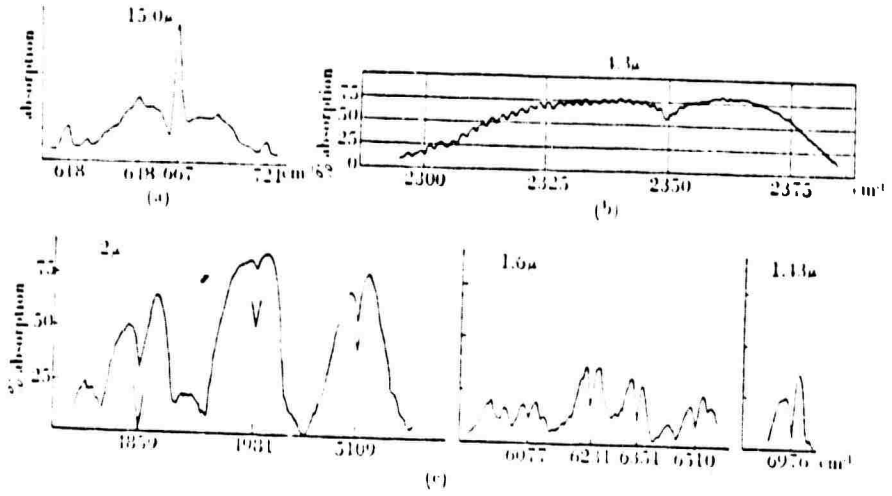

Figure 1-4b. Parts of the Observed Infrared Absorption Spectrum of CO_2 Under Low Dispersion [Ref. 1-3]

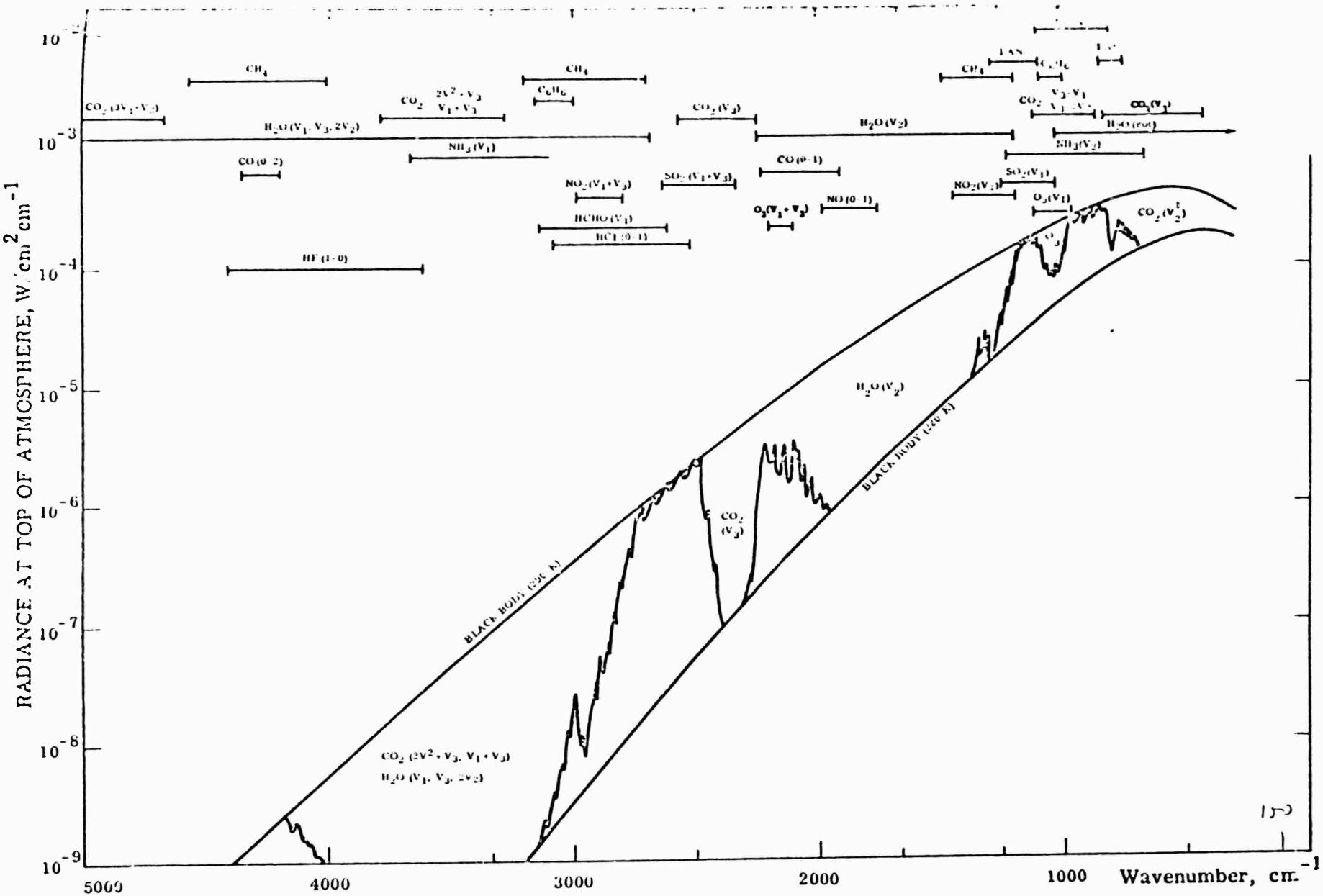

Figure 1-4c. Overview of Atmospheric and Pollutant Absorption Bands [Ref. 1-4]

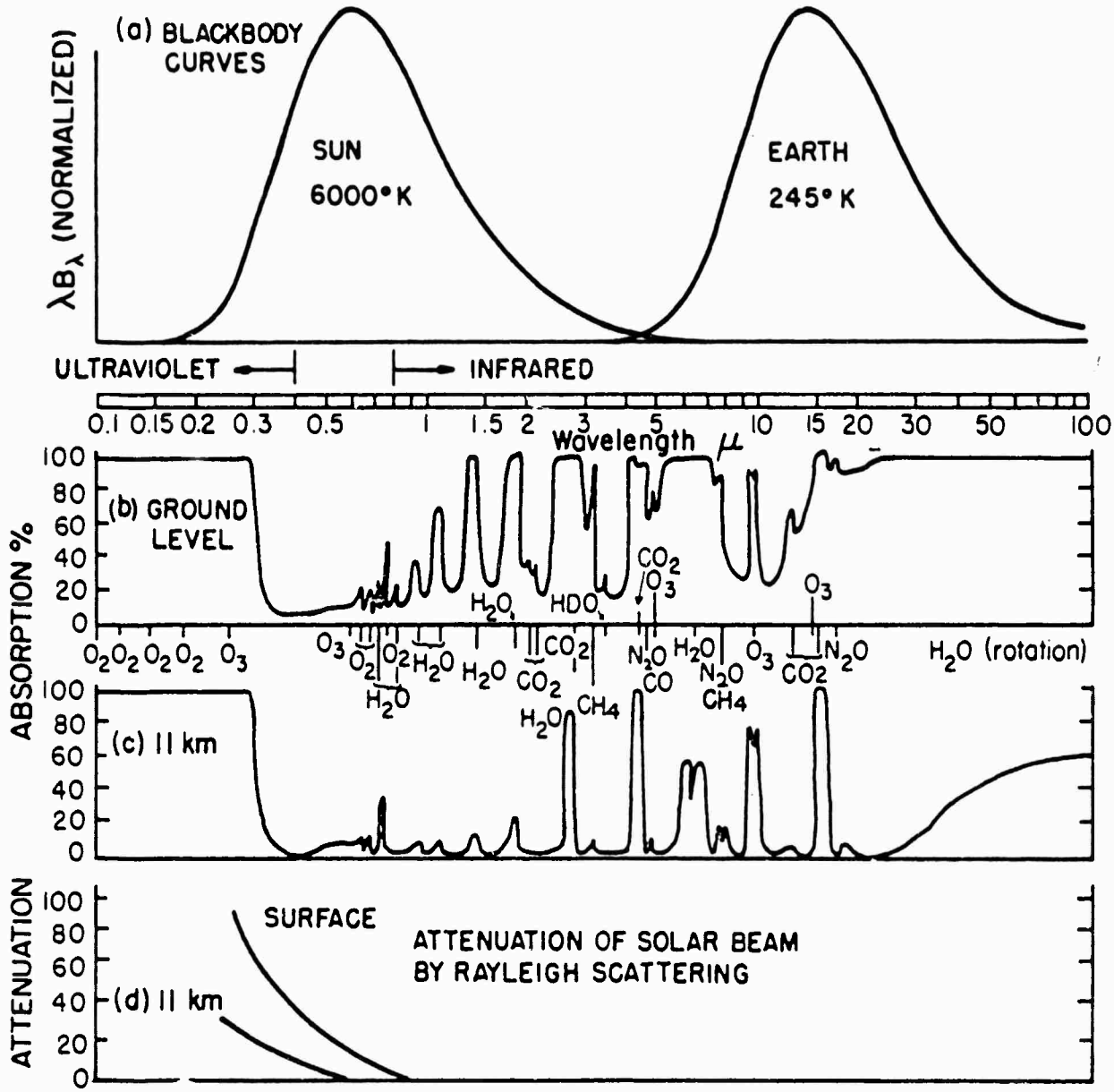

Figure 1-4d. (a) Blackbody Emission for 6000°K and 245°K, Being Approximate Emission Spectra of the Sun and Earth, respectively (Since Inward and Outward Radiation Must Balance, the Curves Have Been Drawn with Equal Areas--Though in Fact 40% of Solar Radiation is Reflected Unchanged; (b) Atmospheric Absorption Spectrum for a Solar Beam Reaching the Ground; (c) The Same for a Beam Reaching the Tropopause in Temperate Latitudes; (d) Attenuation of the Solar Beam by Rayleigh Scattering at the Ground and at the Temperate Tropopause [Ref. 1-5]

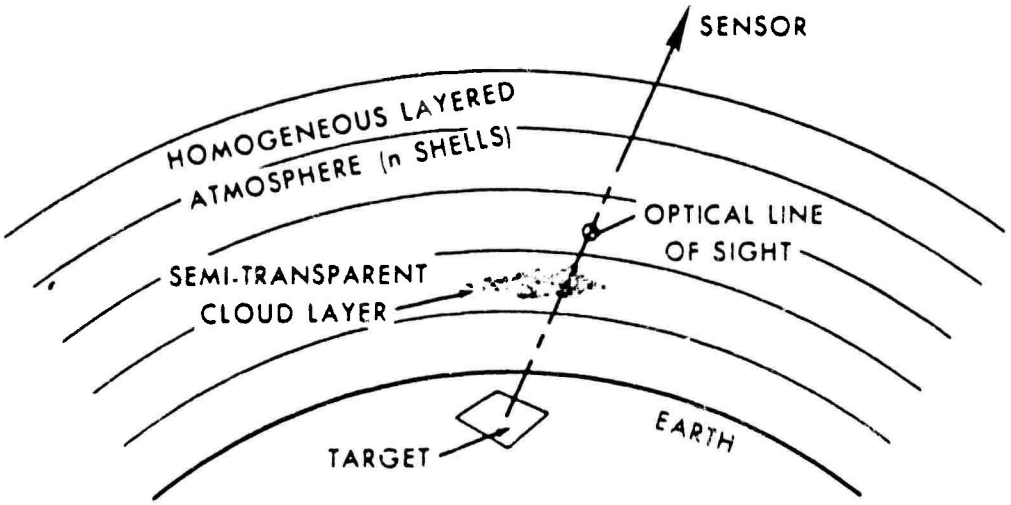

Figure 1-5. Typical Remote Sensing Geometry [Ref. 1-6]

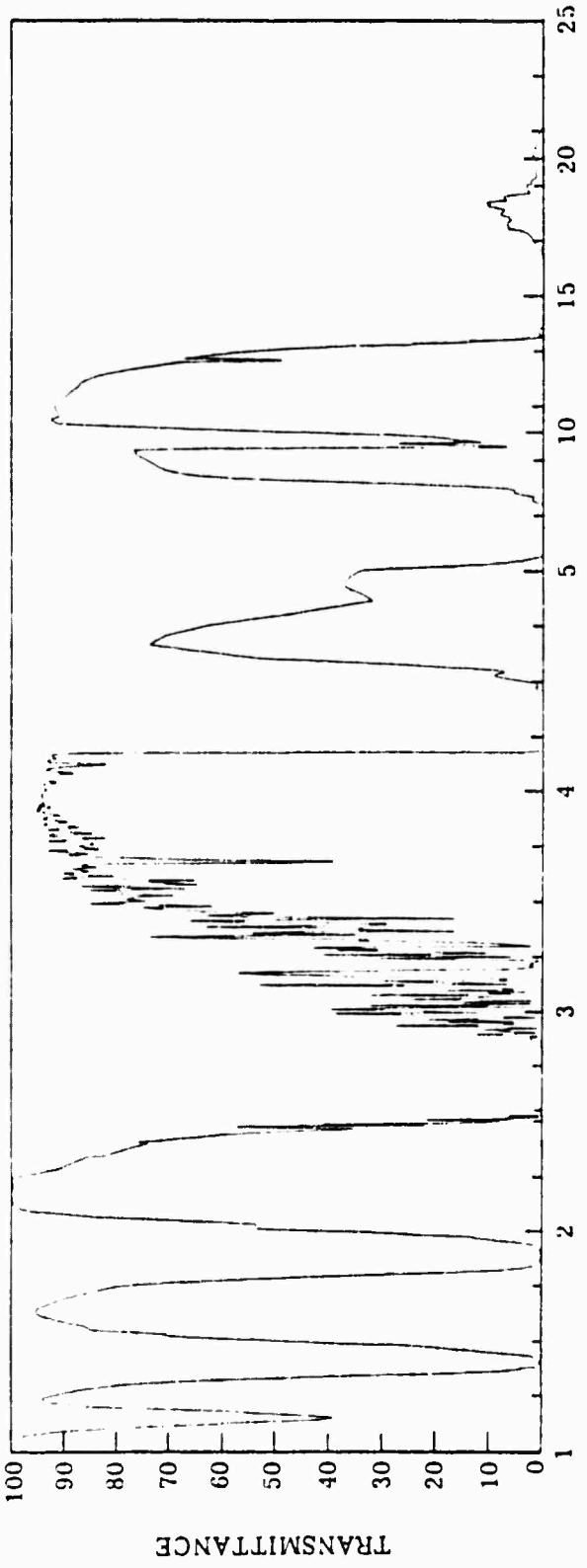

Figure 1-6. Transmission Spectra for a Path from a Typical Satellite Altitude to the Earth. Detector Altitude = 90.000 km; Source Altitude = 0.000 km; Zenith Angle = 120.00 degrees [Ref. 1-6]

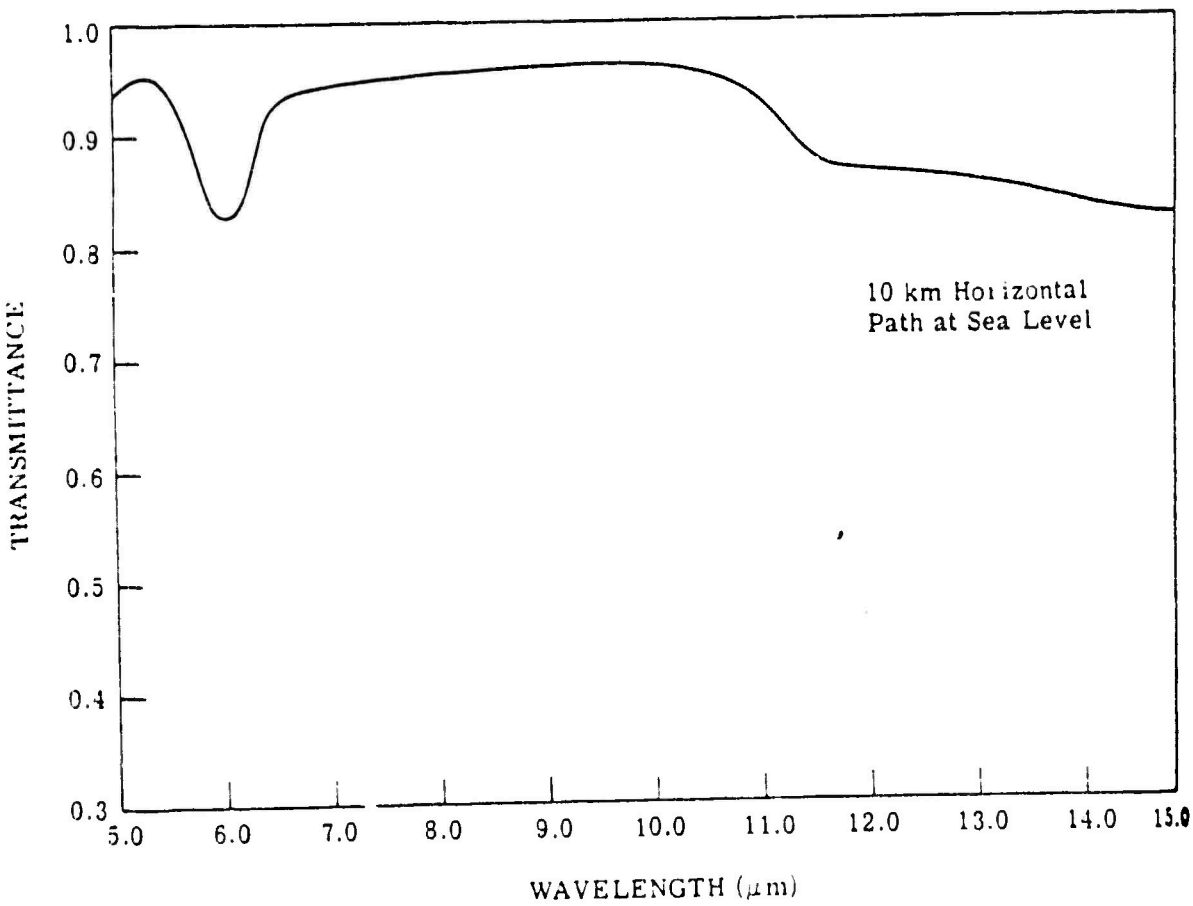

Figure 1-7. Transmission vs Wavelength Due to Haze Extinction [Ref. 1-6]

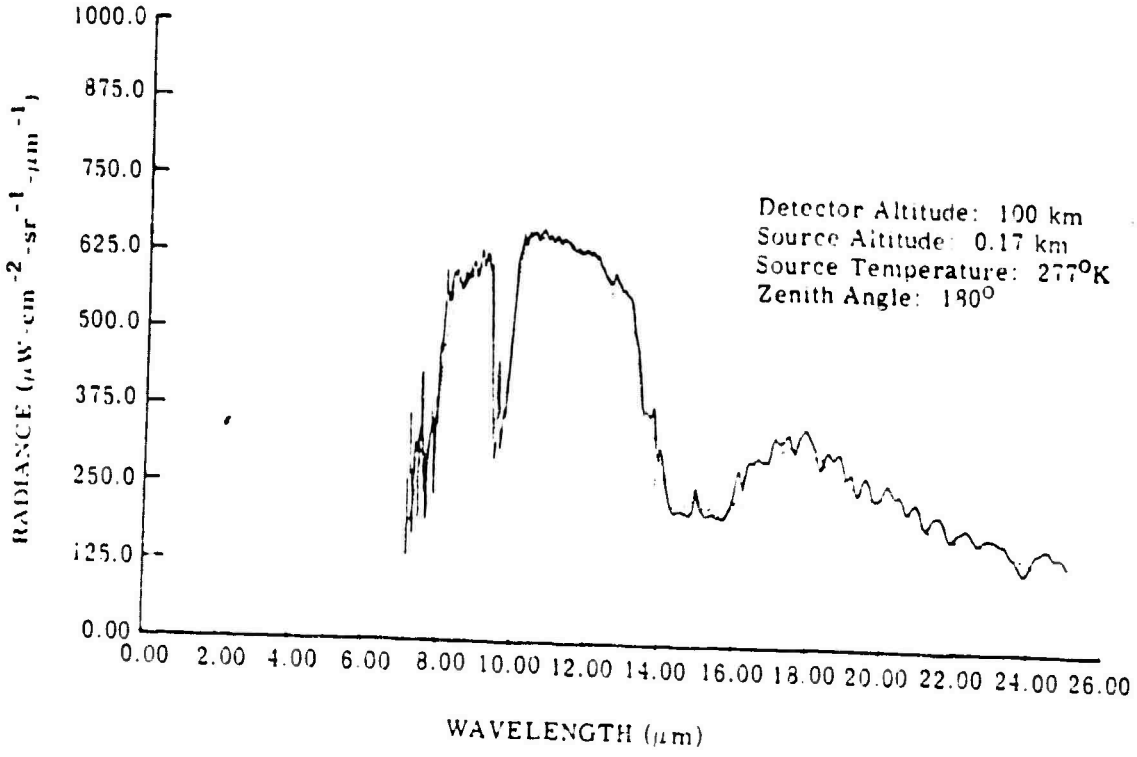

Figure 1-8. Comparison of Calculated Spectral Radiance with Measurements for a Clear Atmosphere. Spectral Radiance (------) Calculated with the University of Michigan Computer Code, and Spectral Radiance (———) Measured by Nimbus III [Ref. 1-6]

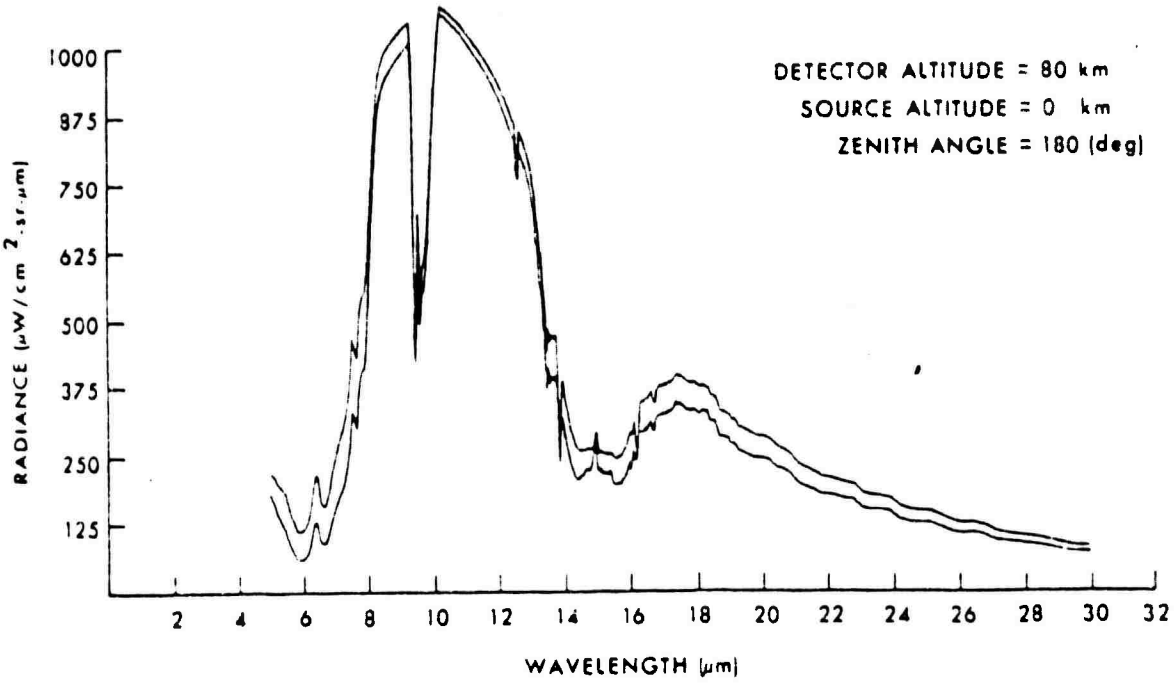

Figure 1-9. The Effect of Temperature Distribution on Radiance [Ref. 1-6]

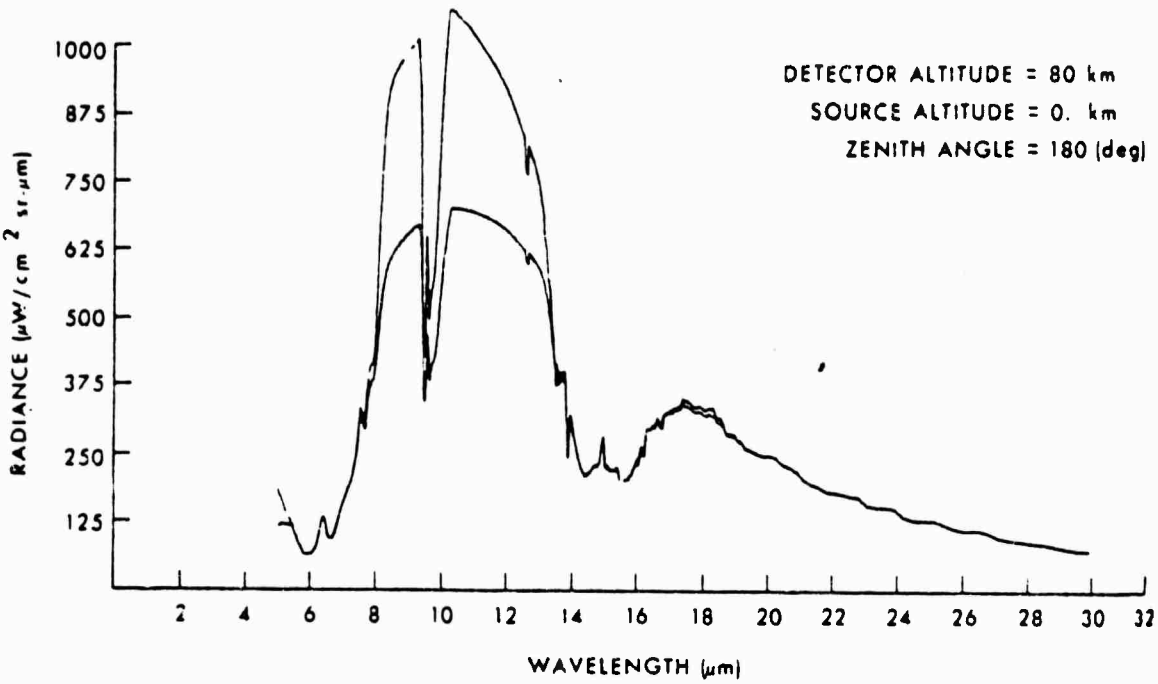

Figure 1-10. The Effect of Surface Temperature on Radiance [Ref. 1-6]

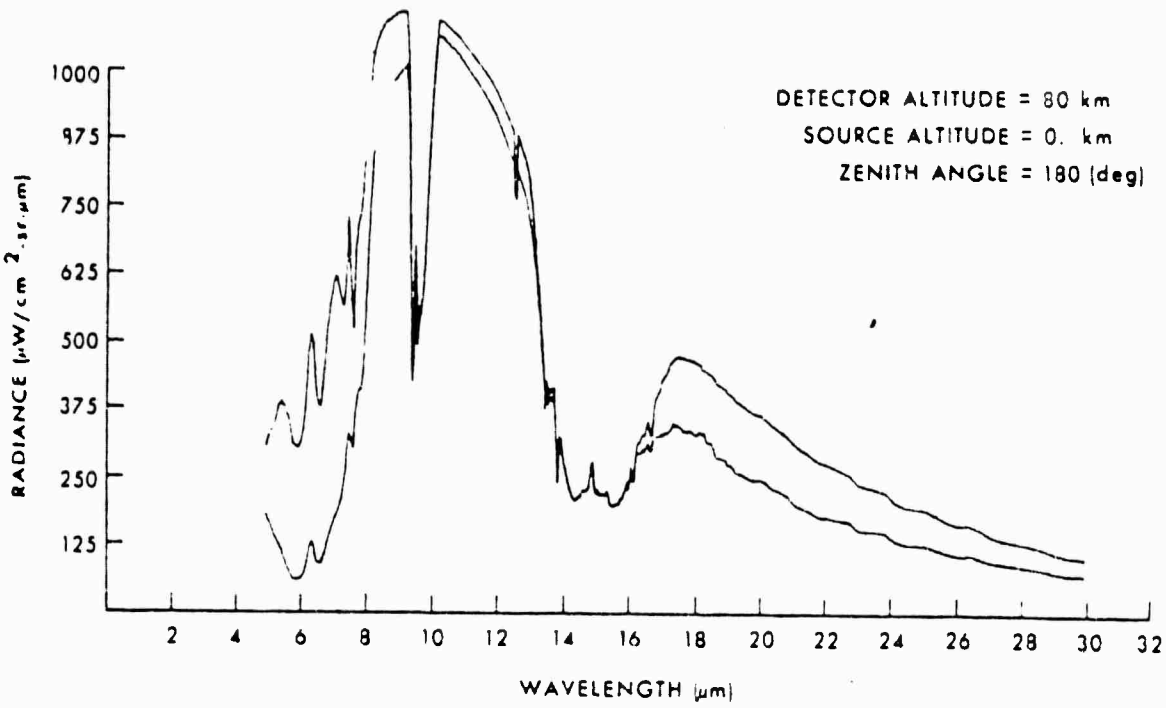

Figure 1-11. The Effect of Water Vapor on Radiance [Ref. 1-6]

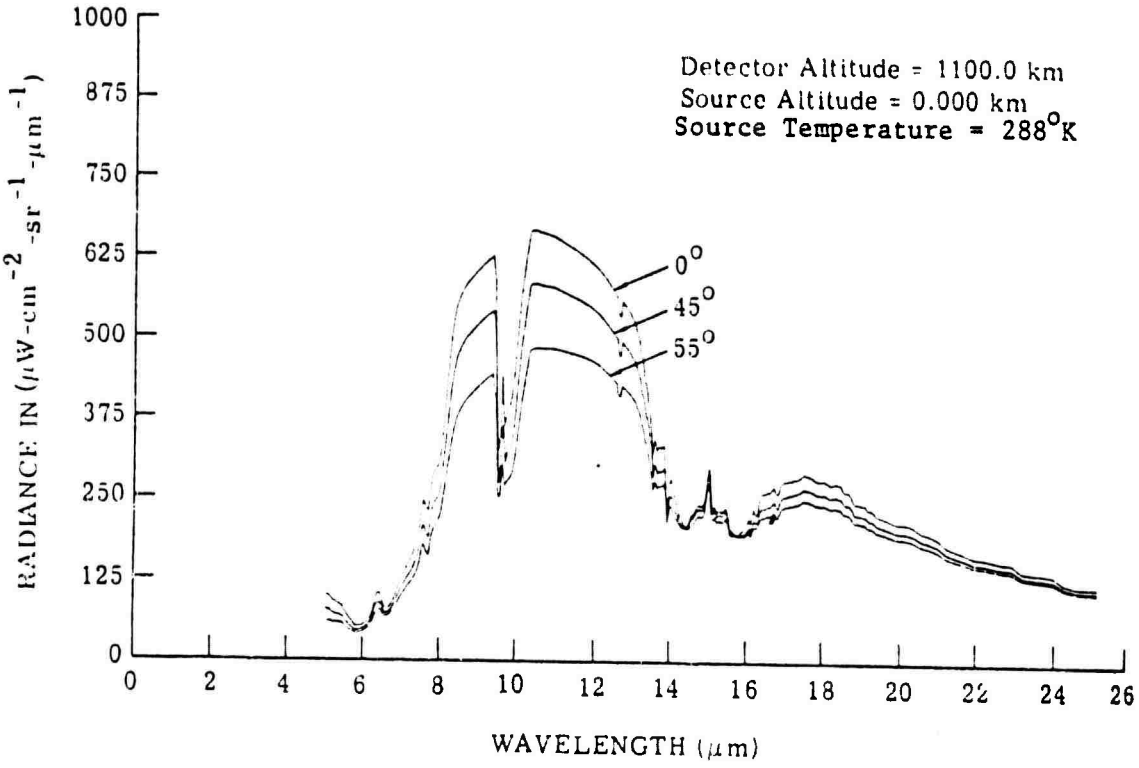

Figure 1-12. Radiance for Three Nadir Angles [Ref. 1-6]

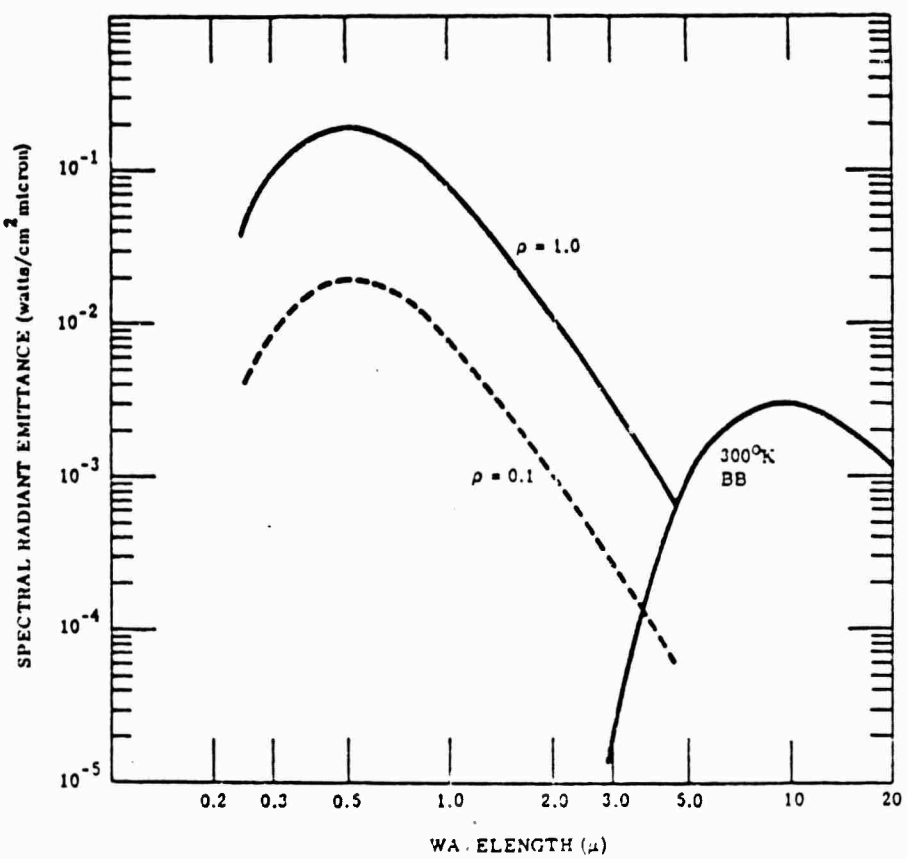

Figure 1-13. Energy Available for Remote Sensing [Ref. 1-7]
(Where ρ is Atmospheric Transmission.)

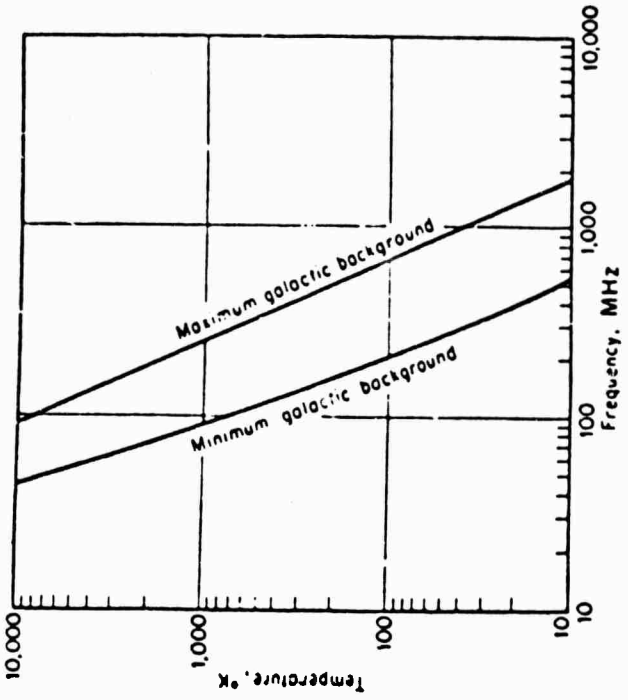

Figure 1-14. Galactic Noise Temperature [Ref. 1-7]

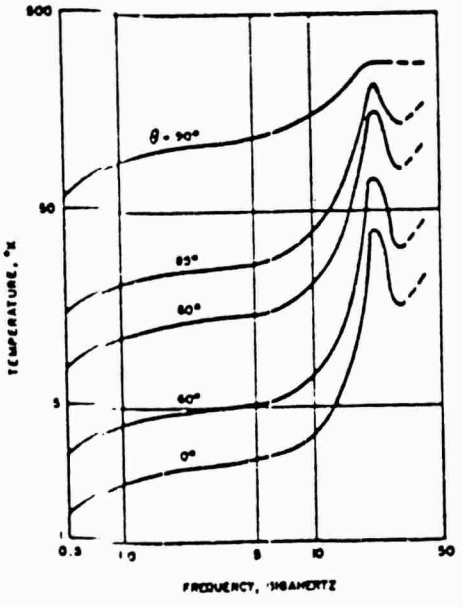

Figure 1-15. Sky Noise Temperature Due to Oxygen and Water Vapor at Various Zenith Angles, (θ) [Ref. 1-7]

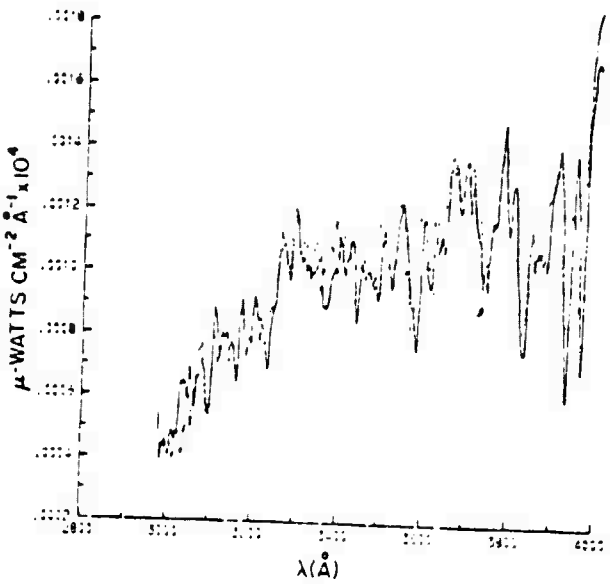

Figure 1-16. Comparison of UVDM Solar Spectrum (Solid Line) with Perkin-Elmer Spectrum (Dashed Line) of Thekaekara (1970) [Ref. 1-8]

Molecules which may exist as trace gases at 300° K near the surface of the earth, and the sources which might produce them, are listed in Table 1-1.

Table 1-1. Atmospheric Trace Gases: Candidates for Assessment

SPECIES	USE
NH_3, NH_2NO, $(NH_2)_2$, $(CH_3)_2N_2H$	NON-CRYOGENIC PROPELLANTS; MANUFACTURE OF PROPELLANTS
FREONS: $CFCl_3$, CF_xCl_y, $C_nF_xCl_y$, ETC.	REFRIGERANTS AND HYDRAULIC FLUIDS
PH_3, MUSTARD GAS, CONSTITUENTS OF BI-COMPONENT NERVE GASES INSECTICIDES	CHEMICAL WARFARE
ETHER, N_2O, $(CF_3)_2O$, $(C_2F_5)_2O$, Xe	ANESTHETICS
GASES ASSOCIATED WITH TNT, RDX, ETC.	EXPLOSIVES
HF, Cl_2, F_2, Br_2, HCl, HNO_3, H_2SO_4	CHEMICAL FACTORIES
BENZENE, CH_3OH, C_2H_5OH, ACETONE, ANILINE, SOLVENTS, LACQUERS, TUNG OIL	FABRICS AND FINISHES
THIOMERCAPTANS: RSH, RCSOH, HYDROCARBONS	PETROLEUM REFINERIES
H_2SO_4, SO_3	SUPERPHOSPHATE MANUFACTURE
CLEANING SOLVENTS, E.G., CCl_4	CHEMICAL FACTORIES
SF_6	UF_6 MANUFACTURE
SiF_4, Si_2F_6	SILICONE AND PLASTICS
AsH_3	STEEL MILLS AND METAL FABRICATION
ACETYLENE, ETHYLENE, N_2O	COMMERCIAL FABRICATION OF PLASTICS, GASES
GASOLINE, KEROSENE	BREATHING OF STORAGE FACILITIES AT REFINERIES AND DOD BASES
TERPENES, HEPTANES, RESINS, LARGE AROMATICS, OILS	NATURAL PRODUCTS FROM FOREST AND DESERT PLANTS
N_2O, CO, CO_2, CH_4, SO_2, H_2S	DECAYING VEGETABLE MATTER
HYDROCARBONS, CH_4, C_2H_6, THIOPHENES	NATURAL OIL SEEPS

REFERENCES TO SECTION 1

1-1. J. L. Pawsey and R. N. Bracewell, Radioastronomy, Oxford Clarendon Press, 1955.

1-2. Symposium on Remote Sensing of the Environment, Willow Run Laboratories, University of Michigan, 1968, p. 36.

1-3. Gerhard Herzberg, Vibrational Infrared and Raman Spectra, D. Von Nostrand Company, Inc., Princeton, New Jersey, 1945.

1-4. C. B. Ludwig, M. Griggs, W. Malkmus, and E. R. Bartle, "Measurement of Air Pollutants from Satellites: Feasibility Considerations," Applied Optics, Vol. 13, No. 6, June 1974.

1-5. W. R. Frisken, "Extended Industrial Revolution and Climate Change," Trans. Geo. Phys., Vol. 52, No. 7, July 1971, pp. 500-508.

1-6. D. C. Anding, H. M. Rose and J. Walker, Proceedings from Symposium on Remote Sensing of the Environment, 1971, pp. 1777-1789.

1-7. Proceedings from Symposium on Remote Sensing of the Environment, Willow Run Laboratories, University of Michigan, 1968, pp. 52, 83.

1-8. J. J. Deluisi, J. Geo. Res. 80, 1975, pp. 345-354.

SECTION 2. THE ELECTROMAGNETIC SIGNATURES

2.1 MAGNETIC SPIN FLIP IN THE EARTH'S MAGNETIC FIELD 1-10 Mc; MAGNETIC MOMENTS OF GASES

Magnetic dipole resonance radiation is a well-known laboratory phenomenon and is to be expected for atmospheric gases which have unpaired electron spins. The spins couple with the various angular momentum vectors which characterize the molecules, and the resultant states of total angular momenta are further split energetically in the earth's magnetic field. There resulted energy transitions between these states by emission and absorption of radiation, and by both of these mechanisms occurring simultaneously, namely by resonance reflection. Resonance reflections for the more abundant free radicals seem already to have been observed with the ionosonder transmitters and receivers on the Alouette satellites [2-1]. These transmitters emit pulses of electromagnetic radiations at 30-second intervals, sweeping in frequency from 0.2 to 14.5 Mc. After each pulse, the onboard receiver listens for 33 msec and records the frequency of the detected signal and the delay time of arrival. From the frequency of the resonantly reflected radiation, the g value of the molecular species causing the scattering may be computed, according to the relation

$$h\upsilon = g\mu H$$

where H = the local earth's magnetic field,

μ = $eh/2$ Mc is the magnetic moment of a free electron of Mass M, and

h = Planck's constant.

The numerical value of g that characterizes a given molecular species is a function of the way the electron spin is coupled in the molecule and is dependent on the strength of the magnetic field. Some g values have been measured for atmospheric free radicals at low magnetic fields and some have been computed. By measuring the frequencies of the returning signals detected by the Alouette receivers, g values have been evaluated and compared with values of g either computed or measured in the laboratory. In this way, it is found that OH, NO, N and O were the species returning the signals, see Figure 2-1 and Table 2-1. Thus, the species responding to the signal causing the excitation may be identified by evaluating their characteristic g values. In weak magnetic fields such as that of the earth, spin orbit coupling is strong and plays a major role in producing g values well below the value 2.00 which characterizes free electron spin flip and synchrotron radiation.

To further strengthen the case for detecting trace gases in the atmosphere at large distances, it may be pointed out that probably the strong decametric radio signals emitted from the atmosphere of Jupiter may be similarly caused by magnetic dipole emissions from the abundant free radicals expected to exist in its reducing atmosphere.

Table 2-1 shows a list of g values, evaluated for the most part from theory. This list seems to comprise the totality of g values that have been computed up to now [Ref. 2-2]. Many more g values should be computed to define the magnetic dipole signatures of the gases which may be candidates for remote assessment such as those listed in Table 1-1. Considering the fact that electron spin resonance (ESR) has been a laboratory diagnostic

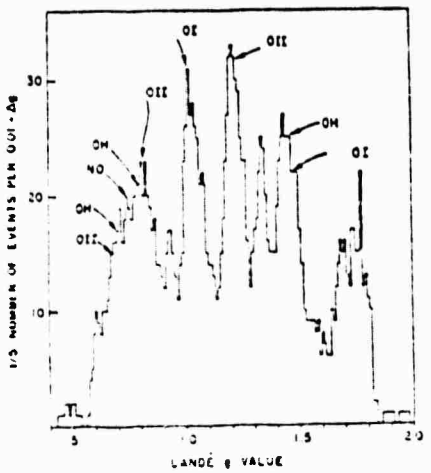

Distribution of g values for about 500 signals taken from over 100 ionograms recorded in Antarctica. Peaks in the distribution are believed to be reflections from free radicals. The labels indicate possible assignments of free radicals. (We believe that the peak at 1.50 may have been somewhat shifted as a result of determinable errors in the fiducial ionogram markers.)

Landé g values for ground and metastable states of atomic and molecular species in Earth's atmosphere.

g Value	Free radical	State	
0.71–0.74	OH	Ground	$^2\Pi_{3/2}$
0.76–0.79	NO	Ground	$^2\Pi_{3/2}$
0.79	OH	Ground	$^2\Pi_{3/2}$
0.80	N I	Metastable	$^4D_{3/2}$
0.80	O II	Metastable	$^4D_{3/2}$
1.00	N II	Metastable	$^1D_2$
1.00	O I	Metastable	$^1D_2$
1.20	N I	Metastable	$^2D_{5/2}$
1.20	O II	Metastable	$^2D_{5/2}$
1.33	N I	Metastable	$^2P_{1/2}$
1.33	O II	Metastable	$^2P_{3/2}$
1.45	OH	Ground	$^2\Pi_{3/2}$
1.50	N II	Metastable	^4P_J
1.50	O I	Ground	$^3P_2$

Figure 2-1. Lande´ g Values for Atomic and Molecular Species Observed in Earth's Ionosphere Over Antarctica Compared with Calculated Values

Table 2-1. Values of g for Expected Electron Spin Resonance Signals from Possible Molecular Species in the Jovian Atmosphere [2-2]

MOLECULAR SPECIES	STATE	g VALUE
NH	$^3\Sigma^-$	-2.0030 -1.00133 -0.66753 -0.50064
CH	$^2\Pi 3/2$	-0.1542 -0.1517 -0.1379 -0.1239
OH	$^2\Pi 1/2$	-0.13399 -0.14121 -0.0025 +0.0033
CH	$^2\Pi 1/2$	-0.0010 -0.0007 -0.0003
NH	$^3\Sigma^-$	-0.0002
CH	$^2\Pi 3/2$	+0.069
NH	$^3\Sigma^-$	+0.10010 +0.16683
CH	$^2\Pi 1/2$	+0.2079
CH	$^2\Pi 3/2$	+0.2592
NH	$^3\Sigma^-$	+0.3367 +0.40049
OH	$^2\Pi 3/2$	0.32442
CH	$^2\Pi 3/2$	+0.3423 +0.4971
OH	$^2\Pi 3/2$	0.48407
NH	$^3\Sigma^-$	+0.60061 0.6674
NO	$^2\Pi 3/2$	0.76-0.79
CH	$^2\Pi 1/2$	0.8702
OH	$^2\Pi 3/2$	0.93399
NH	$^3\Sigma^-$	1.0010

technique for at least 20 years, it is surprising that so few weak field g values have been computed or measured. The reason seems to be that ESR laboratory measurements are usually performed at high field strengths where the electron spin uncouples from the angular momentum vector, and the resulting g is therefore equal to two within a few percent.

If we should want to assess the lower troposphere by exciting it with a decametric transmitter and listening for its reflection, we might ask about the international acceptability of interrogation of the atmosphere by sounding from satellite transmitters. The fact that the succession of Alouette satellites has been so doing at ≈0.2-15 Mc and at an average power of 300 W since 1966 answers the question; namely, there has been no protest against such sounding. Instead, the question may become what may be the maximum frequency and power at which routine sounding may be acceptable.

Another question concerns that of multispectral irradiation of a country by transmitters based in nearby countries. There is much precedence for this practice such as irradiation by The Voice of America, by national radio stations, FM broadcasts, TV stations, amateur radio transmitters, citizens band class transmitters, marker beacons, coast guard and space satellite communications, microwave communications, civilian and military air traffic control radar, emergency aircraft survival, ship navigation, etc. We may recall that the earliest satellites were at a low enough altitude and of such metallic cladding that they were visible by reason of reflecting sunlight to the surface of the earth after sunset, a form of electromagnetic irradiation. Thus, it seems a foregone conclusion that further active irradiation of the earth's surface by electromagnetic assay will continue to be accepted without protest, unless the frequency approaches the ultraviolet.

2.2 ROTATIONAL FREQUENCIES, 1-100 cm^{-1}, MICROWAVE, λ = 1-0.01 cm

A molecule must be asymmetric in order for it to be able to emit electromagnetic radiation by transition between its rotational energy levels in the ground vibrational state. Thus, homopolar molecules such as 0_2, N_2, H_2, etc., are not emitters. Instead, they exchange energy at these frequencies by collision. For asymmetric molecules, the change in energy $\Delta\varepsilon$ by emission and absorption between rotational levels in the ground state is given by (see Figure 2-2):

$$\begin{aligned} \Delta\varepsilon &= 2B(J+1)\,cm^{-1} \\ & J \leftrightarrow J+1 \\ B &= (h/8\pi^2 Ic)\,cm^{-1} \end{aligned} \qquad (2\text{-}1)$$

where I = moment of inertia about a molecular axis.

At ambient environmental air temperature $\approx 300^{\circ}K$ of interest to the remote assessment problem, essentially all molecules are in the ground vibrational state. Thus, to a first approximation, the rotational emission is a series of equally spaced frequencies, as shown in Figure 2-2, for linear molecules. For nonlinear molecules there are corresponding moments of inertia about three geometric axes and therefore as many as three sets of rotational emission and absorption lines.

At $300^{\circ}K$, only the lowest rotational levels are populated, and thus, only the lines corresponding to the transitions $J \leftrightarrow J+1$ where J = 0,1,2,3 play a significant role. The population of the J^{th} level relative to the ground state for diatomic molecules approximately by

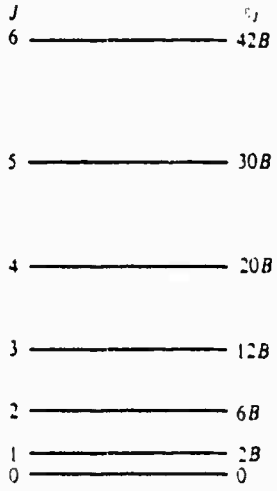

Figure 2-2a. The Allowed Rotational Energy Levels of a Rigid Diatomic Molecule

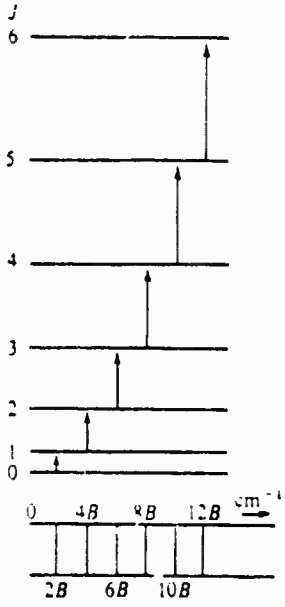

Figure 2-2b. Allowed Transitions Between the Energy Levels of a Rigid Diatomic Molecule and the Spectrum which Arises from Them

$$N_j \equiv (2J + 11)\ e^{-BhcJ(J+1)/kT} \qquad (2\text{-}2)$$

as described Herzberg's books [2-4]. For example, for $B \equiv 10\ cm^{-1}$ at °C, the peak population occurs at $J = 3$, and for $J > 10$, the population has decreased by a factor of >40.

At 300° K, the energies E of these lines are broadened by ΔE by the Doppler effect, namely, by kinetic motion of the emitting and absorbing molecules, where $\Delta E/E \approx 0.30$.

The most energetic of these rotational frequencies in themselves provide largely an academic signature of trace gases in the lower troposphere because absorption by atmospheric water vapor inhibits their assessment by observation through the atmosphere (see Figures 1-2 and 1-3). Nevertheless, despite attenuations of up to 100 dB in traversing the atmosphere, the emission from rotational transitions of at least 20 molecules as complex as seven atoms, emitting from interstellar media, have been observed with ground-based radio-telescopes. Furthermore, submillimeter rotational radiation in the earth's atmosphere has been measured from airplanes for atmospheric polar molecules such as H_2O, N_2O, NO, SO_2, O_3, HNO_3, and NO_2.

Rotational and vibrational frequencies combine to produce vibration-rotation or vibronic spectra, some of which lie in the observable "window" in the near infrared, and some of which may be observed by Raman backscatter, for our purpose of remote assessment of gases in the low troposphere.

The rotational frequencies for several diatomic molecular species which exist as components of room temperature gases, computed from Equation 2-1, and their respective intensities computed from Equation 2-2, are listed in Table 2-2.

Table 2-2. Rotational Absorption and Emission Frequencies of Diatomic Gases at $300^{o}K$

	B_e	ν_1	ν_2	ν_3	ν_4
Cl_2	0.2438				
Cl_F	0.5165	0.033	2.066	3.099	4.132
ClO	---				
H_2	60.809				
HBr	8.473	16.946	33.892	50.838	67.798
HCl	10.5909	21.182	42.364	63.545	84.727
HF	20.939	41.08	82.19	123.15	164.00
HI	6.551	13.102	26.204	39.305	---
HS	[9.47]	18.94	37.88	56.82	---
I_2	0.02735				
ICl	0.11416	0.2283	0.4566	0.685	0.9133
BF	1.518	3.03	6.07	9.11	12.14
B_2	1.212				
BBr	0.480	0.98	1.96	2.94	3.92
BH	12.018	24.04	48.07	72.11	96.14

Table 2-2. Rotational Absorption and Emission Frequencies of Diatomic Gases at 300°K (Cont.)

	B_e	ν_1	ν_2	ν_3	ν_4
BCl	0.6838				
Br_2	0.08091				
BrF	0.3572	---	1.429	2.143	2.858
BrO	---				
CO	[1.9212]	3.8424	7.685	11.527	15.370
C_2	1.6326				
CH	14.457	28.914	57.828	86.742	115.656
CN	1.8996	3.799	7.598	11.398	15.197
CP	0.7986	1.597	3.194	4.792	6.389
CS	0.8205	1.641	3.282	4.923	6.564
IO	---				
N_2	2.010				
NH	16.65	33.3	66.6	99.9	---
NO	1.8046	3.409	6.818	10.228	13.637
O_2	1.4456				

Table 2-2. Rotational Absorption and Emission Frequencies of Diatomic Gases at $300^{o}K$ (Cont.)

	B_e	ν_1	ν_2	ν_3	ν_4
OH	18.871	37.74	75.484	113.23	---
P_2	0.3033				
PH	[4.363]	8.726	75.484	113.23	---
PN	0.7862	1.572	3.145	4.717	6.290
PO	0.7613	1.523	3.045	4.568	6.090
SiH	7.496	14.992	29.984	44.976	59.97
SiN	0.7310	1.462	2.924	4.396	5.848
SiO	0.7263	1.453	2.905	4.358	5.810
SiS	0.3036	0.607	1.214	1.822	2.429
SO	0.7089	1.418	2.836	4.253	5.671
OCS	0.2027	---	0.8109	1.2163	1.6217
CH_3F	0.8512	---	3.4047	5.1070	6.8090

2.3 VIBRATIONAL FREQUENCIES, 10^2 - 10^4 cm^{-1}, INFRARED, λ = 1-100μ

At $\simeq 300^{\circ}K$, nearly all molecules are in the ground vibrational state so that vibrational transitions occur only from the ground state ($\nu = 0$). Transition to the next vibrational state, $\nu = 1$, is the fundamental absorption, and besides this there are the much weaker first and second overtones caused by the transitions ($\nu = 0$) $\rightarrow$ ($\nu = 2$) and ($\nu = 0$) $\rightarrow$ ($\nu = 3$) (see Figures 2-3 and 2-4). The corresponding vibration frequencies for emission and absorption are given by

$$\begin{aligned} \nu_o &= \omega_e(1 - 2x_e) \\ \nu_1 &= 2\omega_e(1 - 3x_e) \\ \nu_2 &= 3\omega_e(1 - 4x_e) \end{aligned} \qquad (2\text{-}3)$$

where ω_e is the zero point vibrational frequency, and x_e is the correction for anharmonicity, both of which are listed in Herzberg's tables [2-4].

To a first approximation, the energy of a vibrating, rotating molecule is the sum of the separate vibrational and rotational energies. Under this simplification, one finds that the vibrational-rotational transitions are given by

$$\nu = \omega_o + 2B \quad \Delta m \qquad (2\text{-}4)$$

where $\Delta m = \pm 1, \pm 2$.

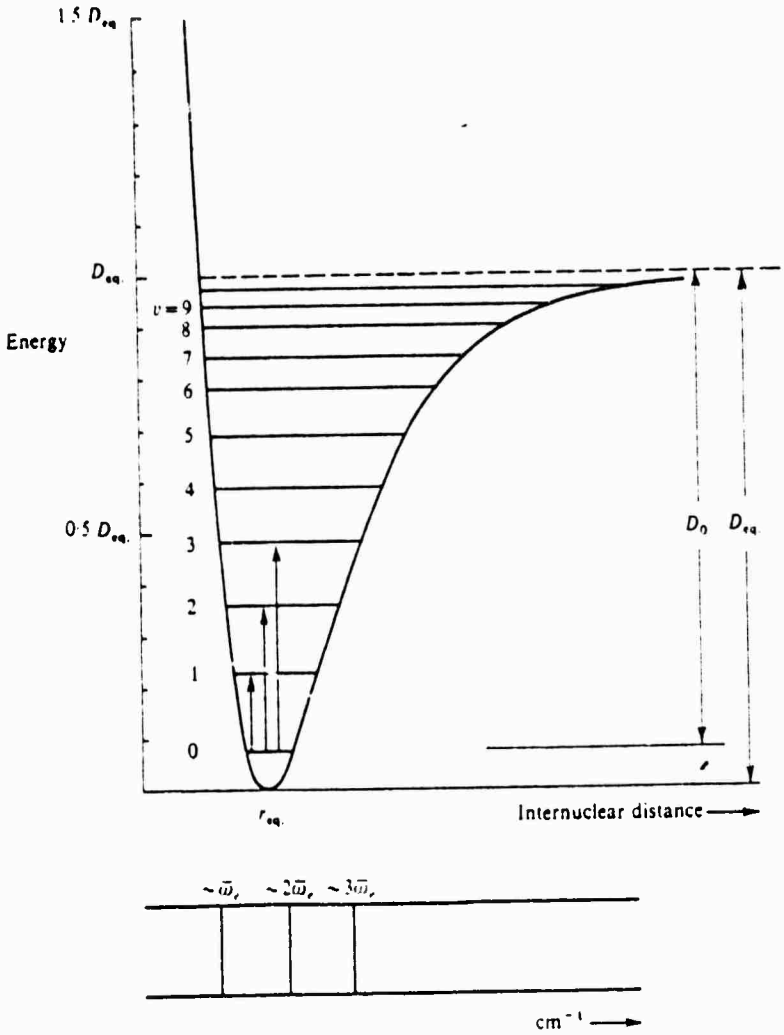

Figure 2-3. The Allowed Vibrational Energy Levels and Some Transitions Between Them for a Diatomic Molecule Undergoing Anharmonic Oscillations

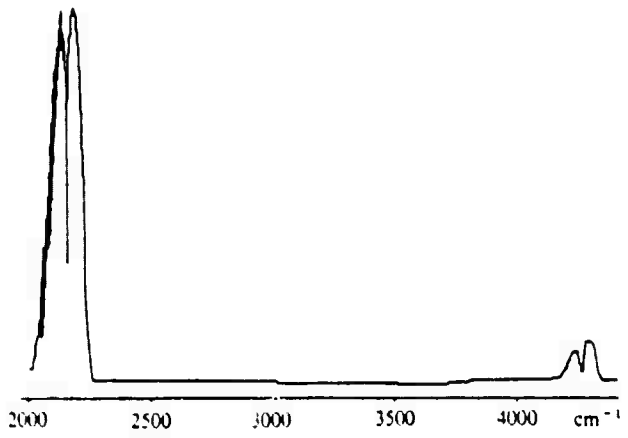

Figure 2-4. The Fundamental Absorption (Centered at about 2143 cm^{-1}) and the First Overtone (Centered at abqut 4260 cm^{-1}) of Carbon Monoxide; the Fine Structure of the P Branch in the Fundamental is Partially Resolved (Gas Pressure 650 mm Hg in a 10-cm Cell)

Positive values of the quantum number Δm account for frequencies in the R-band and negative values for the P-band (see Figures 2-5 and 2-6). Lines arising from $\Delta J = 0$ are called the Q-branch (see Figure 2-7). The maximum intensity in the rotational spectrum (characterized by J, see Equation 2-1) occurs at a vibrational-rotational frequency displaced from ν_0 by $\pm\Delta\nu$ where

$$\Delta\nu = \sqrt{8kT\ B/hc} + 2B. \qquad (2\text{-}5)$$

The quantities ν_0, ν_1, ν_2 and $\Delta\nu$ have been computed for several diatomic gases and diatomic subcomponents of molecules at $300^{\circ}K$ and are listed in Table 2-3, in units of cm^{-1}.

For polyatomic molecules there are many more vibrational frequencies characterizing each molecule, and the frequencies are less well measured so that the anharmonic correction x_e may not be known. Since it is a small correction, lack of its definition will not be too detrimental to remote assessment by measuring infrared frequencies. Measurement of two or more characteristic frequencies should allow the active molecule or a subgroup of the molecule to be determined.

Characteristic infrared frequencies for polyatomic gaseous molecules and their subgroups, as computed from Herzberg's tables [2-4], are listed in Table 2-4 in units of cm^{-1}. Characteristic frequencies for many kinds of subgroups and ligands in hydrocarbon molecules are listed in Table 2-5.

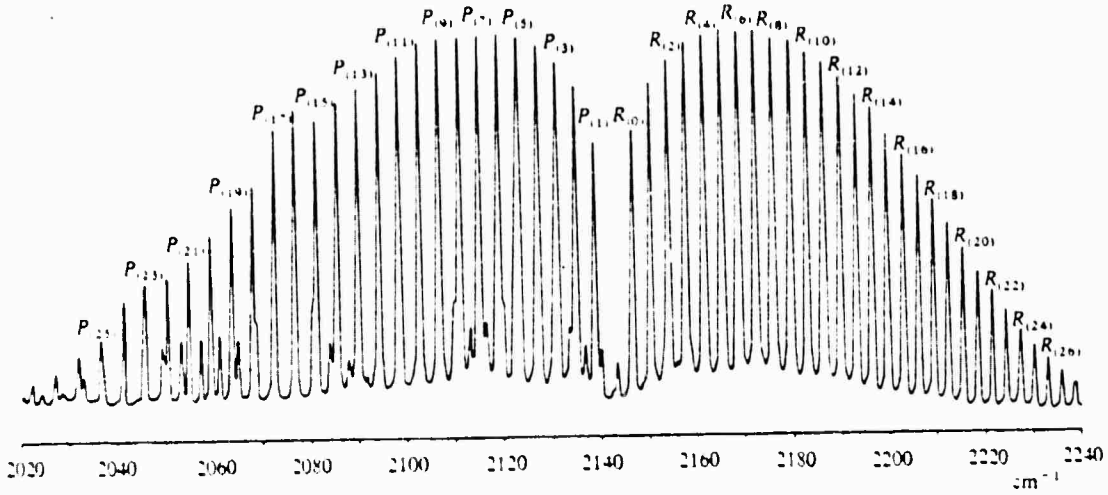

Figure 2-5. The Center of the Fundamental Band of Carbon Monoxide Under Higher Resolution than in Figure 2-4. (Gas Pressure 100 mm Hg in a 10-cm Cell.) The Lines are Labeled According to Their J Values. The P Branch is Complicated by the Presence of a "Hot Band" Centered at about 2100 cm^{-1}; Some of the Rotational Lines from this Band Appear between P Branch Lines, Others are Overlapped by a P Branch Line and Give it an Enhanced Intensity (e.g., lines $P_{(16)}$, $P_{(17)}$, $P_{(23)}$, and $P_{(24)}$)

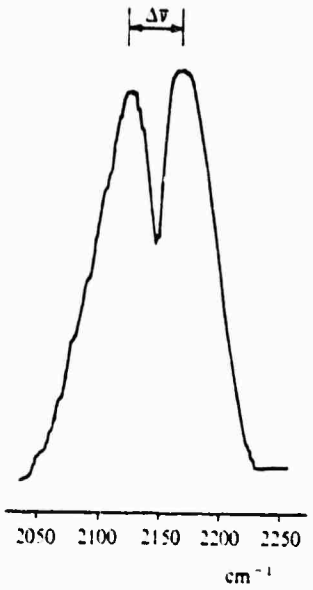

Figure 2-6. The Fundamental Band of Figure 2-5 under Very Low Resolution; All Rotational Fine Structure Has Been Lost, and a Typical PR Contour is Seen

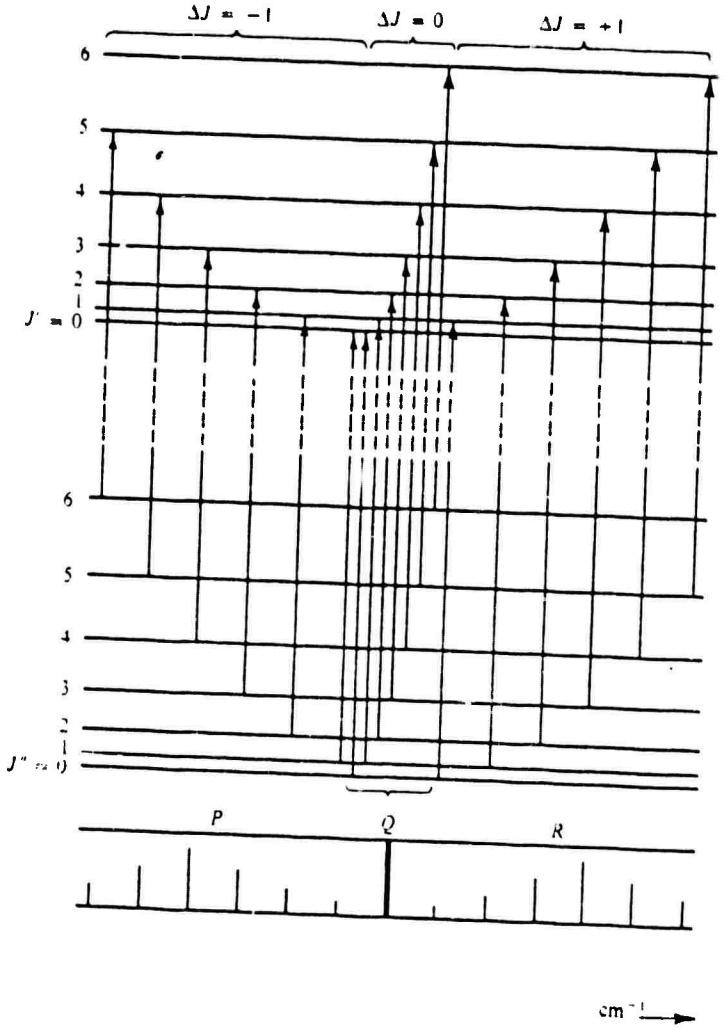

Figure 2-7a. The Rotational Energy Levels for Two Vibrational States Showing the Effect on the Spectrum of Transitions for Which $\Delta J = 0$.

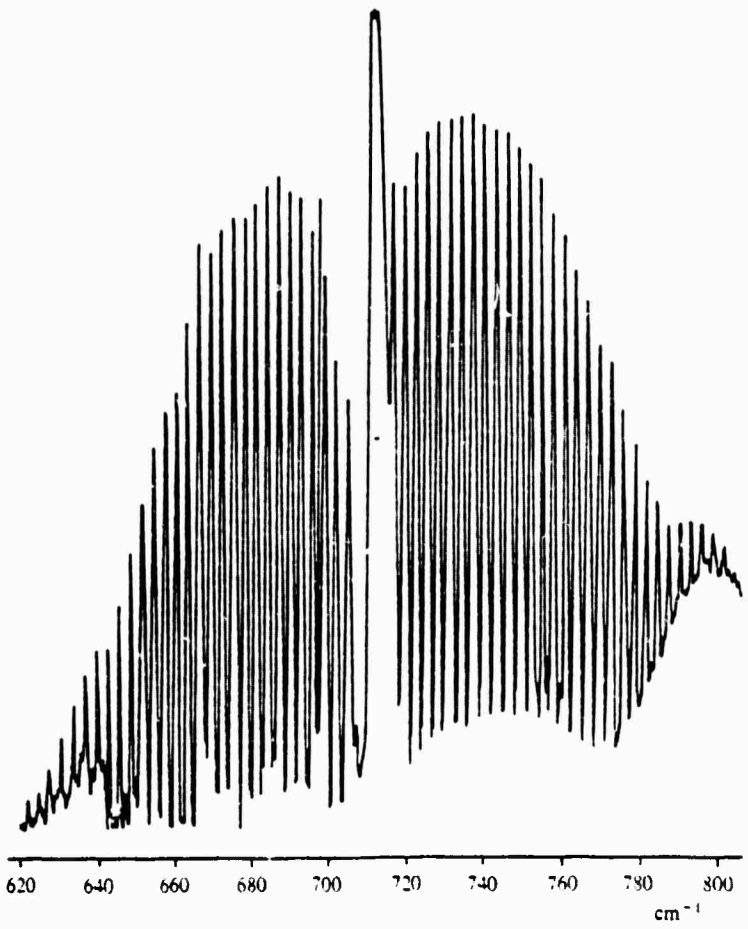

Figure 2-7b. Spectrum of the Bending Mode of the HCN Molecule Showing the PQR Structure. The Broad Absorption Centered at 800 cm^{-1} is Due to an Impurity

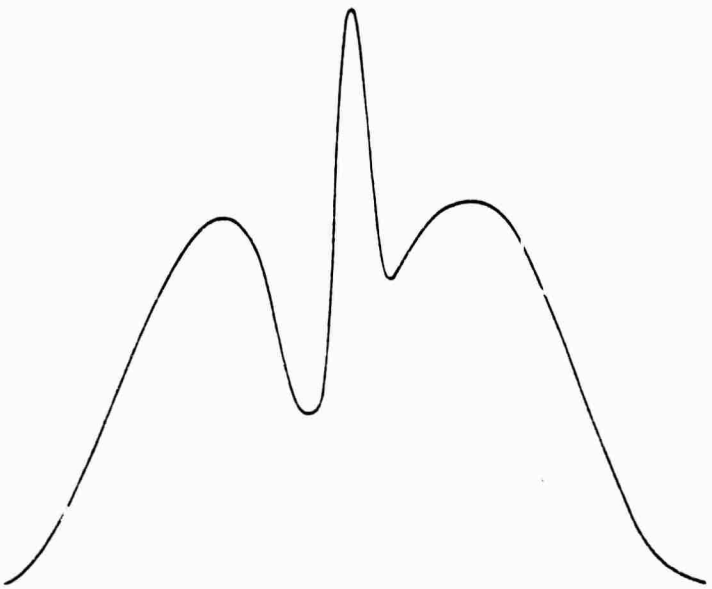

Figure 2-7c. The Contour of a PQR Band Under Low Resolution

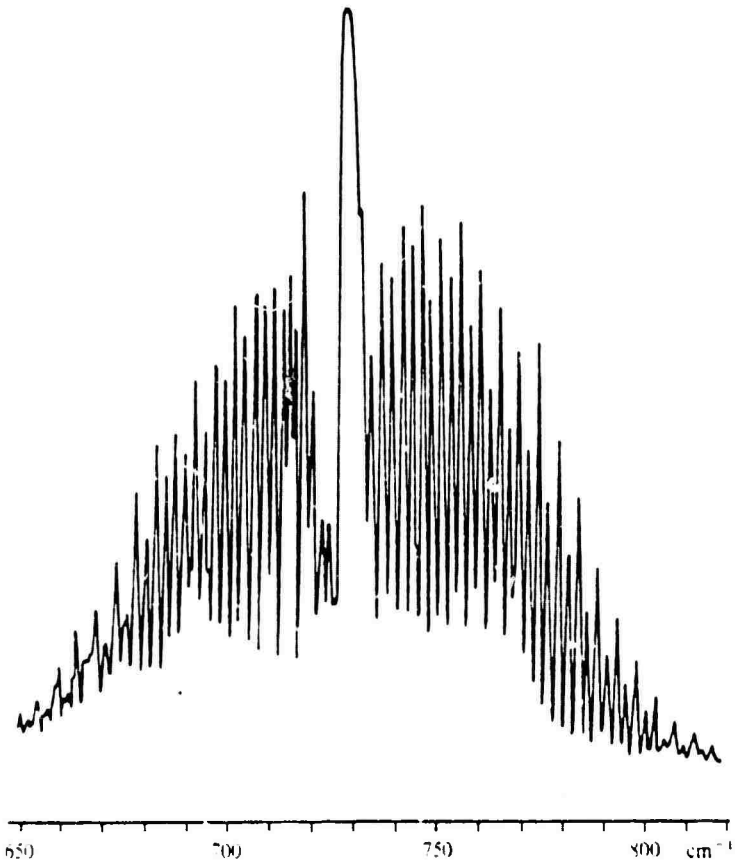

Figure 2-7d. The Spectrum of a Bending Mode of Acetylene, HC = CH, Showing the Strong, Weak, Strong, Weak, ... Intensity Alternation in the Rotational Fine Structure Due to the Nuclear Spin of the Hydrogen Atoms

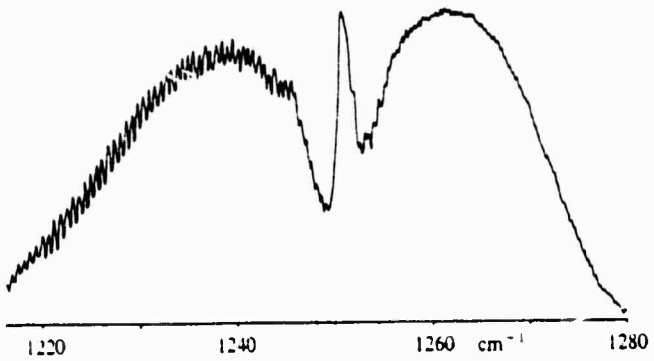

Figure 2-7e. The Parallel Stretching Vibration, Centered at 1251 cm^{-1}, of the Symmetric Top Molecule Methyl Iodide, CH_3I, Showing the Typical PQR Contour

Table 2-3. Vibrational Frequencies for Diatomic Molecules and Bandwidth $\Delta\nu$ in Units of cm^{-1}

	ω_e	x_e	ν_0 $\omega_e(1-2x_e)$	ν_1 $2\omega_e(1-3x_e)$	ν_2 $3\omega_e(1-4x_e)$	B	$\Delta\nu$
Cl_2	564.9	0.0071	557	1105	1647	0.2438	20.4
ClF	793.2	0.0125	773	1527	2261	0.5165	30
ClO	780		780	1560	2340		
F_2	892.1	0.0504	802	1514	2136		
I_2	214.57	0.0029	213	425	636	0.0374	7.8
IBr	268.4	0.0029	267	532	796		
ICl	384.28	0.0038	382	760	1135	0.1142	13.8
IO	687	0.0073	677	1344	2001		
N_2	2359.6	0.0061	2331	4633	6906	2.010	61
NH	3300		3300	6600	9900	16.65	197
NO	1904.0		1904	3808	5712	1.7046	55
NS	1220.0		1220	2440	3660		
O_2	1876.4	0.0088	1843.4	3654	5431	1.4456	51
OH	3735.2	0.0222	3569	6973	10211	18.871	212
PH	2380		2380	4760	7140	4.363	93
PN	1337.2	0.0052	1323	2633	3928	0.7862	37
PO	1230.6	0.0053	1218	2422	3614	0.7613	37
SiH	2080		2080	4160	12480	7.496	125
SiF	856.7	0.0055	847	1685	2514		
SiCl	535.4	0.0041	531	1058	1580		
SiF	856.7	0.0055	847	1685	2514		
SiN	1151.7	0.0057	1139	2265	3379	0.7310	36
SiO	1242.0	0.0049	1230	2447	3653	0.7263	36
SiS	749.5	0.0034	744	1484	2218	0.3036	23
SO	1123.7	0.0054	1112	2211	3298	0.7089	35

PAGE 1 OF 2

Table 2-3. Vibrational Frequencies for Diatomic Molecules and Bandwidth $\Delta\nu$ in Units of cm^{-1} (Cont.)

	ω_e	x_e	ν_0 $\omega_e(1-2x_e)$	ν_1 $2\omega_e(1-3x_e)$	ν_2 $3\omega_e(1-4x_e)$	B	$\Delta\nu$
HF	4138.5	0.0218	3958.1	7735.7	11332.9	20.939	226
HCl	2990.6	0.0174	2886	5668	8347	10.5909	152
HBr	2649.7	0.0171	2559.1	5027.5	7405.4	8.473	134
HI	2309.5	0.0172	2230.4	4381.8	6451.8	6.551	116
H_2	4395.2	0.0268				60.809	435
HS						9.47	143
CO	2169.7	0.0061	2143.2	4260.0	6350.3	1.9212	60
NO	1904.0	0.0073	1876.2	3724.6	5545.2	1.7046	56
ICl	384.2	0.0038	381.3	759.6	1135.1	0.1142	14
N_2	2360						
B_2	1051.3	0.0089	1032.6	2046.5	3041.6	1.212	47
BF	1265.6	0.0072	1247.4	2476.5	3687.5	1.518	53
BCl	839.1	0.0061	828.9	1647.5	2455.9	0.6838	35
BBr	684.3	0.0051	677.3	1347.7	2011.0	0.490	29
BH	2366	0.0207	2268	4438.1	6510.3	12.018	163
Br_2	233.2	0.0030	231.8	437.4	641.7	0.0809	12
BrCl	430	0.0067	424	843	1255		
BrF	671	0.0045	665	1315	1959	0.3572	25
BrO	713	0.0010	711	1422	2130		
CH	2861.6	0.0225	2732	5337	7812	14.457	182
CO	2170.2	0.0062	2143	4260	6349	1.9212	60
CN	2068.7	0 0064	2042	4058	6047	1.8996	59

Table 2-4. Infrared Vibrational Frequencies for Polyatomic Molecules

	ν_1 (cm^{-1})	ν_2 (cm^{-1})	ν_3 (cm^{-1})	ν_4 (cm^{-1})	ν_5 (cm^{-1})	ν_6 (cm^{-1})
NO_2	1320	750	1618			
N_2O	2224	1285	589			
CK_3CHO	2967	2840	3736	1793	1441	1390
HC_2CHO	3326	2858	2106	1696	1389	944
Trans C_2H_2Cl	3071	1576	1270	844	349	898
Cis	3086	1591	1179	711	173	876
C_2HCl	3096	1590	1250	850	633	452
C_4N_2	2267	2119	692	2241	1154	504
$C_2O_2Cl_2$	1778	1078	619	465	176	360
C_2U_4	1571	447	237		1000	347
CH_3NH_2	3361	2961	2820	1623	1473	1430
$H_2-C=C=CH_2$	3015	1443	1073	865	3007	1957
$CH_3-C\equiv CH$	3335	2941	2142	1382	931	3008
C_2H_4O	3005	1490	1266	1120	877	3063
SF_6	769	640	940	614	522	344
UF_6	667	535	626	189	200	144
B_2H_6	2524	2104	1180	794	829	1745
C_2H_6	2954	1388	945	278	2896	1379
C_2H_5I	2914	1197	951	500	262	
C_2H_3CHO	3102		3000	2800	1723	1625
H_2O	3652	1595	3756			
H_2S	2611	1290	2684			
H_2Se	2260	1074	2350			
SO_2	1151	524	1361			
NO_2	1320	648	1621			
F_2O	830	490	1110			
Cl_2O	680	330	973			

PAGE 1 OF 4

Table 2-4. Infrared Vibrational Frequencies for Polyatomic Molecules (Cont.)

	ν_1 (cm^{-1})	ν_2 (cm^{-1})	ν_3 (cm^{-1})	ν_4 (cm^{-1})		
NH_3	3337	950	3414	1628		
PH_3	2327	991	2421	1121		
PF_3	890	531	840	486		
PCl_3	510	257	480	190		
PBr_3	380	162	400	116		
AsF_3	707	341	644	274		
$AsCl_3$	410	193	370	159		
CH_4	2914	1526	3020	1306		
SiH_4	2187	978	2183	910		
CF_4	904	437	1265	630		
SiF_4	800	260	1022	420		
CCl_4	424	150	608	221		
CBr_4	267	123	672	183		
$SiBr_4$	249	90	487	137		
CO_2	1337	667	2349			
CS_2	657	397	1523			
HCN	2089	712	3312			
ClCN	729	397	2201			
BrCN	580	368	2187			
ICN	470	321	2158			
SCO	859	527	2079			
NNO	1285	589	2224			
BF_3	888	691	1446	480		
BCl_3	471	462	958	243		
BBr_3	279	372	806	151		
SO_3	1069	652	1330	532		

Table 2-4. Infrared Vibrational Frequencies for Polyatomic Molecules (Cont.)

	ν_1 (cm^{-1})	ν_2 (cm^{-1})	ν_3 (cm^{-1})	ν_4 (cm^{-1})	ν_5 (cm^{-1})	ν_6 (cm^{-1})
C_2H_2	3374	1974	3287	612	729	
C_2N_2	2322	842	2149	506	2226	
H_2CO	2766	1746	1501	1167	2843	
CH_3Cl	2968	1355	733	3044	1488	1017
CH_3Br	2972	1305	611	3056	1443	954
CH_3I	2953	1251	533	3060	1438	883
$H_2C=C=O$	3070	2152	1388	1118	588	528
$H_2C-N\equiv N$	3077	2102	1414	1170	564	406
H-C-OH=O	3570	2943	1770	1387	1229	1105
$N\equiv C-C\equiv CH$	3326	2271	2077	876	663	500
C_3O_2	2200	830	2258	1573	577	550
CF_3I	1073	286	1185	540	265	
$H_2C=CH_2$	3026	1622	1342	1027	3103	1236
CH_3SH	2869	2607	1335	704	3010	1475 1430
CH_3CN	2954	2268	1389	920	3009	1454
CH_3NO	2564	842	400			
C_2H_3Cl	3121	3086	3030	1608	1369	1279
C_4H_2	3329	2184	874	3329	2020	627
O_3	1110	705	1042			
$C_2N_4H_2$				737		
$CH_3C_2H_3$	3089	3013	2992	2933	2870	1652
$(CH_3)_2O$	2997	2821	1448	1242	1053	929
$(CH_3)_2S$	2911	2832	1445	1325	1041	685
C_4H_4O	3120	3090	1486	1381	1137	1067
C_4H_4S	3110	3080	1404	1358	1077	1032
C_4H_4Se	3096	3062	1428	1349	1019	923

Table 2-4. Infrared Vibrational Frequencies for Polyatomic Molecules (Cont.)

		ν_1 (cm^{-1})	ν_2 (cm^{-1})	ν_3 (cm^{-1})	ν_4 (cm^{-1})	ν_5 (cm^{-1})	ν_6 (cm^{-1})
	$C_3N_3H_3$	3042	1132	991			837
	$(C_2H_3)_2$	3101	3014	3014	1643	1442	1279
	$(CH_2)_3O$	2959	2930	1473	1461	1342	1134
	$(CH_3)_2CO$	2922	2871	1710	1356	1066	787
	C_4H_4NH	3400	3133	3100	1467	1384	1237
	$C_4H_4N_2$	3054	1570	1230	1015	596	950
1,3	$C_4H_4N_2$	3083	3048	3001	1570	1463	1146
1,2	$C_4H_4N_2$	3063	3043	1572	1414	1283	1160
	C_5H_6	3088	2973	2880	1496	1368	1105
	C_5H_5N	3054	3054	3036	1583	1482	1218
	$C_5H_4O_2$	3140	3120	1689	1666	1564	1466
	C_6H_6	3073	995	1350	674	3057	1010
	$CH_3-C\equiv C-C\equiv CH_3$	2914	2264	1381	1228	554	
	$(CH_3CO)_2$	3023	2940	1725	1444	1275	690
	HCN	3310 710		3310			~40 ~40
	$HC\equiv CH$	730		730			~30
	CH_3I	1251 840		1251			~15 ~60

MANY OTHERS MEASURED AND PARTIALLY EVALUATED [REF. 2-4].

Table 2-5. Vibrational Frequencies of Various Groups

Group	*Approximate Frequency* (cm^{-1})	*Group*	*Approximate Frequency* (cm^{-1})
—OH	3600	$\rangle C{=}O$	1750–1600
$-NH_2$	3400	$\rangle C{=}C\langle$	1650
$\equiv CH$	3300	$\rangle C{=}N\diagdown$	1600
	3060	$\rangle C-C\langle$ $\rangle C-N\langle$ $\rangle C-O\diagdown$	1200–1000
$=CH_2$	3030		
		$\rangle C{=}S$	1100
$-CH_3$	2970 (asym. stretch) 2870 (sym. stretch) 1460 (asym. deform.) 1375 (sym. deform.)	$\rangle C-F$	1050
		$\rangle C-Cl$	725
$-CH_2-$	2930 (asym. stretch) 2860 (sym. stretch) 1470 (deformation)	$\rangle C-Br$	650
		$\rangle C-I$	550
—SH	2580		
$-C{\equiv}N$	2250		
$-C{\equiv}C-$	2220		

Group	Bond-stretching vibration	Group	Bond-stretching vibration	Group	Bond-bending vibration
$\equiv C-H$	3300	$-C{\equiv}C-$	2050	$\equiv C-H$	700
$=C-H$	3020	$\diagdown C{=}C\diagup$	1650	$=C\begin{matrix}H\\H\end{matrix}$	1100
$-C-H$	2960	$\diagdown C-C\diagup$	900	$-C\begin{matrix}H\\H\\H\end{matrix}$	1000
—O—H	3680[47b]	$\diagdown C-F$	1100	$C\begin{matrix}H\\H\\H\end{matrix}$	1450
—S—H	2570	$\diagdown C-Cl$	650	$C\begin{matrix}H\\H\end{matrix}$	1450
—N—H	3350	$\diagdown C-Br$	560	$C-C{=}C$	300
$\diagdown C{=}O$	1700	$\diagdown C-I$	500		
$-C{\equiv}N$	2100				
	cm^{-1}		cm^{-1}		cm^{-1}

2.4 RAMAN - INFRARED

Rayleigh scattering is well known to be elastic scattering of an electromagnetic quantum by a vibrating electron. It can occur only if there is an asymmetrically arranged electron able to vibrate, that is only if the molecule containing the electron has an electric dipole moment. In contrast, Raman scattering is inelastic scattering of the photon and occurs because the electromagnetic field of the photon induces an electric dipole moment in addition to any dipole moment which may exist in the unperturbed molecule. Then if the frequency of the photon is ν_{ph} and the frequency of vibration (or rotation) of the unperturbed molecules is ν, the new frequency is $\nu_{ph} \pm \nu$, and photons are scattered with frequency changed from ν_{ph} to the Raman frequency $\nu_{ph} \pm \nu$. Thus, symmetric molecules such as N_2, O_2, and H_2 which normally cannot emit or absorb infrared radiation because of their lack of an intrinsic dipole moment, can scatter photons Raman shifted by a frequency which characterizes the molecule provided that the molecular rotation or vibration causes a periodic change in the induced dipole moment.

For rotational Raman spectra, the Raman-shifted wave numbers are given by

$$\nu = [\nu_{ph} \pm B(4J + 6)] \qquad (2\text{-}6)$$

corresponding to the selection rule $\Delta J = 2$, and of these, the most important are given by the minus sign because the lower rotational levels are the more populated at low temperatures (see Figure 2-8).

The fundamental frequency of the Raman-shifted vibrational spectrum is given by

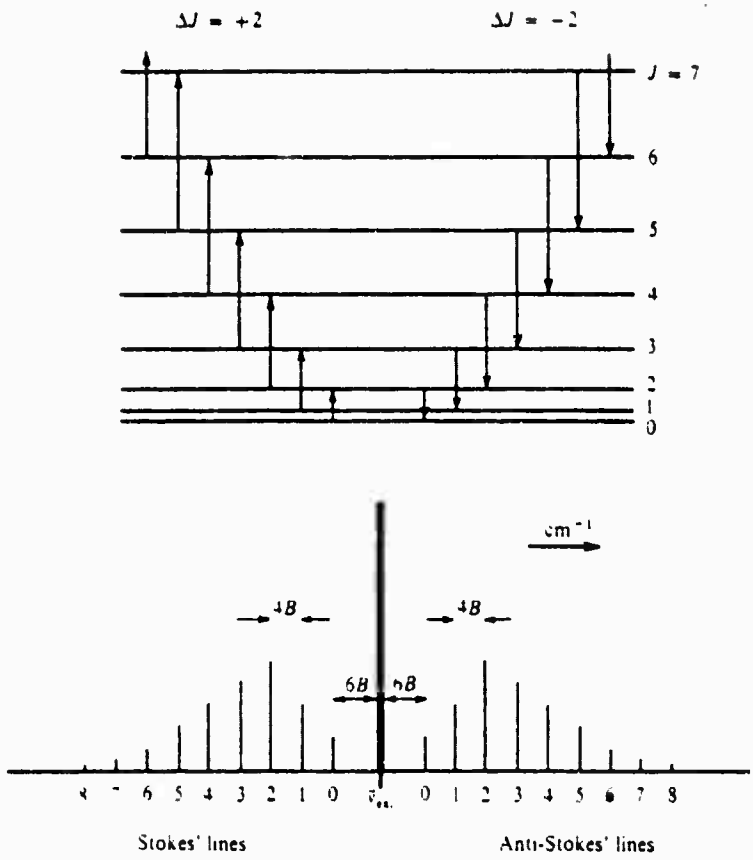

Figure 2-8. The Rotational Energy Levels of a Diatomic Molecule and the Rotational Raman Spectrum Arising from Transitions between Them. Spectral Lines are Numbered According to Their Lower J Values

$$(v = 0) \leftrightarrow (v = 1); \quad \nu_0 = \omega_e(1 - 2x_e) \qquad (2\text{-}7)$$

corresponding to $\Delta v = \pm 1$.

Since Raman-scattered light is of low intensity, the overtones ν_1, ν_2, etc., may be neglected.

An example of a Raman-shifted irradiation frequency ν_{ph} observed both for rotational and for rotational-vibrational modification is shown in Figure 2-9.

Raman-shifted light usually is polarized. This is because the induced electric dipole must be in a plane normal to the direction of the incident light no matter whether or not the incident light is polarized. Observation of the polarization characteristics of Raman-scattered light may help to characterize the molecule causing the scattering. Examples of polarizations observed in Raman spectra are shown in Table 2-6 and of the modes of vibration causing polarizations in Table 2-7. As an example, spectrograms of visible Hg lines Raman-shifted by CCl_4 and $CHCl_2Br$ are shown in Figure 2-10. Vibrational frequencies which have been observed in the Raman mode are shown in Table 2-8.

2.5 ELECTRONIC TRANSITIONS, $>10^4$ cm^{-1}, NEAR ULTRAVIOLET AND VISIBLE $\lambda < 10{,}000$ Å

Few gases absorb visible light, which is of course why there is a visible and near infrared "window" in the earth's atmosphere. Instead, electronic transitions in gases lie for the most part at wavelengths shorter than 3000 Å. Electronic wavelengths characterizing subgroups in hydrocarbons and some of their ligands are shown in Table 2-9.

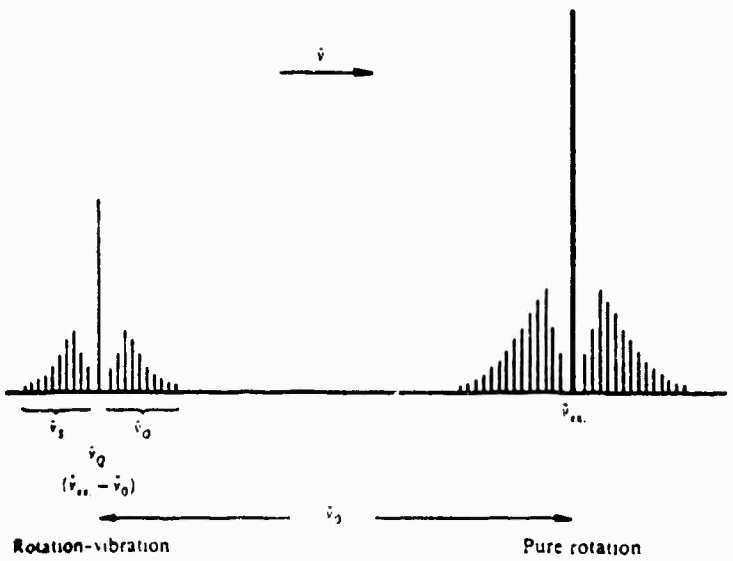

Figure 2-9. The Pure Rotation and the Rotation-Vibration Spectrum of a Diatomic Molecule Having a Fundamental Vibration Frequency of $\bar{\nu}_0$ cm^{-1}. Stokes' Lines Only are Shown

Table 2-6a. Infrared and Raman Bands of Sulphur Dioxide

WAVENUMBER	INFRARED CONTOURS	RAMAN
519	TYPE BAND	POLARIZED
1151	TYPE BAND	POLARIZED
1361	TYPE BAND	DEPOLARIZED

Table 2-6b. Infrared and Raman Spectra of Nitrous Oxide

$\bar{\nu}(cm^{-1})$	INFRARED	RAMAN
589	STRONG: PQR CONTOUR	-----
1285	VERY STRONG: PR CONTOUR	VERY STRONG:POLARIZED
2224	VERY STRONG: PR CONTOUR	STRONG: DEPOLARIZED

Table 2-7. Activities of Vibrations of Planar and Pyramidal AB_3 Molecules

Symmetric Planar	*Activity* (*R* = Raman, *I* = Infra-Red)	*Vibration*	*Pyramidal*	*Activity* (*R* = Raman, *I* = Infra-Red)
	*R*: active (pol.) strong *I*: inactive	ν_1 symmetric stretch	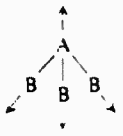	*R*: active (pol.) strong *I*: active ⊥
 (⊕ = upwards ⊖ = downwards)	*R*: inactive *I*: active ⊥	ν_2 out-of-plane symmetric deformation		*R*: active (pol.) strong *I*: active ⊥
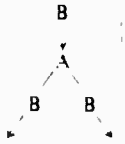	*R*: active (depol.) weak *I*: active ⊥	ν_3 asymmetric stretch	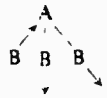	*R*: active (depol.) weak *I*: active ⊥
	*R*: active (depol.) weak *I*: active ⊥	ν_4 asymmetric deformation		*R*: active (depol.) weak *I*: active ⊥

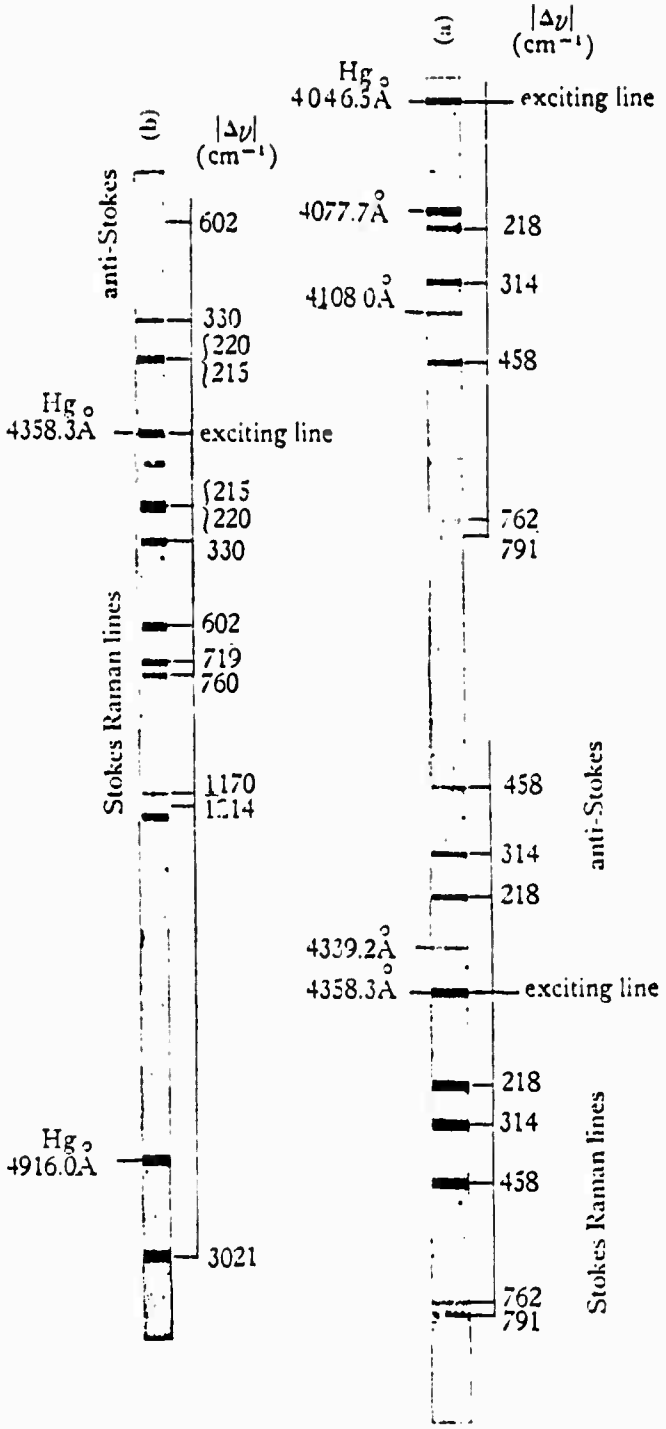

Figure 2-10. Raman Spectra of CCl_4 and $CHCl_2BR$ Showing Anti-Stokes Lines after Glocker. Raman Lines are Indicated at the Top of Each Spectrogram; Hg Lines at the Bottom. The Exciting Line Has Been Reduced in Intensity by a Screen. In (a) the Stokes Raman Lines of CCl_4 Occur Both Through Excitation by the Line 4358.3 Å and by the Line 4046.5 Å

Table 2-8. A Summary of Characteristic Raman Frequencies [2-5]

Frequency (cm^{-1})	Vibration	Compound
3,400–3,300	Bonded antisymmetric NH_2 stretch	Primary amines
3,380–3,340	Bonded OH stretch	Aliphatic alcohols
3,374	CH stretch	Acetylene (gas)
3,355–3,325	Bonded antisymmetric NH_2 stretch	Primary amides
3,350–3,300	Bonded NH stretch	Secondary amines
3,335–3,300	≡CH Stretch	Alkyl acetylenes
3,300–3,250	Bonded symmetric NH_2 stretch	Primary amines
3,310–3,290	Bonded NH stretch	Secondary amides
3,190–3,145	Bonded symmetric NH_2 stretch	Primary amides
3,175–3,154	Bonded NH stretch	Pyrazoles
3,103	Antisymmetric $=CH_2$ stretch	Ethylene (gas)
3,100–3,020	CH_2 Stretches	Cyclopropane
3,100–3,090	Aromatic CH stretch	Benzene derivatives
3,095–3,070	Antisymmetric $=CH_2$ stretch	$C=CH_2$ Derivatives
3,062	CH Stretch	Benzene
3,057	Aromatic CH stretch	Alkyl benzenes
3,040–3,000	CH Stretch	C=CHR Derivatives
3,026	Symmetric $=CH_2$ stretch	Ethylene (gas)
2,990–2,980	Symmetric $=CH_2$ stretch	$C=CH_2$ Derivatives
2,986–2,974	Symmetric NH_3^+ stretch	Alkyl ammonium chlorides (aq. soln)
2,969–2,965	Antisymmetric CH_3 stretch	*n*-Alkanes
2,929–2,912	Antisymmetric CH_2 stretch	*n*-Alkanes
2,884–2,883	Symmetric CH_3 stretch	*n*-Alkanes
2,861–2,849	Symmetric CH_2 stretch	*n*-Alkanes
2,850–2,700	CHO Group (2 bands)	Aliphatic aldehydes
2,590–2,560	SH Stretch	Thiols
2,316–2,233	C≡C Stretch (2 bands)	$R\text{-}C{\equiv}C\text{-}CH_3$
2,301–2,231	C≡C Stretch (2 bands)	$R\text{-}C{\equiv}C\text{-}R'$
2,300–2,250	Pseudoantisymmetric N=C=O stretch	Isocyanates
2,264–2,251	Symmetric C≡C-C≡C stretch	Alkyl diacetylenes
2,259	C≡N Stretch	Cyanamide
2,251–2,232	C≡N Stretch	Aliphatic nitriles
2,220–2,100	Pseudoantisymmetric N=C=S stretch (2 bands)	Alkyl isothiocyanates
2,220–2,000	C≡N Stretch	Dialkyl cyanamides
2,172	Symmetric C≡C-C≡C stretch	Diacetylene
2,161–2,134	N≡C Stretch	Aliphatic isonitriles
2,160–2,100	C≡C Stretch	Alkyl acetylenes
2,156–2,140	C≡N Stretch	Alkyl thiocyanates
2,104	Antisymmetric N=N=N stretch	CH_3N_3
2,094	C≡N Stretch	HCN
2,049	Pseudoantisymmetric C=C=O stretch	Ketene
1,974	C≡C Stretch	Acetylene (gas)
1,964–1,958	Antisymmetric C=C=C stretch	Allenes
1,870–1,840	Symmetric C=O stretch	Saturated 5-membered ring cyclic anhydrides

Table 2-8. A Summary of Characteristic Raman Frequencies (Cont.)

Frequency (cm^{-1})	Vibration	Compound
1,820	Symmetric C=O stretch	Acetic anhydride
1,810–1,788	C=O Stretch	Acid halides
1,807	C=O Stretch	Phosgene
1,805–1,799	Symmetric C=O stretch	Noncyclic anhydrides
1,800	C=C Stretch	$F_2C=CF_2$ (gas)
1,795	C=O Stretch	Ethylene carbonate
1,792	C=C Stretch	$F_2C=CFCH_3$
1,782	C=O Stretch	Cyclobutanone
1,770–1,730	C=O Stretch	Halogenated aldehydes
1,744	C=O Stretch	Cyclopentanone
1,743–1,729	C=O Stretch	Cationic α-amino acids (aq. soln)
1,741–1,734	C=O Stretch	*O*-Alkyl acetates
1,740–1,720	C=O Stretch	Aliphatic aldehydes
1,739–1,714	C=C Stretch	$C=CF_2$ Derivatives
1,736	C=C Stretch	Methylene cyclopropane
1,734–1,727	C=O Stretch	*O*-Alkyl propionates
1,725–1,700	C=O Stretch	Aliphatic ketones
1,720–1,715	C=O Stretch	*O*-Alkyl formates
1,712–1,694	C=C Stretch	RCF=CFR
1,695	Nonconjugated C=O stretch	Uracil derivatives (aq. soln)
1,689–1,644	C=C Stretch	Monofluoroalkenes
1,687–1,651	C=C Stretch	Alkylidene cyclopentanes
1,686–1,636	Amide I band	Primary amides (solids)
1,680–1,665	C=C Stretch	Tetralkyl ethylenes
1,679	C=C Stretch	Methylene cyclobutane
1,678–1,664	C=C Stretch	Trialkyl ethylenes
1,676–1,665	C=C Stretch	*trans*-Dialkyl ethylenes
1,675	Symmetric C=O stretch (cyclic dimer)	Acetic acid
1,673–1,666	C=N Stretch	Aldimines
1,672	Symmetric C=O stretch (cyclic dimer)	Formic acid (aq. soln)
1,670–1,655	Conjugated C=O stretch	Uracil, cytosine, and guanine derivatives (aq. soln)
1,670–1,630	Amide I band	Tertiary amides
1,666–1,652	C=N Stretch	Ketoximes
1,665–1,650	C=N Stretch	Semicarbazones (solid)
1,663–1,636	Symmetric C=N stretch	Aldazines, ketazines
1,660–1,654	C=C Stretch	*cis*-Dialkyl ethylenes
1,660–1,650	Amide I band	Secondary amides
1,660–1,649	C=N Stretch	Aldoximes
1,660–1,610	C=N Stretch	Hydrazones (solid)
1,658–1,644	C=C Stretch	$R_2C=CH_2$
1,656	C=C Stretch	Cyclohexene, cycloheptene
1,654–1,649	Symmetric C=O stretch (cyclic dimer)	Carboxylic acids
1,652–1,642	C=N Stretch	Thiosemicarbazones (solid)

Table 2-8. A Summary of Characteristic Raman Frequencies (Cont.)

Frequency (cm^{-1})	Vibration	Compound
1,650–1,590	NH_2 Scissors	Primary amines (weak)
1,649–1,625	C=C Stretch	Allyl derivatives
1,648–1,640	N=O Stretch	Alkyl nitrites
1,648–1,638	C=C Stretch	H_2C=CHR
1,647	C=C Stretch	Cyclopropene
1,638	C=O Stretch	Ethylene dithiocarbonate
1,637	Symmetric C=C stretch	Isoprene
1,634–1,622	Antisymmetric NO_2 stretch	Alkyl nitrates
1,630–1,550	Ring stretches (doublet)	Benzene derivatives
1,623	C=C Stretch	Ethylene (gas)
1,620–1,540	Three or more coupled C=C stretches	Polyenes
1,616–1,571	C=C Stretch	Chloroalkenes
1,614	C=C Stretch	Cyclopentene
1,596–1,547	C=C Stretch	Bromoalkenes
1,581–1,465	C=C Stretch	Iodoalkenes
1,575	Symmetric C=C stretch	1,3-Cyclohexadiene
1,573	N=N Stretch	Azomethane (in soln)
1,566	C=C Stretch	Cyclobutene
1,560–1,550	Antisymmetric NO_2 stretch	Primary nitroalkanes
1,555–1,550	Antisymmetric NO_2 stretch	Secondary nitroalkanes
1,548	N=N Stretch	1-Pyrazoline
1,545–1,535	Antisymmetric NO_2 stretch	Tertiary nitroalkanes
1,515–1,490	Ring stretch	2-Furfuryl group
1,500	Symmetric C=C stretch	Cyclopentadiene
1,480–1,470	OCH_3, OCH_2 Deformations	Aliphatic ethers
1,480–1,460	Ring stretch	2-Furfurylidene or 2-furoyl group
1,473–1,446	CH_3,CH_2 Deformations	*n*-Alkanes
1,466–1,465	CH_2 Deformation	*n*-Alkanes
1,450–1,400	Pseudoantisymmetric N=C=O stretch	Isocyanates
1,443–1,393	Ring stretch	2-Substituted thiophenes
1,442	N=N Stretch	Azobenzene
1,440–1,340	Symmetric CO_2^- stretch	Carboxylate ions (aq. soln)
1,415–1,400	Symmetric CO_2^- stretch	Dipolar and anionic α-amino acids (aq. soln)
1,415–1,385	Ring stretch	Anthracenes
1,395–1,380	Symmetric NO_2 stretch	Primary nitroalkanes
1,390–1,370	Ring stretch	Naphthalenes
1,385–1,368	CH_3 Symmetric deformation	*n*-Alkanes
1,375–1,360	Symmetric NO_2 stretch	Secondary nitroalkanes
1,355–1,345	Symmetric NO_2 stretch	Tertiary nitroalkanes
1,350–1,330	CH Deformation	Isopropyl group
1,320	Ring vibration	1,1-Dialkyl cyclopropanes
1,314–1,290	In-plane CH deformation	*trans*-Dialkyl ethylenes
1,310–1,250	Amide III band	Secondary amides
1,310–1,175	CH_2 Twist and rock	*n*-Alkanes

Table 2-8. A Summary of Characteristic Raman Frequencies (Cont.)

Frequency (cm^{-1})	Vibration	Compound
1,305–1,295	CH_2 In-phase twist	*n*-Alkanes
1,300–1,280	CC Bridge bond stretch	Biphenyls
1,282–1,275	Symmetric NO_2 stretch	Alkyl nitrates
1,280–1,240	Ring stretch	Epoxy derivatives
1,276	Symmetric N=N=N stretch	CH_3N_3
1,270–1,251	In-plane CH deformation	*cis*-Dialkyl ethylenes
1,266	Ring "breathing"	Ethylene oxide (oxirane)
1,230–1,200	Ring vibration	*para*-Disubstituted benzenes
1,220–1,200	Ring vibration	Mono- and 1,2-dialkyl cyclopropanes
1,212	Ring "breathing"	Ethylene imine (aziridine)
1,205	C_6H_5-C Vibration	Alkyl benzenes
1,196–1,188	Symmetric SO_2 stretch	Alkyl sulfates
1,188	Ring "breathing"	Cyclopropane
1,172–1,165	Symmetric SO_2 stretch	Alkyl sulfonates
1,150–950	CC Stretches	*n*-Alkanes
1,145–1,125	Symmetric SO_2 stretch	Dialkyl sulfones
1,144	Ring "breathing"	Pyrrole
1,140	Ring "breathing"	Furan
1,130–1,100	Symmetric C=C=C stretch (2 bands)	Allenes
1,130	Pseudosymmetric C=C=O stretch	Ketene
1,112	Ring "breathing"	Ethylene sulfide
1,111	NN Stretch	Hydrazine
1,070–1,040	S=O Stretch (1 or 2 bands)	Aliphatic sulfoxides
1,065	C=S Stretch	Ethylene trithiocarbonate
1,060–1,020	Ring vibration	*ortho*-Disubstituted benzenes
1,040–990	Ring vibration	Pyrazoles
1,030–1,015	In-plane CH deformation	Monosubstituted benzenes
1,030–1,010	Trigonal ring "breathing"	3-Substituted pyridines
1,030	Trigonal ring "breathing"	Pyridine
1,029	Ring "breathing"	Trimethylene oxide (oxetane)
1,026	Ring "breathing"	Trimethylene imine (azetidine)
1,010–990	Trigonal ring "breathing"	Mono-, meta-, and 1,3,5-substituted benzenes
1,001	Ring "breathing"	Cyclobutane
1,000–985	Trigonal ring "breathing"	2- and 4-Substituted pyridines
992	Ring "breathing"	Benzene
992	Ring "breathing"	Pyridine
939	Ring "breathing"	1,3-Dioxolane
933	Ring vibration	Alkyl cyclobutanes
930–830	Symmetric COC stretch	Aliphatic ethers
914	Ring "breathing"	Tetrahydrofuran

Table 2-8. A Summary of Characteristic Raman Frequencies (Cont.)

Frequency (cm^{-1})	Vibration	Compound
906	Symmetric CON stretch	Hydroxylamine
905–837	CC Skeletal stretch	*n*-Alkanes
900–890	Ring vibration	Alkyl cyclopentanes
900–850	Symmetric CNC stretch	Secondary amines
899	Ring "breathing"	Pyrrolidine
886	Ring "breathing"	Cyclopentane
877	OO Stretch	Hydrogen peroxide
851–840	Symmetric CON stretch	*O*-Alkyl hydroxylamines
836	Ring "breathing"	Piperazine
835–749	C_4 Skeletal stretch	Isopropyl group
834	Ring "breathing"	1,4-Dioxane
832	Ring "breathing"	Thiophene
832	Ring "breathing"	Morpholine
830–720	Ring vibration	*para*-Disubstituted benzenes
825–820	C_2O Symmetric skeletal stretch	Secondary alcohols
818	Ring "breathing"	Tetrahydropyran
815	Ring "breathing"	Piperidine
802	Ring "breathing"	Cyclohexane (chair form)
785–700	Ring vibration	Alkyl cyclohexanes
760–730	C_4O Symmetric skeletal stretch	Tertiary alcohols
750–650	C_3 Symmetric skeletal stretch	*tert*-Butyl group
740–585	CS Stretch (1 or more bands)	Alkyl sulfides
735–690	"C=S Stretch"	Thioamides, thioureas (solids)
733	Ring "breathing"	Cycloheptane
730–720	CCl Stretch, P_C conformation	Primary chloroalkanes
715–620	CS Stretch (1 or more bands)	Dialkyl disulfides
709	CCl Stretch	CH_3Cl
703	Ring "breathing"	Cyclooctane
703	Symmetric CCl_3 stretch	CH_2Cl_2
690–650	Pseudosymmetric N=C=S stretch	Alkyl isothiocyanates
688	Ring "breathing"	Tetrahydrothiophene
668	Symmetric CCl_3 stretch	$CHCl_3$
660–650	CCl Stretch, P_H conformation	Primary chloroalkanes
659	Symmetric CSC stretch	Pentamethylene sulfide
655–640	CBr Stretch, P_C conformation	Primary bromoalkanes
630–615	Ring deformation	Monosubstituted benzenes
615–605	CCl Stretch, S_{HH} conformation	Secondary chloroalkanes
610–590	CI Stretch, P_C conformation	Primary iodoalkanes
609	CBr Stretch	CH_3Br
577	Symmetric CBr_2 stretch	CH_2Br_2
570–560	CCl Stretch, T_{HHH} conformation	Tertiary chloroalkanes
565–560	CBr Stretch, P_H conformation	Primary bromoalkanes
540–535	CBr Stretch, S_{HH} conformation	Secondary bromoalkanes
539	Symmetric CBr_3 stretch	$CHBr_3$
525–510	SS Stretch	Dialkyl disulfides

Table 2-8. A Summary of Characteristic Raman Frequencies (Cont.)

Frequency (cm^{-1})	Vibration	Compound
523	CI Stretch	CH_2I
520–510	CBr Stretch, T_{HHH} conformation	Tertiary bromoalkanes
510–500	CI Stretch, P_H conformation	Primary iodoalkanes
510–480	SS Stretch	Dialkyl trisulfides
495–485	CI Stretch, S_{HH} conformation	Secondary iodoalkanes
495–485	CI Stretch, T_{HHH} conformation	Tertiary iodoalkanes
484–475	Skeletal deformation	Dialkyl diacetylenes
483	Symmetric CI_2 stretch	CH_2I_2
459	Symmetric CCl_4 stretch	CCl_4
437	Symmetric CI_3 stretch	CHI_3 (in soln)
425–150	"Chain expansion"	*n*-Alkanes
355–335	Skeletal deformation	Monoalkyl acetylenes
267	Symmetric CBr_4 stretch	CBr_4 (in soln)
200–160	Skeletal deformation	Aliphatic nitriles
178	Symmetric CI_4 stretch	CI_4 (solid)

Table 2-9. Characteristic Frequencies for Visible and Ultraviolet Electronic Transitions of Various Groups of Atoms Bound in Hydrocarbon Molecules

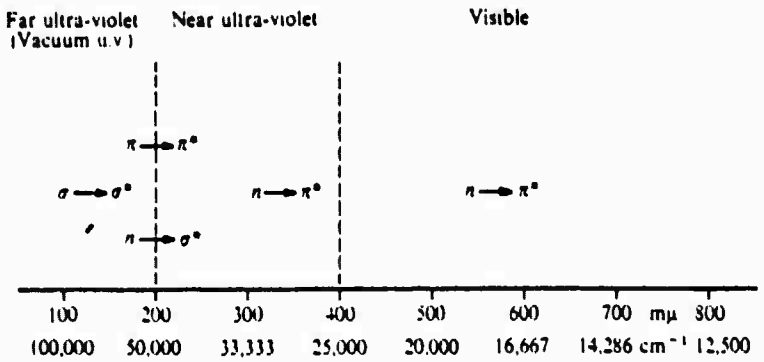

The regions of the electronic spectrum and the type of transition which occurs in each.

	$\lambda_{max.}$ (mμ)	ε
−C=C−	170	16,000
−C=C−C=C−	220	21,000
−C=C−C=C−C=C−	260	35,000

while for oxygen-containing molecules we have both $\pi \rightarrow \pi^*$ and $n \rightarrow \pi^*$ transitions:

	$\pi \rightarrow \pi^*$ (*strong*) (mμ)	$n \rightarrow \pi^*$ (*weak*) (mμ)
−C=O	166	280
−C=C−C=O	240	320
−C=C−C=C−C=O	270	350
	245	435

	$\pi \rightarrow \pi^*$ (*strong*) (mμ)	$n \rightarrow \pi^*$ (*weak*) (mμ)
>C=C<	170	—
−C≡C−	170	—
>C=O	166	280
>C=N−	190	300
−N=N−	?	350
>C=S	?	500

Some gases having electronic transitions in the visible or near ultraviolet, namely, at wavelengths longer than 3000 Å, are listed in Table 2-10. Because of the cutoff absorption by atmospheric ozone at wavelengths shorter than 3000 Å, transitions at shorter wavelengths are not useful for remote assessment of trace atmospheric gases.

Table 2-10. Some Vapors and Gases Having Electronic Transitions in the Visible and Near Ultraviolet

CHEMICAL FORMULA	WAVE LENGTH (Å)	
NO_2	3000-6000	NITROGEN DIOXIDE
N_2O	2800-3065	NITROUS OXIDE
CH_3CHO	2500-3500	ACETALDEHYDE
CH_2CHO	3900-4200	PROPYNAL
$C_2O_2Cl_2$	300-3800	OXALYLCHLORIDE
UF_6	3300-4100	URANIUM HEXAFLUORIDE
C_4H_4S	3130-3180	THIOPHENE
C_2H_3CHO	300-3940; 4025-4122	ACROLEIN
$C_2N_4H_2$	4700-5600	S-TETRAZINE
SO_2	3400-3900	SULFUR DIOXIDE
$C_3N_3H_3$	2700-3170; 3800-5000	S-TRIAZENE
$(CH_3)_2CO$	2200-3300	ACETONE
CS_2	3900-4300	CARBON DISULFIDE
$1,4C_4H_4N_2$	2900-3300; 3560-3760	PYRAZINE
H_2CO	2300-3530; 3600-3967	FORMALDEHYDE
CH_3I	2000-3600	METHYL IODIDE
$H_2C=C=O$	2600-3850	KETENE
$CH_2-N\equiv N$	3200-4750	ARAZOMETHANE
C_3O_2	2400-3300	CARBON SUBOXIDE
$H_2-C=CH_2$	2600-3400	ETHYLENE
CH_3NO	5900-7100	NITROSOMETHANE
$H_2C_2O_2$	2300-3200; 3900-5400; 5150-5750	GLYOXAL
O_3	3000-3740; 5500-6100	OZONE
BH	4328	
Br_2	5110 AND AN ABSORPTION CONTINUUM AT SHORTER WAVE LENGTHS	
BrCl	VISIBLE ABSORPTION BANDS REPORTED IN HERZBERG BUT NOT PUBLISHED	

Table 2-10. Some Vapors and Gases Having Electronic Transitions in the Visible and Near Ultraviolet (Cont.)

CHEMICAL FORMULA	WAVE LENGTH (Å)	
PrF	5172	
Br_2O	3330,4011	
Cl_2	4796 AND AN ABSORPTION CONTINUUM AT SHORTER WAVELENGTHS	
ClF	5275	
F_2	CONTINUOUS ABSORPTION WITH MAXIMUM AT 2899	
HI	CONTINUOUS ABSORPTION STARTING AT 3636 WITH MAXIMUM AT 2083	
IBr	5924	
I_2	6393	
ICl	5508	
SiH_2	5000-6000	
HCP	3050-4100	
SO_2	3400-3900; 2600-3400	
ClO_2	2700-5100	
CH_3I	2000-3600	

REFERENCES TO SECTION 2

2-1. J. D. Barry, P. J. Coleman, W. F. Libby and L. M. Libby, "Radio Reflection by Free Radicals in the Earth's Atmosphere," Science, 156, 1967, pp. 1730-1732. The discussion of limits on detectable pollutant concentrations given in the text (pp. 3-1 to 3-3) is descriptive of the actual satellite experiments. In engineering such an experiment for satellite detection of pollutants at the earth's surface, the solid angle from which signals would come would be considerably less.

2-2. L. M. Libby and W. F. Libby, "Comparison of Magnetospheres and Radio Emissions of Jupiter with Earth," Proceedings of the 14th International Cosmic Ray Conference, Munich, August 1975.

2-3. C. N. Banwell, Fundamentals of Modern Spectroscopy, McGraw-Hill, 1966.

2-4. G. Herzberg, Infrared and Raman Spectra, Van Nostrand-Reinhold Co., 1945; also Spectra of Diatomic Molecules, Van Nostrand-Reinhold Co., 1950; also Electronic Spectra of Polyatomic Molecules, Van Nostrand-Reinhold Co., 1966.

2-5. J. W. Robinson, ed., Handbook of Spectroscopy, Vol. II, CRC Press, Cleveland, Ohio, 1974, pp. 119-124.

SECTION 3. METHODS OF ASSESSMENT BY PASSIVE METHODS: SUCCESSFUL EXPERIMENTS

3.1 EXCITATION BY DECAMETRIC RADIATION FROM GROUND-BASED AND SATELLITE TRANSMITTERS FOLLOWED BY EMISSION AND DETECTION OF MAGNETIC SPIN FLIP RADIATION

Consider first the operation of the Alouette satellites, as top-side ionosonders. The experimental observations discussed in this section were actually excited by active irradiation from a source in the satellite. We discuss this experiment here to illustrate the sensitivity of assessment. We suggest in this section that these emissions may be excited by existing ground sources of several megacycle frequencies and so assessed by passive means. The transmitter and receiver simultaneously sweep from 0.2 to 14.5 Mc/sec during each 30-sec interval. At the beginning of each interval, the transmitter emits a 100-μsec pulse at a frequency of 0.2 Mc/sec and an average power of 300 watts. After a 2 μsec delay there follows a receiving period of 33 msec, then the transmitter emits a second pulse of higher frequency, followed by another listening period, and so on. For each 30-sec interval an ionogram displays the frequency ν of any detected signal, its time of arrival, its intensity, and the real time. When the frequency of the transmitter equals the resonant magnetic dipole frequency of a given species of free radicals in the atmosphere, the radicals are induced to radiate photons of the resonant frequency, some portion of which arrives at the satellite receiver and is recorded. From the time of arrival at the receiver after emission of the stimulating frequency from the transmitter, the distance between the satellite and the free radical can be computed. The resonant frequency ν is given by

$$\nu = \frac{g\mu B}{h}, \quad \mu = \frac{eh}{2\ Mc} \approx 10^{-20} \text{ erg/gauss}$$

where g is the Lande' factor characterizing the radical, determined by spin-orbit coupling, B is the local magnetic field of the earth, and μ is the electron magnetic moment. The B field at the satellite as a function of its geographical coordinates may be computed from a polynomial expansion of the geomagnetic field.

With $\mu \approx 10^{-20}$ erg/gauss, approximately equal concentrations of a particular species have dipoles parallel and antiparallel to the local magnetic field at $\approx 300^{\circ}$K. For radicals resonant with the Alouette signal, the probability of reflection in terms of the Einstein coefficient for stimulated emission is given by [2-1]

$$W = [2\pi(\mu^2/3)/h^2c](dI/d\nu) = 2 \times 10^4 (dI/d\nu) \ sec^{-1}$$

where $(dI/d\nu)$ is the energy flux from the sounder-transmitter per unit frequency interval. The average radiated power of the Alouette transmitters, 300 watts, is spread over a bandwidth of about 30 kcs. If one neglects absorption between the satellite and a point at distance R, the energy flux at R is

$$dI/d\nu = 10^5/4\pi R^2 [erg/cm^2 sec(cy/sec)].$$

We neglect the angular dependence and assume that the power P reflected by a population of N magnetic dipoles per cubic centimeter, given by

$$P(R) = W(N/2)h\nu = 2 \cdot 10^9 (N/2)h\nu/4\pi R^2 (erg/cm^3 sec)$$

is radiated isotropically. The intensity of the signal arriving at the satellite at time t, measured from the time at which the 100 μsec pulse begins, is given by

$$S(t) = \int_{R_1}^{R_2} [P(R)/4\pi R^2]dV(erg/cm^2sec)$$

where the integral is taken over the volume, V, of origin of reflected radiation reaching the satellite at time t. The volume is a spherical shell centered at the satellite. For a pulse of 100 msec, the inner surface of the shell has radius $R_1 = c(t - 10^{-4})/2$, and the outer surface has radius $R_2 = ct/2$ where t is measured in seconds and c is the velocity of light.

Using $\nu \approx 10^6$ sec^{-1}, it follows that

$$S(t) = 3 \times 10^{-13} N \int_{R_1}^{R_2} dR/R^2.$$

Furthermore, the signal must be at least 10^{-4} seconds long so that

$$\int_{R_1}^{R_2} dR/R^2 = 6 \times 10^{-7}.$$

If the signal is to be detected at the satellite, S(t) must be greater than the threshold of the receiver, that is $S(t) > 3 \times 10^{-15}$ erg/cm^{2}sec. Then

$$(3 \times 10^{-13})(6 \times 10^{-7}) \quad N > 3 \times 10^{-15}/cm^3$$
$$N > 2 \times 10^{+4}/cm^3$$

is the minimum concentration for a detectable signal at $R = 3 \times 10^6$cm (20 miles). At a distance of 100 miles the minimum concentration is $N > 5 \times 10^5/cm^3$, corresponding to $N > 10^{-5}$ ppb of air.

The top-side ionosonder Alouette satellites have been in orbit since 1965, and there have been no protests against their transmissions. They are in polar orbits so that they orbit over all the countries of the world, including Antarctica.

However, there is an alternative way of stimulating the magnetic spin flip emissions, namely, by electromagnetic irradiation from ground-based transmitters such as ham radios, television stations, ship to shore transmitters, navigational beacons, civilian aviation radio and radar, ground to satellite communications, microwave relay, and the like. Any frequency at shorter wavelength ship stimulate spin flip emission $\nu - \nu_o$ in the Raman mode. That is, the photon of frequency ν is scattered inelastically by the magnetic dipole to a frequency lower by ν_o so that the scattered photon has frequency $\nu - \nu_o$, where $\nu_o = g\mu B/h$ as before. Thus if the satellite observes both ν and $\nu - \nu_o$, then g can be evaluated, and in this way, the molecular species causing the Raman scattering can be identified.

Consider the scattering of light of frequency ν by a bound electron of characteristic frequency ν_o. The total elastic scattering cross section is given by the classical formula [3-1]:

$$\sigma = \frac{8\pi}{3} r_o^2 \; ; \quad r_o = \frac{e}{mc^2} . \tag{3-1}$$

When a photon of incident wave number k_o is inelastically scattered so that it loses energy ΔE, the differential elastic scattering cross section is given by

$$\frac{d\sigma}{d\Omega} = \frac{4r_o^2 h^2}{\mu} k k_o \frac{(\Delta E)^2}{[(\Delta E)^2 - k_o^2]^2} . \tag{3-2}$$

In the case of resonant (elastic) scattering, for the total cross section,

$$\sigma \simeq 16\, r_o^2 \sim 10^{-25} cm^2 .$$

For the Alouette experiment where resonant magnetic-dipole scattering was observed, the cross section is decreased by $(\mu/er_o)^2 \sim 10^{-4}$.

If Raman scattering in the inelastic magnetic-dipole mode is observed, as we propose here, the electric dipole scattering probability will be decreased by $(\Delta E/h\nu)^2$. Let $\Delta E \sim 1$ Mc, appropriate to magnetic spin flip of free radicals in the earth's troposphere, and let $h\nu \sim 20$ Mc by the incident radiation. The the effective cross section relative to that in the Alouette experiment will be decreased by $(1/20)^2 = 1/400$. Then the minimum density N of a magnetic species observable at distance d will be:

$$d = 20 \text{ miles}; \; N \geq 8 \times 10^6/cm^3 \; (5 \times 10^{-7} \text{ppm})$$

$$d = 100 \text{ miles}; \; N \geq 6 \times 10^8/cm^3 \; (4 \times 10^{-5} \text{ ppm}) .$$

Amateur frequencies of greater than 1 Mc are listed in Table 3-1. Their input power is lower by 1/6 than Alouette, which would increase the minimum detectable concentrations N accordingly. The electromagnetic spectrum at frequencies above 30 Mc is shown in Figure 3-1. The civilian air traffic navigational frequencies used by ground-based transmitters at various airports world wide in the frequency band 108-135 megacycles may be obtained from sets of charts published by Jeppeson Company [3-3].

Besides these sources of radiation which are able to stimulate magnetic-dipole spin flip, there is the powerful Over-the-Horizon (OTH) radar which irradiates most of China, Russia, and the Near East, at 20 Mc [3-4 to 3-7 and Appendix A , described in New Scientist, November 1974].

Table 3-1. A Summary of the U.S. Amateur Bands. (Figures are Megacycles. A_ϕ Means an Unmodulated Carrier, A1 Means C.W. Telegraphy, A2 is Tone-Modulated C.W. Telegraphy, A3 is Amplitude-Modulated Phone, A4 is Facsimile, A5 is Television, N.F.M. Designates Narrow-Band Frequency- or Phase-Modulated Radiotelephony, F.M. Means Frequency Modulation, Phone (Including N.F.M.) or Telegraphy, and F1 is Frequency-Shift Keying) [3-8]

80 meters	3,500-4000	-- A1
	3,500-3,800	- F1
	3,800-4000	-- A3 and n.f.m.
40 meters	7,000-7,300	-- A1
	7,000-7,200	-- F1
	7,200-7,300	-- A3 and n.f.m.
20 meters	14,000-14,350	-- A1
	14,000-14,200	-- F1
	14,200-14,300	-- A3 and n.f.m.
	14,300-14,350	-- F1
15 meters	21,000-21,450	-- A1
	21,000-21,250	-- F1
	21,250-21,450	-- A3 and n.f.m.
11 meters	26,960-27,230	-- A_ϕ, A1, A2, A3, A4, f.m.
10 meters	28,000-29,700	-- A1
	28,500-29,700	-- A3 and n.f.m.
	29,000-29,700	-- f.m.
6 meters	50-54	-- A1, A2, A3, A4, n.f.m.
	51-54	-- A_ϕ
	52.5-54	-- f.m.
2 meters	144-148	-- A_ϕ, A1, A2, A3, A4, f.m.
	220-225	
	420-450[1]	-- A_ϕ, A1, A2, A3, A4, A5. f.m.
	1,215-1,300	
	2,300-2,450	
	3,300-3,500	-- A_ϕ, A1, A2, A3, A4, A5, f.m. pulse
	5,650-5,925	
	10,000-10,500	
	21,000-22,000	
All above 30,000		

[1]Input power must not exceed 50 watts.

PAGE 1 OF 2

Table 3-1. A Summary of the U.S. Amateur Bands (Cont.) [3-8]

In addition, A1 and A3 on portions of 1,800-2,000, as follows:

Area	Band, kc.	Power Day	Power Night
Minn, Iowa, Wis, Mich, Pa., Md., Del, and states to North	1800-1825 1875-1900	500	200
N.D., S.D., Nebr., Colo, N. Mex., States west, incl. Hawaii	1900-1925 1975-2000	500*	200*
Okla., Kans., Mo., Ark., Ill., Ind., Ky., Tenn., Ohio, W. Va., Va., N.C., S.C., and Texas (west of 99° W or North of 32° N)	1800-1825 1875-1900	200	50

No operation elsewhere.

*Except in state of Washington, 200 watts day, 50 watts night.

Novice licensees may use the following frequencies, transmitters to be crystal-controlled and have a maximum power input of 75 watts.

3700-3750 A1 21,00-21,250 A1
7,150-7,200 A1 145-147 A1, A2, A3, f.m.

Technician licensees are permitted all amateur privileges in 50 Mc. and in the bands 220 Mc. and above.

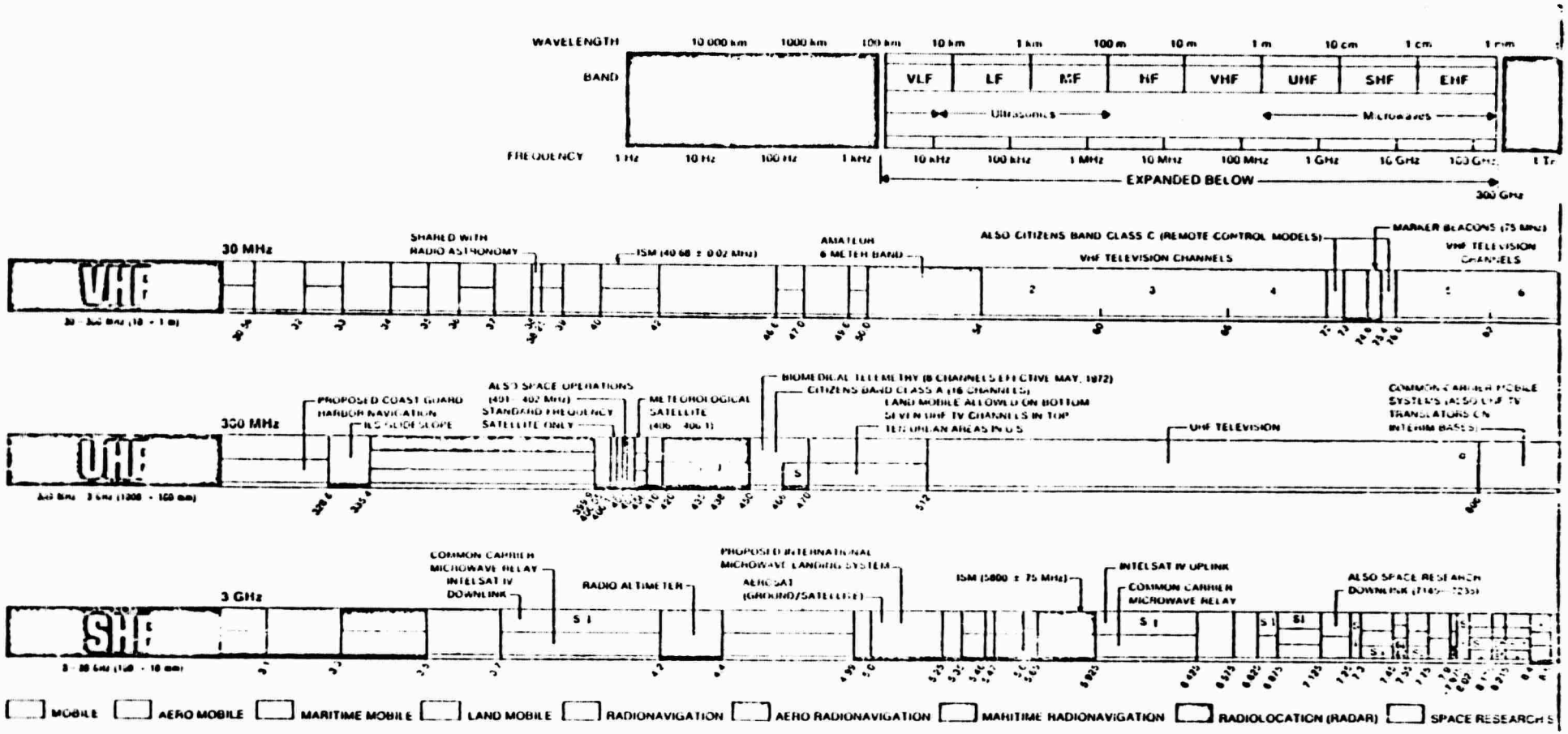

Figure 3-1. Radio Spectrum as Depicted by the International Telecommunications System

1. The radio spectrum is divided into bands allocated for broad services defined by the International Telecommunications Union. While consistent with worldwide assignments, the chart applies specifically to services and subservices for users within the United States.
2. Included are the provisions of the 1971 World Administrative Radio Conference held in Geneva. The new services became effective on January 1, 1973.
3. R indicates an aeronautical radio band reserved for aircraft flying major air routes. OR bands are used for "off-route" service. In the United States, OR bands designate military users, and R bands apply to civil users.

According to the New Scientist article, the known transmitters and receivers are at Cypress and Okinawa. The beam is aimed low, at 2-4° above the horizontal, the frequency is adjustable around 20 Mc, and the power for the transmitter is about 300 kW. This geometry is ideal for observation of Raman-scattered radiation by a satellite receiver moving above the irradiated area. The signal bounces alternately off the ground and the ionosphere making several hops as it crosses the irradiated terrain. Presumably OTH uses a constant wave transmitter; thus the advantage of pulsed transmission plus observation of reflected signal vs delay time is lost. On the other hand, the Raman shift separates the returned signal in frequency from resonance scattering of the incident radiation and prevents confusion, simplifying its detection.

3.2 REMOTE DETECTION OF EMISSION AND ABSORPTION IN THE INFRARED AND VISIBLE USING PASSIVE SENSING

Detection of absorption and emission of pollutant gases in the lower troposphere, depending on excitation by reflected sunlight, uses excitation of vibration-rotation and electronic motions at photon frequencies able to penetrate the atmosphere. The satellite or airplane-borne detection equipment may be either a spectrometer or a set of filters together with a photomultiplier able to record the selected photons. To illustrate this principle, we describe several experiments in which remote detection has already been reduced to practice as follows:

3.2.1 Experiment No. 1a [Ref. 3-9]

Source of Excitation:

Sunlight reflected from the surface of the earth.

Wavelength Studied:

2720 Å to 4220 Å for SO_2 detection by absorption.

4000 Å to 5500 Å for NO_2 detection by absorption.
4800 Å to 6300 Å for I_2 for calibration by absorption.

Equipment: (See Figures 3-2 and 3-3.)

A grating spectrometer which views the radiation coming from the troposphere below. The dispersed spectrum is fed through a mask which has slits where the pollutant absorption lines should occur. The dispersed spectrum is wiggled periodically across this mask. If the signal from the photomultiplier reaches minimum periodically, then there is a resonant beat signal which means that the observed absorption spectrum fits the expected spectrum, and the pollutant is positively identified.

Sensitivity:

Less than 0.2 ppm of pollutant gas seems to be detectable under realistic conditions, using measuring equipment in a balloon over Chicago at 35 km altitude.

This experiment measured the product of (pollutant concentration) x (path length). In the second experiment made simultaneously from the ground, the concentration was evaluated.

Over another country, it may not be feasible to make the ground measurement so that the concentration cannot be evaluated directly in this way. On the other hand, the Nimbu is daily measuring the atmospheric temperature profile around the world. If the relative intensities in the various infrared lines of the spectrum characterizing a given pollutant are measured, then, taking into account the temperature profile from the Nimbus, the concentration of pollutant as a function of altitude can be deduced. If, alternatively, the client wishes only tc identify

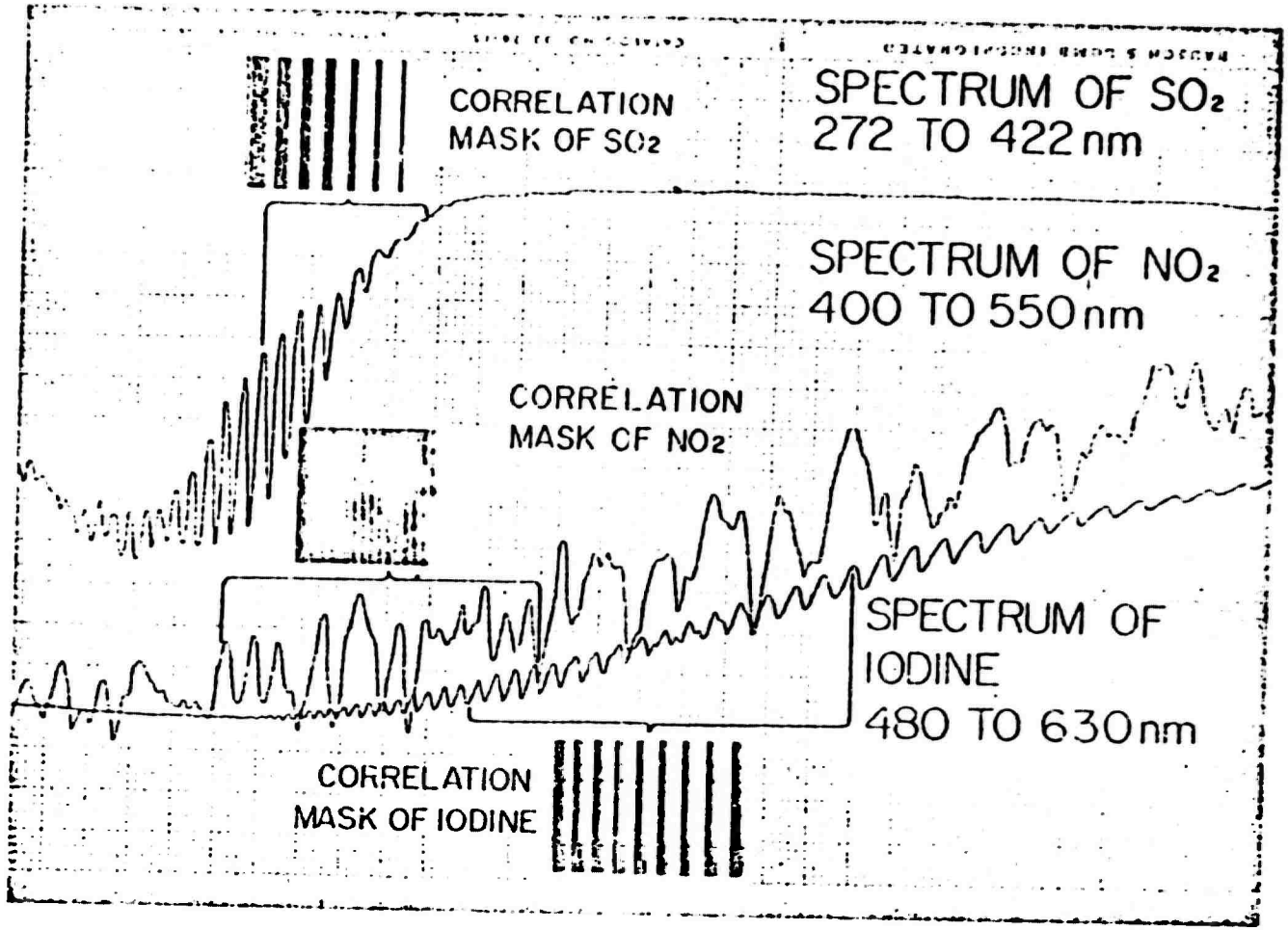

Figure 3-2. Schematic Signals Received in a Correlation Spectrometer

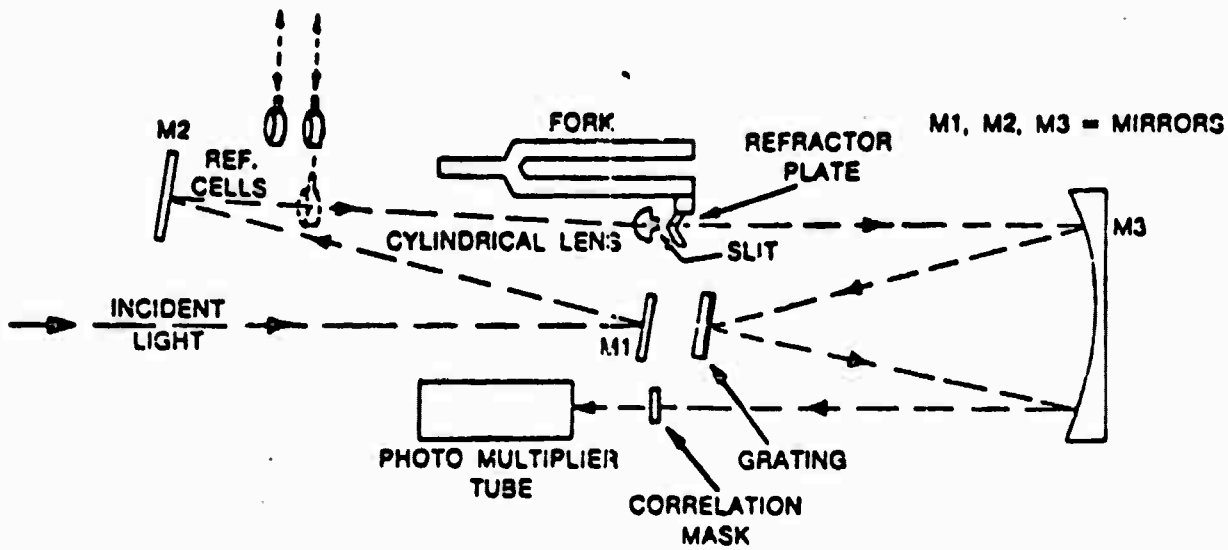

Figure 3-3. Dispersive System for Vapor Detection Using Spectrum Correlation Filter

the pollutant and does not care about the concentration profile, the answer is obtained directly from the experiment described above.

The geometry is illustrated in Figure 3-4. The results of Experiment No. 1 are described in Figures 3-5 and 3-6. The equipment used in this comparison is called a Correlation Spectrometer.

3.2.2 Experiment No. 1b [Ref. 3-10]

The wavelengths, equipment and sensitivity are identical with those described in Experiment No. 1a.

In this experiment, tests of an airborne installation were made from a helicopter using a remote sensing instrument (described in Experiment No. 1a) and from a fixed wing Aero Commander 500 A. Surveys were made along the Toronto water front and around Washington, D.C. Individual plumes from the electrical generating stations and shore line industries are readily identified, with signals reproducible to 10 percent. The product of pollutant concentration x path length was measured as the plane climbed from 500 to 15,000 feet. In this way, it was determined that the major part of the pollutant was confined below a 4000 ft altitude. With an effective path length of 5000 meters, which may not be unusual over an industrial area, the correlation spectrometer can detect concentrations as low as two parts per billion, corresponding to a minimum signal of about 20-30 ppm-meter. The correlation spectrometer technology obviously is applicable over the whole of the visible and infrared windows of the atmosphere and may be varied by adjusting the spacing of the lines scribed on the grating and by varying the positions of the photomultipliers and masks along the circumference of focus of the grating spectrometer.

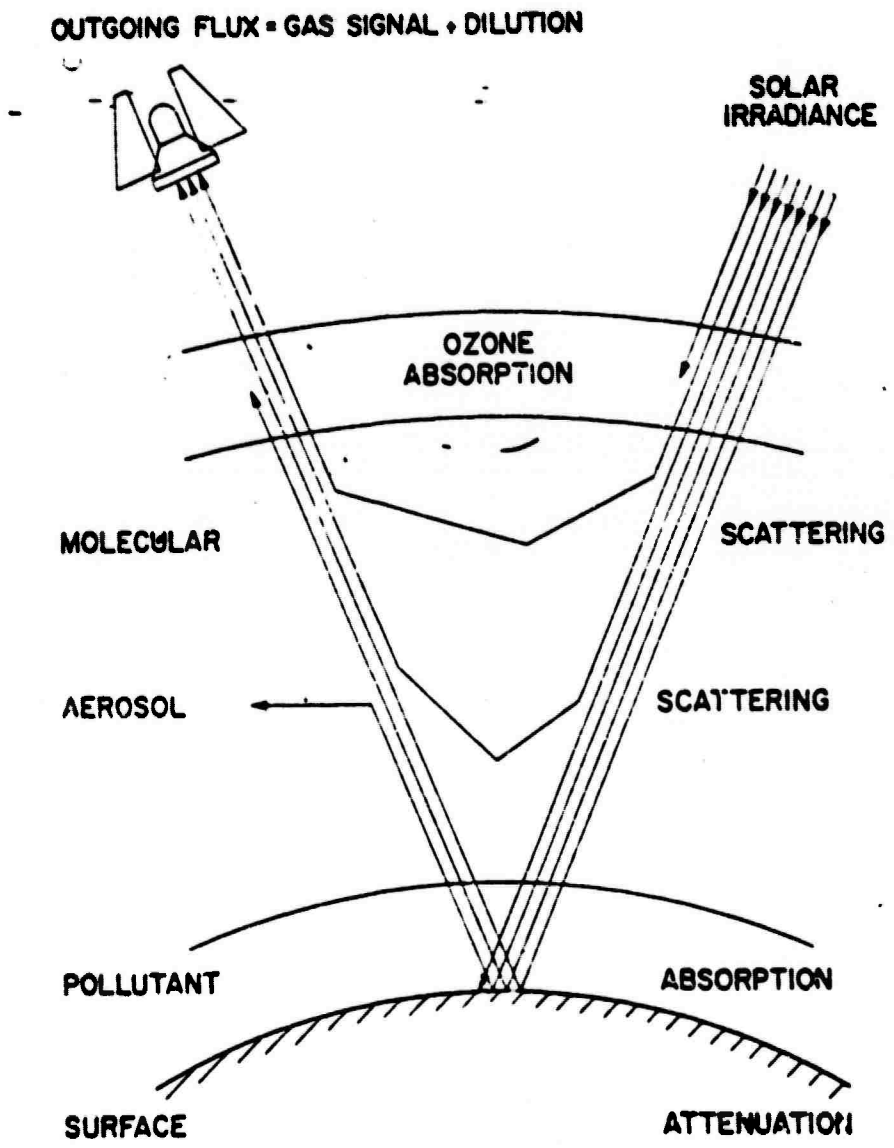

Figure 3-4. Attenuation and Dilution

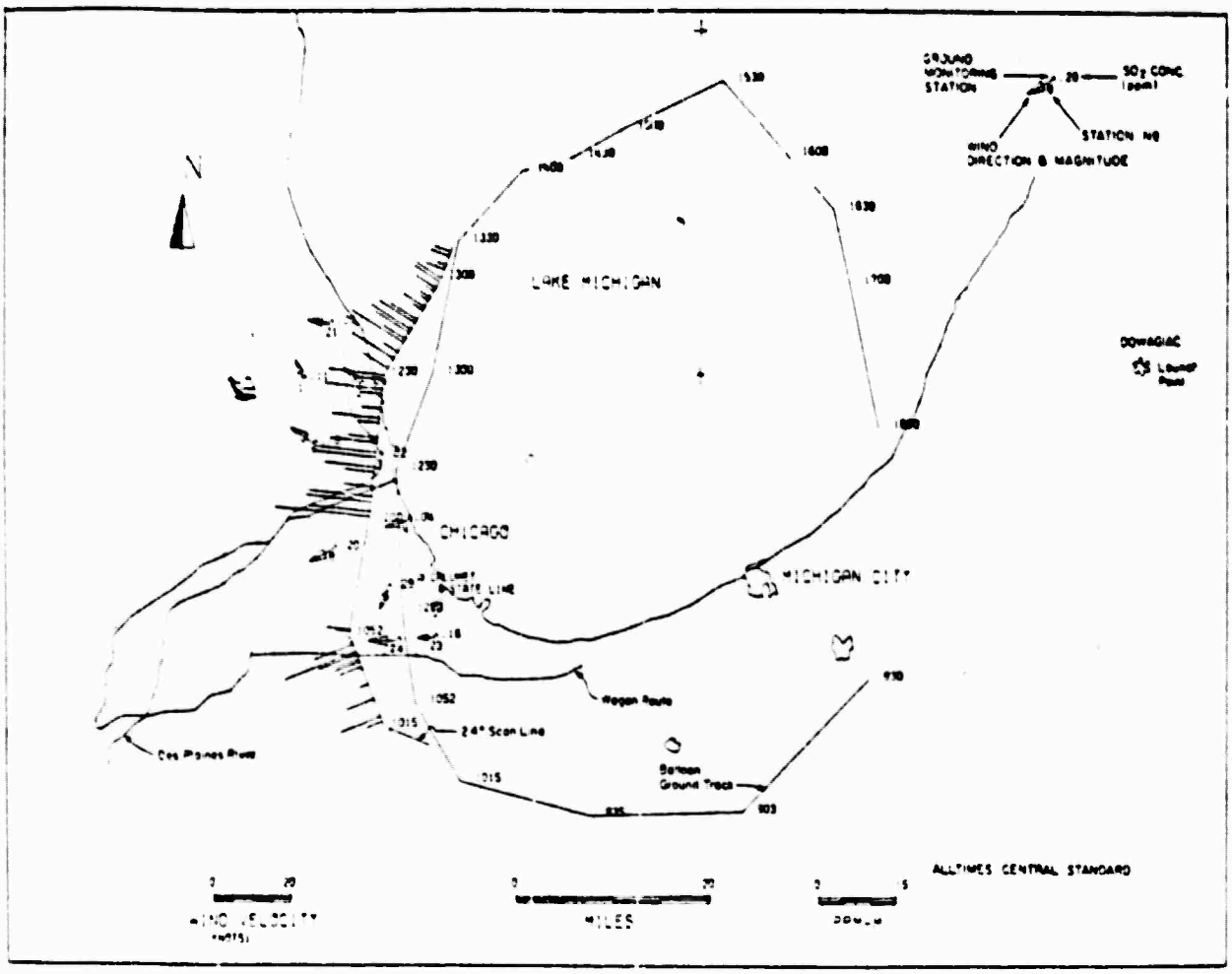

Figure 3-5. Balloon Flight SO2 Profile: Chicago Area, September 3, 1969

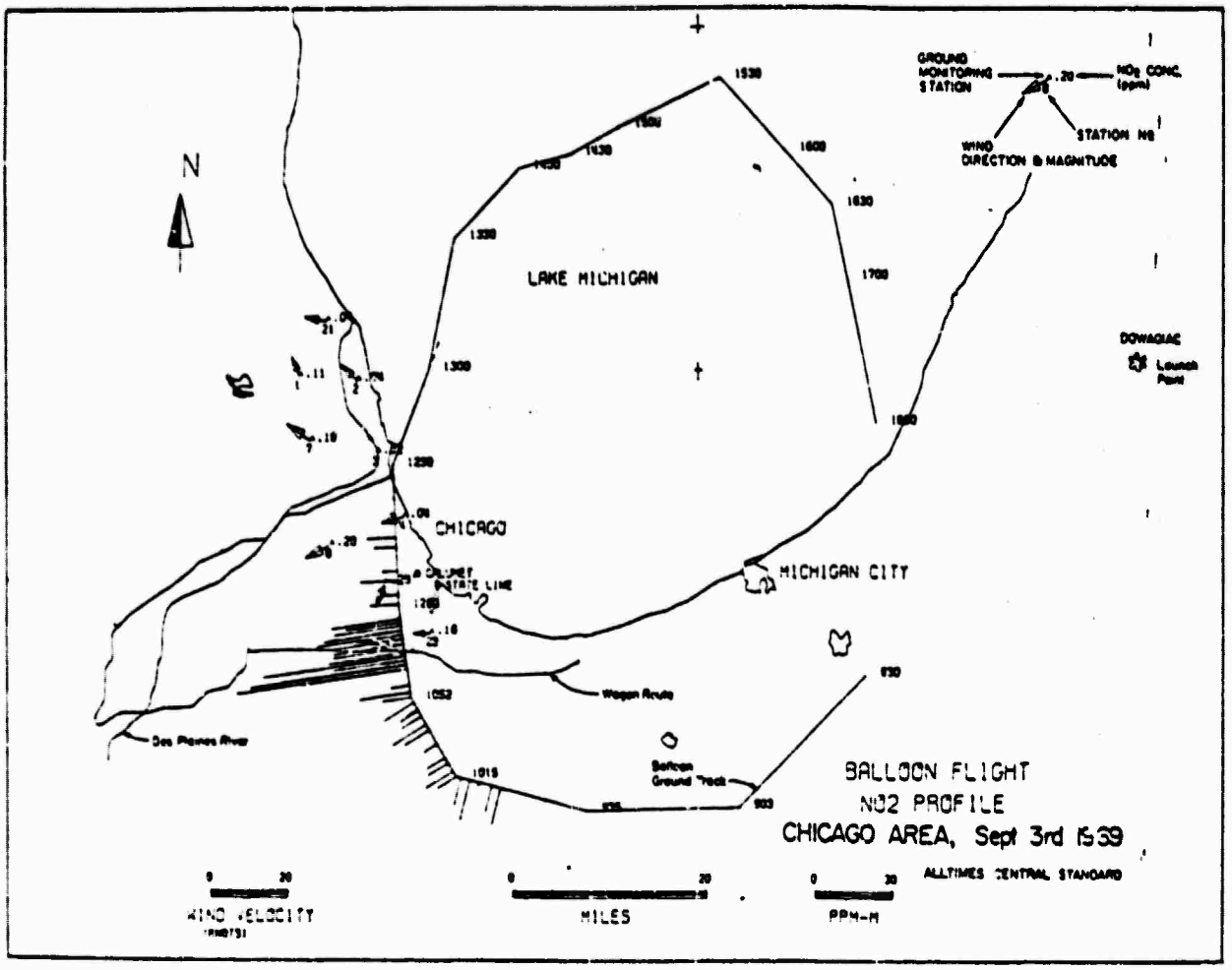

Figure 3-6. Balloon Flight NO2 Profile: Chicago Area, September 3, 1969

Experiments 1a and 1b show that any gas pollutant with an infrared and/or visible signature may be searched for by a passively sensing correlation spectrometer carried at satellite altitudes. In these two experiments, positive results were obtained for identifying the signatures of NO_2 and SO_2 at minimum concentrations of ~0.02 ppm. We may expect similar sensitivities for detection of any of the gases listed in the foregoing tables which have characteristic vibronic and/or electronic signatures in the frequency intervals corresponding to windows in the atmosphere.

Some interesting applications of this remote sensing technique have been listed in Ref. 3-10. For example,

- The monitoring of volcanic emissions of sulphur dioxide and other gases to provide warnings of impending volcanic activity.

- The detection of fumarole emissions as a guide to the location of sources of geothermal energy.

- The measurement of trace gases emitted by oxidizing mineral deposits and the use of this information as a guide to exploration.

- The measurement of gaseous emissions of iodine vapor associated with oil field brines as a guide to potential oil-bearing regions.

- The applications of optical remote sensing techniques to the detection of fish oil slicks associated with large schools of fish.

In Figures 3-7 thru 3-11 and Tables 3-2 and 3-3, the data of Barringer et al., measured with their airplane-borne technology, are illustrated. With respect to detecting oil slicks, the infrared signatures of some oils one might expect to find on surfaces of water in rivers, lakes, harbors, and oceans are shown in Figure 3-12. The atmospheric windows through which these signatures might be detected in absorption are also indicated.

3.2.3 Experiment No. 2 [Ref. 3-11]

An infrared spectrophotometer is used either to measure emitted radiation from warm gases as in gas plumes emitting against a cold background or in absorption of solar radiation reflected from the earth's surface. It has been used in particular for measuring ozone bands at about 8700 Å. The intensities are measured in up to 64 narrow channels in the 8,500 - 12,500 Å atmospheric window. An analog-to-digital converter puts the measured intensities into a computer for comparison of their intensities with laboratory intensities obtained for the pollutant of interest at similar temperatures and pressures. These laboratory intensities are called "training spectra." The computer connected by transmission to the receiver can simultaneously evaluate the least squares frequency and amplitude equation for up to ten infrared-absorbing (or emitting) pollutants. For example, the error in the 9500 Å channel for evaluation of the ozone signature corresponds to about ±1 percent absorption.

3.2.4 Experiment No. 3 [Ref. 3-12]

In this experiment, various kinds of rocks on the earth's surface have been identified by their characteristic emittance features caused by molecular vibrations of atoms in the various crystal structures. The Earth Resources Technology Satellite carries sensors which selectively observe reflected sunlight (from the earth's surface) in channels of 0.475 - 0.575 μm, 0.580 - 0.680 μm,

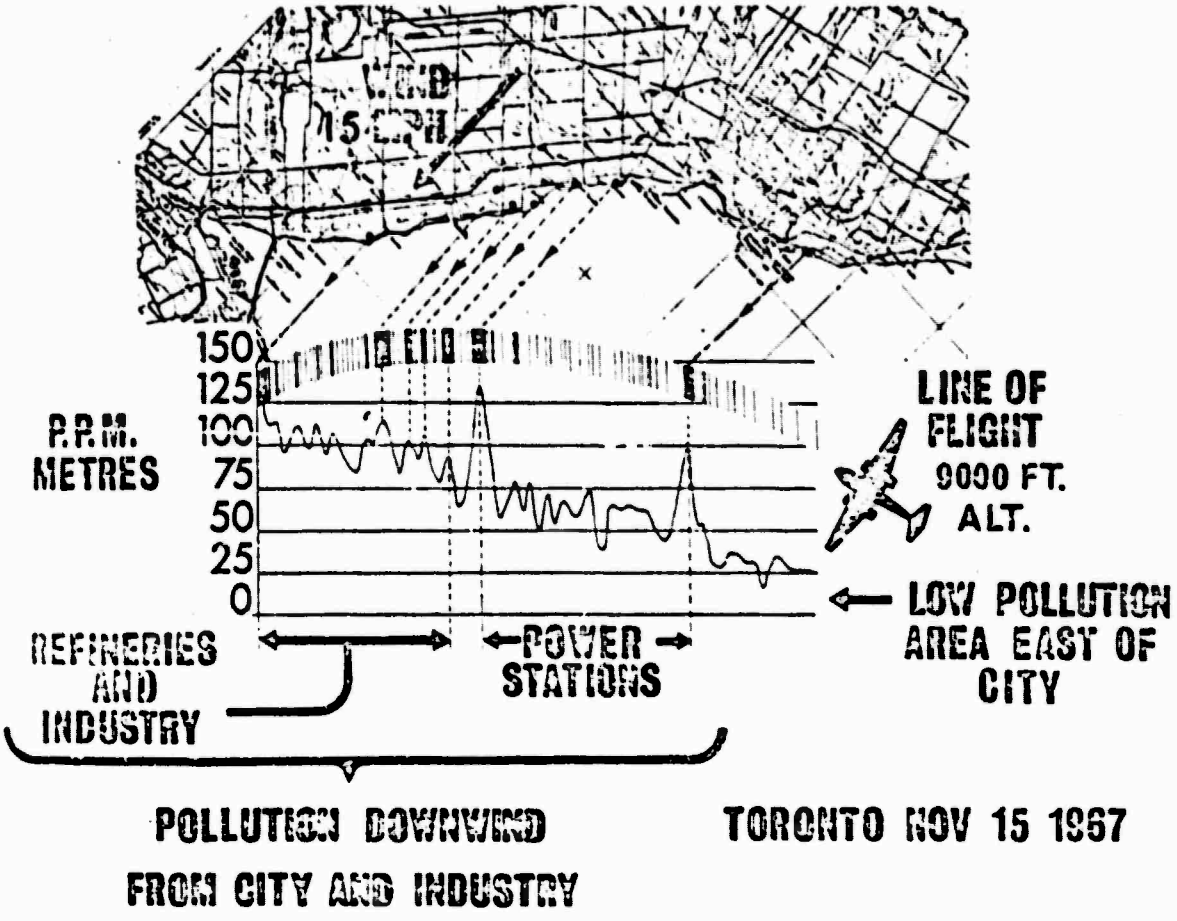

Figure 3-7. Sulfur Dioxide Concentration--Total Vertical Burden
Toronto, November 15, 1967

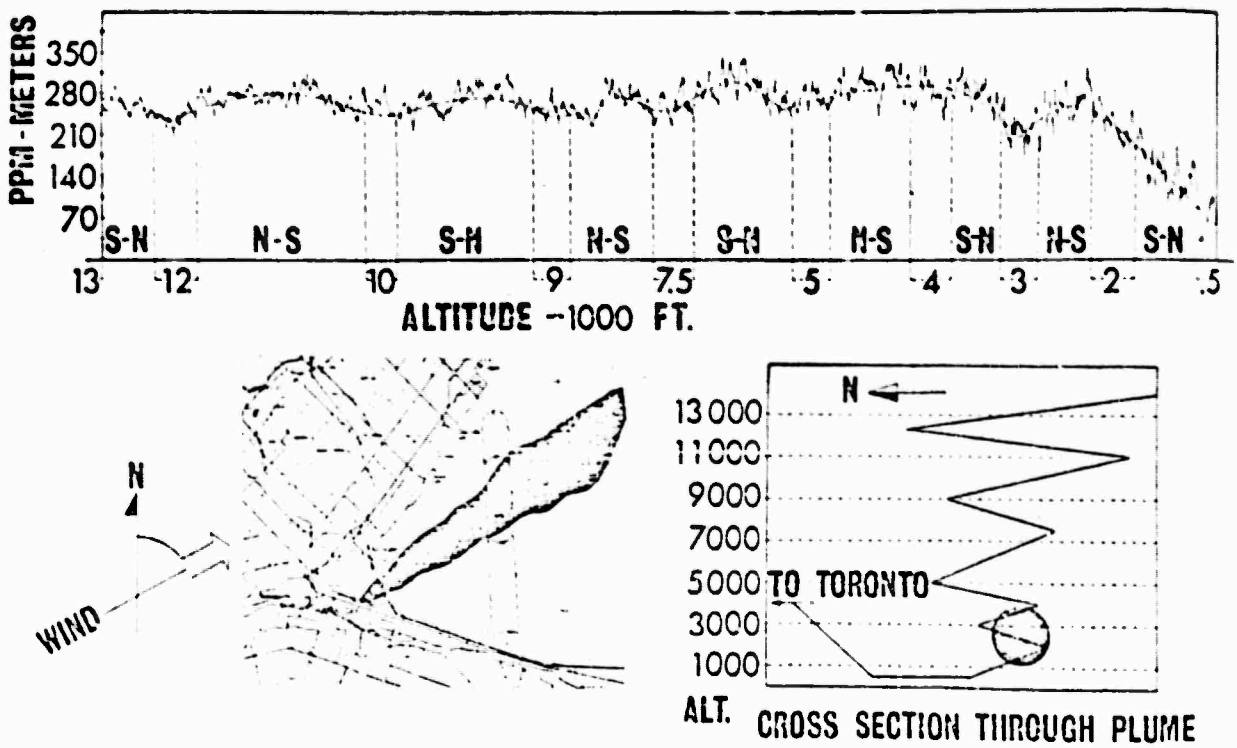

Figure 3-8. SO_2 Profile Over Lake Ontario

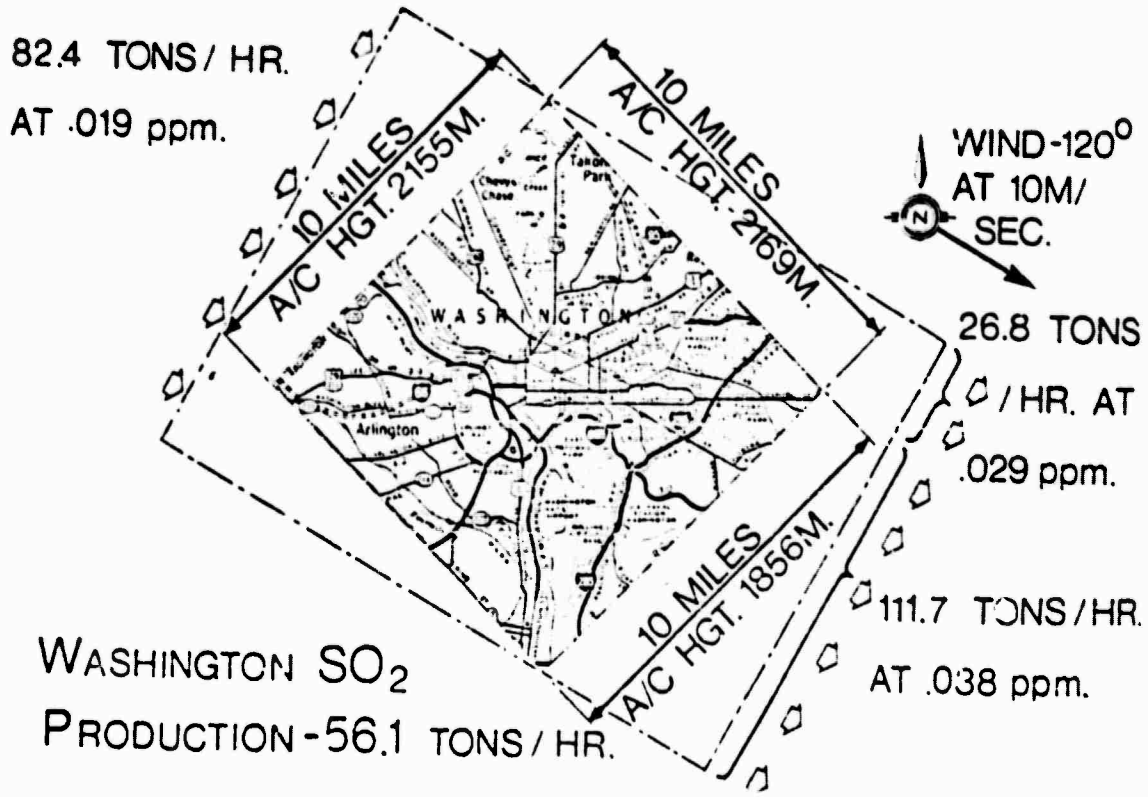

Figure 3-9. SO_2 Mass Balance--Washington, D.C.

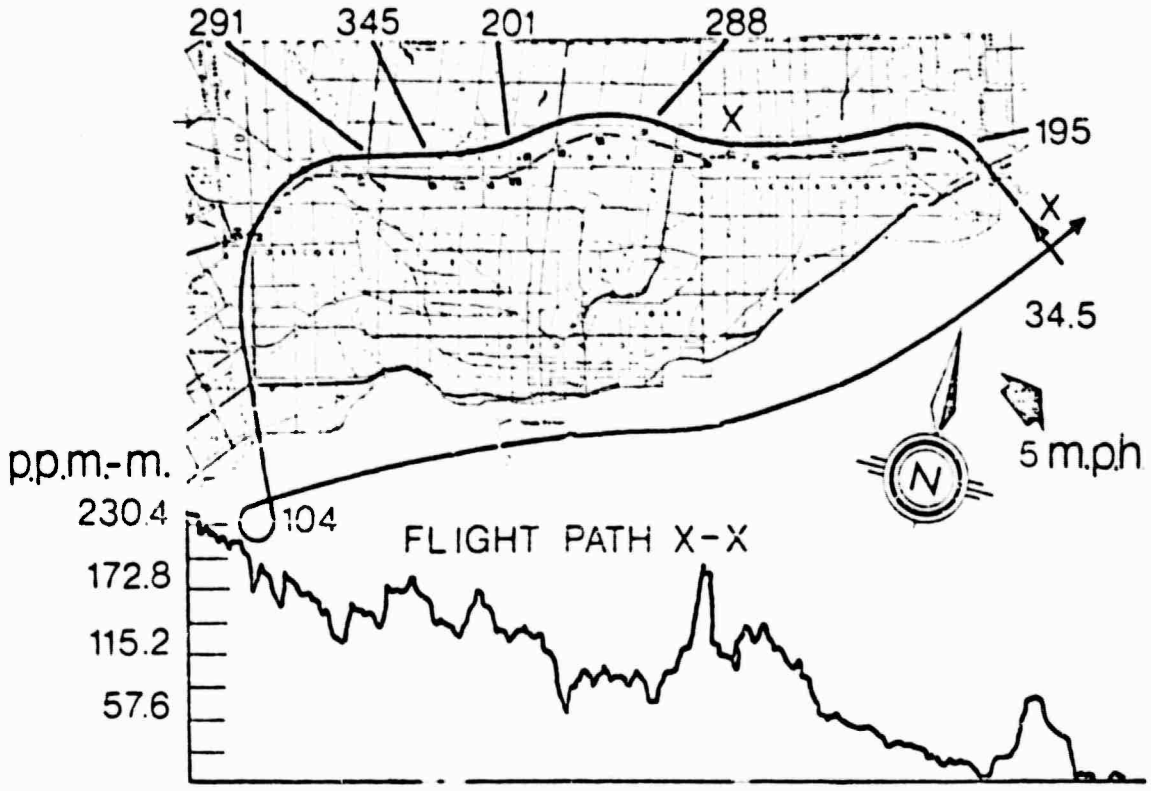

Figure 3-10. NO_2 Profile--Toronto, March 7, 1968

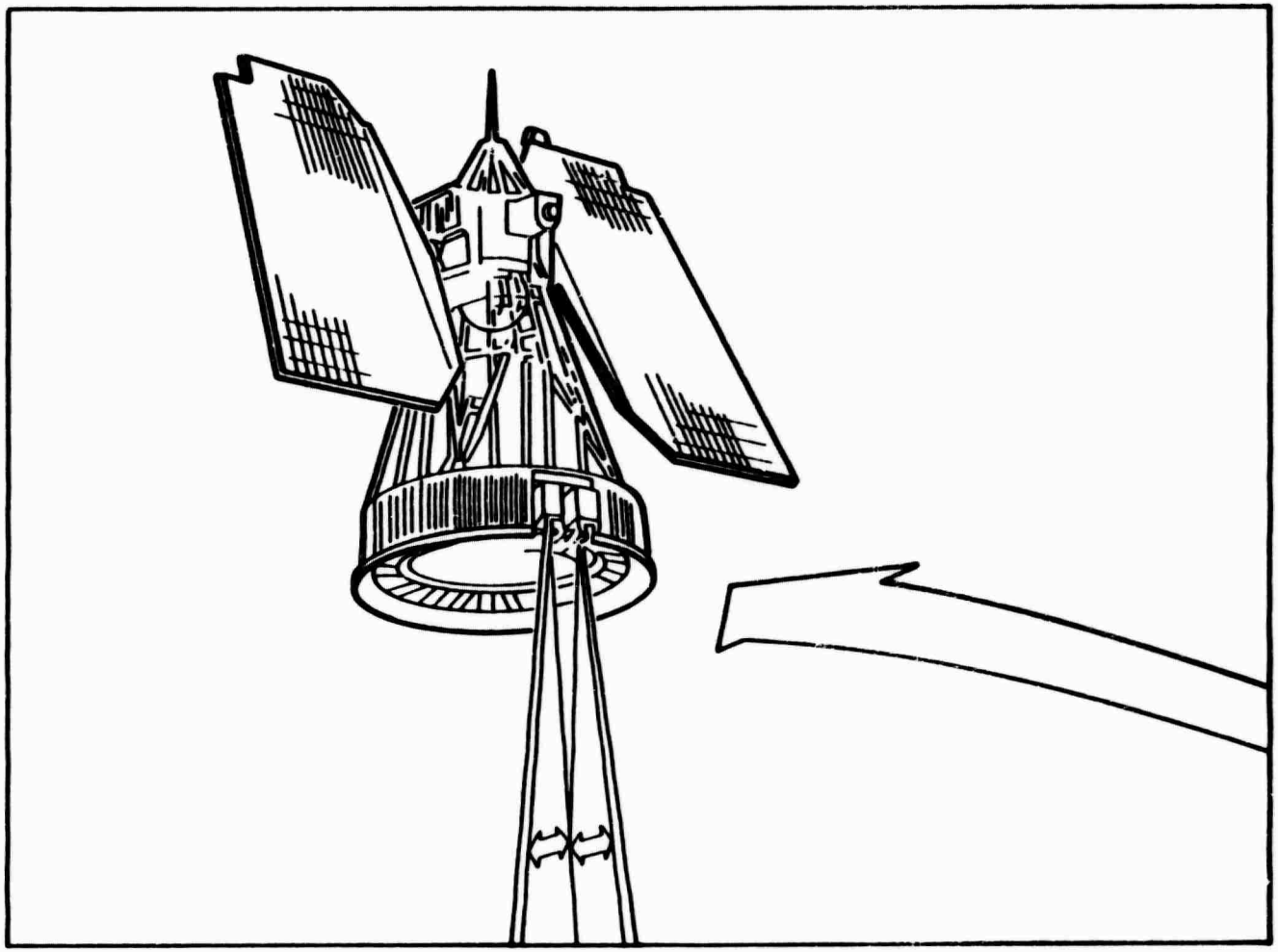

Figure 3-11. Artist's Impression of a Nimbus Satellite in Orbit Carrying Two Correlation Spectrometers for Remote Sensing of Pollutant Gases

Table 3-2. SO_2 Determinations

TIME E.S.T.	LOCATION	LEG	PRESS ALT. (FT.)	ACT. ALT. M.S.C. (FT.)	MEAN STC EL (FT.)	HEIGHT h (M)	SUN ANGLE (θ°)	m FACTOR	PATH LENGTH (M)	INSTRUMENT READING (PPM-METERS)	MEAN SO_2 CONC. (PPM)
0856	DALLCARLIA RLS.		7500	7250							
0859	16TH ST. & SPRING(NW)SILVER SPRING	1	7500	7250	250	2140	73.8	3.05	6527	112	.018
0902	SILVER SPRING		7500	7220							
0904:50	1 MILE E. OF ST. PLEASANT	2	7500	7250	147	2160	72.9	2.92	6307	266	.045
0909	SEAT PLEASANT		6500	6220							
0913	W. WILSON BRIDGE	3	6500	6220	140	1850	71.9	2.97	5495	192.5	.057
0923:30	DALLCARLIA RLS.		7500	7220							
0926	SILVER SPRING	1	7500	7215	250	2120	70	3.02	6402	126	.021
0929	SILVER SPRING		7500	7215							
0931:30	PR. GEORGE C.C.	2	7500	7215	147	2160	69.5	2.98	6431	172	.028
0936	SEAT PLEASANT		6500	6225							
0940	W. WILSON BR.	3	6500	6225	140	1855	68.5	2.92	5417	284	.055
0923:30	DALLCARLIA RLS.		7500	7250							
	1 MI. NW SILVER SPRING	1	7800	7540	250	2180	67.0	3.04	6627	126	.020
0959	EASTERN AVE.&SOUTHERN AVE.		7500	7250							
1002	EASTERN AVE.&SOUTHERN AVE.	2	7500	7250	147	2165	66.3	3.01	6517	143	.023
1006	1 MI. SE OF SEAT PLEASANT		6500	6225							
1011	W. WILSON BRIDGE	3	6500	6240	140	1860	65.6	2.99	5561	141	.027
1020	DALLCARLIA RLS.		7500	7250							
1023	1 MI. NW SILVER SPRING	1	7800	7540	250	2180	64.5	3.01	6562	108	.017
1027	NE of EASTERN AVENUE		7600	7340							
1030	EASTERN & SOUTHERN AVE.	2	7600	7340	147	2190	64	2.98	6526	132	.021
1036	EASTERN AVE. & SOUTHERN		6500	6240							
1040	W. WILSON BR.	3	6500	6240	140	1860	63.2	2.94	5468	160	.031

Note 1 - Mean Temperature of Ambient Air (Aircraft Thermometer) was -6 °C.
Mean Pressure Taken = 12.6 psia

Table 3-3. Summary of Airborne Results

TRAVERSE		MEAN CONCENTRATIONS		
		Leg 1	Leg 2	Leg 3
No	Time			
1	0856-0915	.018	.045	.037
2	0923-0940	.021	.028	.055
3	0952-1011	.020	.023	.027
4	1020-1040	.017	.021	.031
MEAN SO_2		.019	.029	.038

C.A.M.P. STATION
MEASUREMENTS (BY H.E.W.)

TIME	SO_2 CONCENTRATIONS HOURLY AVERAGE
0800-0900	0.12
0900-1000	0.10
1000-1100	0.09

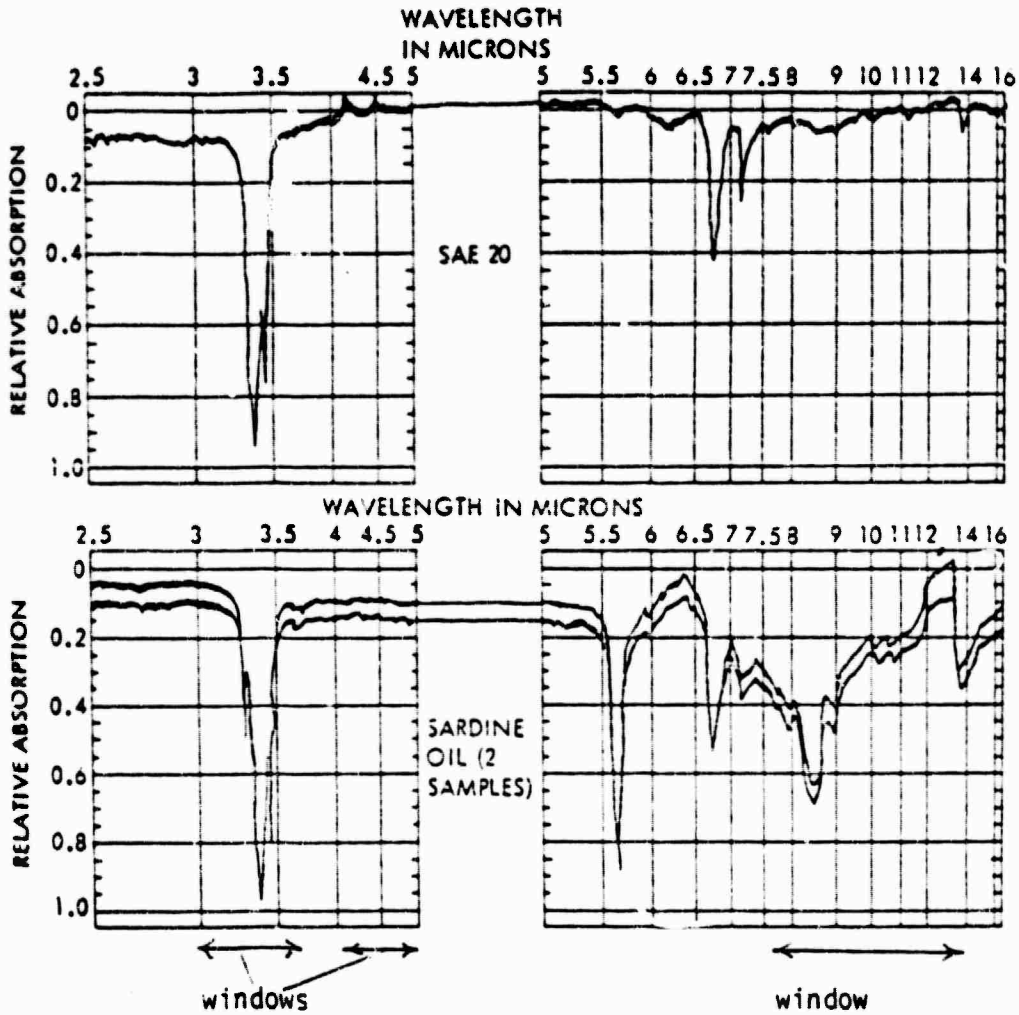

Figure 3-12. Fish and Mineral Oil Spectral Signatures [Ref. 3-12]

3.069 - 0.830 μm, and 0.6 - 0.7 μm, 0.7 - 0.8 μm, 0.8 - 1.1 μm, and 10.4 - 12.6 μm. Iron oxides have been surveyed using the fact that ferrous compounds have electronic transitions reflecting strongly at 1.0 μm whereas ferric compounds reflect mainly at 0.87 and 0.70 μm. The ratios of signals in these two channels as seen from altitude give a measure of iron ores on the surface of the earth. This experiment was made on an overflight at about a 1-km altitude. Evaluations of observed relative reflectances in the several infrared sensing channels are shown in Figure 3-13 and Table 3-4.

By similar analyses, based on previous calibration of reflectances in the laboratory, it should be possible to assess remotely the composition of slag piles and mine tailings.

3.2.5 Experiment No. 4 [Ref. 3-13]

Passive remote sensing of electromagnetic radiations of an 8 to 10 cm wavelength allowed temperatures of the surface of the Baltic Sea to be evaluated by comparison of relative intensities of the OH bands from the sea surface. The temperatures computed from these observations are shown in Figure 3-14, and are compared there with temperatures measured by ships. One sees that with an additive constant correction, this method of remote assessment by passive infrared spectral measurement is very good.

3.2.6 Experiment No. 5 [Ref. 3-14]

(a) A Radiometer was used to measure atmospheric emission with a resolution better than 2 cm^{-1} in the region 1-30 microns; (b) a spectrometer was used to measure atmospheric absorption using the sun as a source with a resolution of about 0.3 cm^{-1} in the 1- to 30-micron region. The equipment was borne on a balloon. (Note: for down-looking observations of atmospheric absorption, the sun's glitter could be substituted as a source.) A liquid

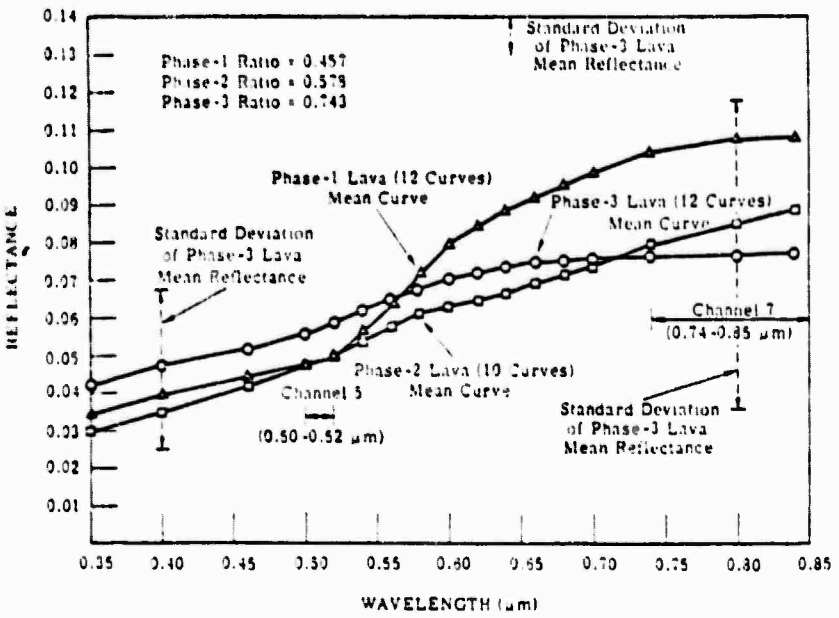

Figure 3-13. Mean Reflectance of Three Lavic Phases of Pisgah Crater Basalts

Table 3-4. Average Reflectance (Relative to MgO) of Typical Spectra of Various Minerals and Vegetation

Rock	Band 1 ρ_{Band_1} (0.5-0.6 μm)	Band 2 ρ_{Band_2} (0.6-0.7 μm)	Band 3 ρ_{Band_3} (0.7-0.8 μm)	Band 4 ρ_{Band_4} (0.8-1.1 μm)	$\frac{\rho_1}{\rho_4}$	$\frac{\rho_3}{\rho_4}$
Gabbro (Plagioclase)	.57	.24	.19	.11	5.20	1.36
Basalt	.68	.70	.71	.73	1.07	.97
Limonite	.11	.30	.33	.29	0.38	1.14
Hematite	.09	.13	.17	.20	0.45	.85
Vegetation (Green)	.13	.13	.38	.47	0.28	.81

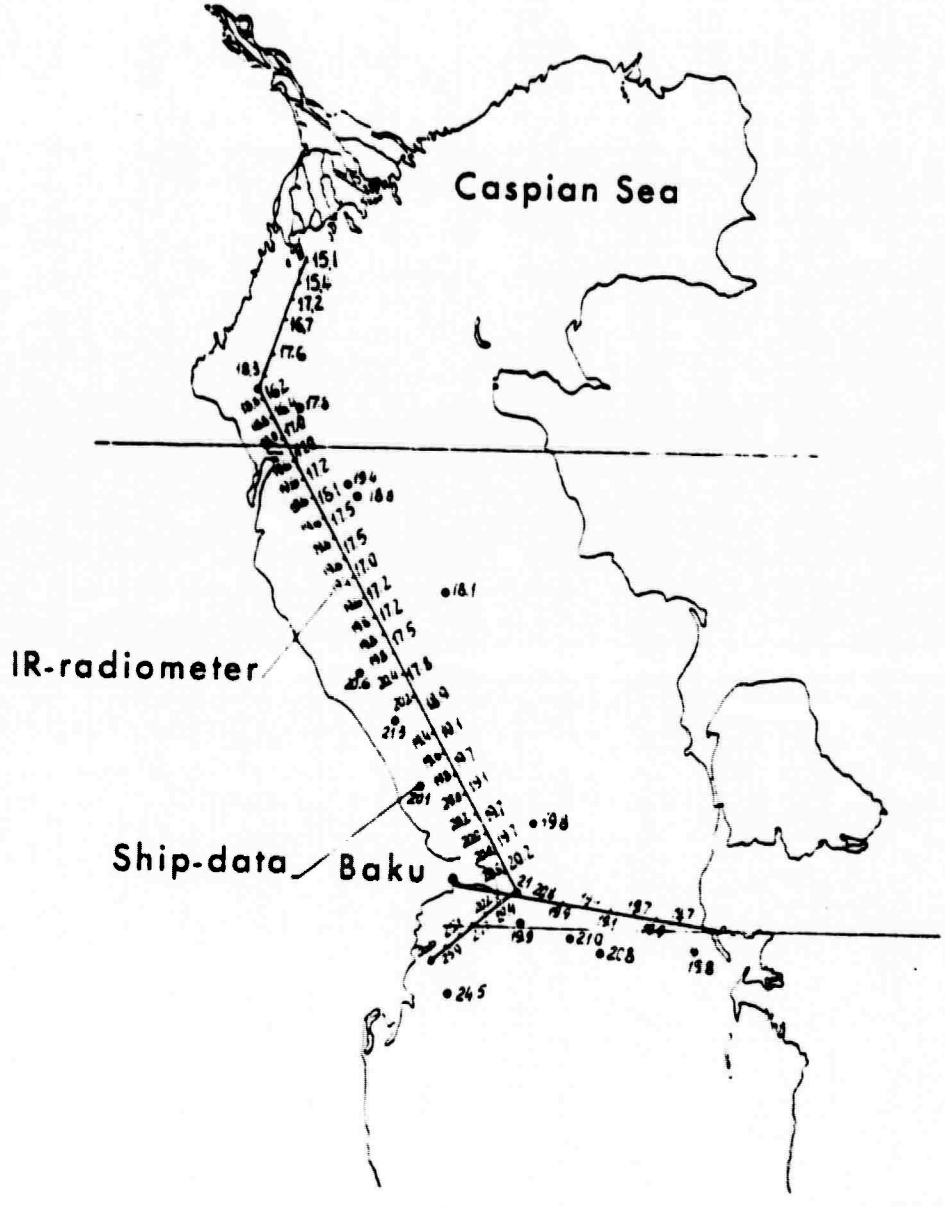

Figure 3-14. Temperature Map of the Caspian Sea, Obtained from Infrared and Microwave Radiometer Data λ = 3-10 cm, Microwave and Infrared, Passive

nitrogen cooled Ge:Cu detector appears to be used for both techniques. The grating spectrometer has a 1/2 meter focal length with a grating. The radiometer uses a filter wheel with positions for 5 filters. Typical spectra are shown in Figures 3-15 thru 3-19. Vertical profiles for H_2O, CO, N_2O and HNO_3 obtained by analysis of the spectra, are shown in Figure 3-20. The maximum sensitivity obtained appears to be about 0.02 ppm.

3.2.7 Experiment No. 6 [Ref. 3-15]

A correlation interferometer has been developed for measurement of CO and CH_4 at 2.35 microns. The instrument has been used in laboratory tests, solar-looking ground-based tests (and therefore could probably be used for looking down at the sun's reflection from a body of water), and downwarn looking airplane-based tests [on a Falcon]. CO and CH_4 were successfully detected. It is computed that the method could be used to detect NO_2 at 0.4 - 0.04 ppb and SO_2 at 0.04 - 0.009 ppb. The interferometer is shown schematically in Figure 3-21. The filter had a half width of 10 cm^{-1}.

An example of the interferogram measured for detection of CO is shown in Figure 3-21. In order to determine the detectability of a number of atmospheric trace gases by this method, calculations were made to simulate the operation of the correlation interferometer as follows:

- Spectra with 0.5 cm^{-1} resolution were obtained in the laboratory for individual gases, see Table 3-5.

- Using a computer, spectra of various combinations of gases were simulated for various filters, using the laboratory-measured spectra.

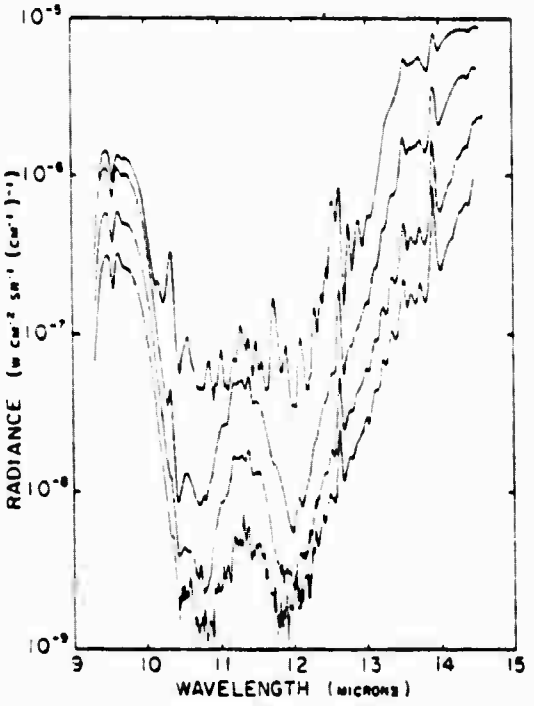

Figure 3-15a. Typical Spectral Atmospheric Radiance Measured 10 December 1969 at Altitudes of 3.4, 10.0, 20.1, and 24.7 km. (The zenith angle was 45° for all records.)

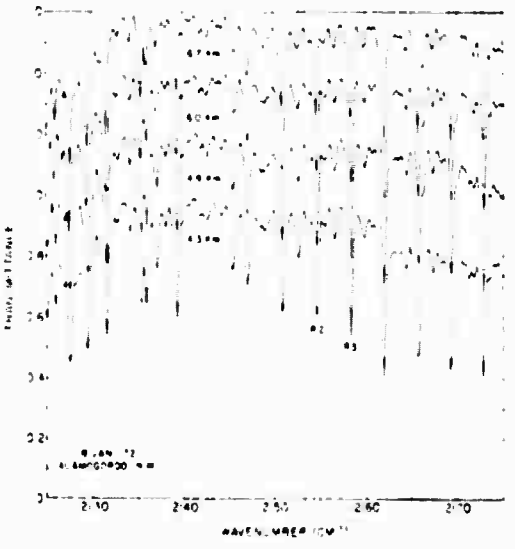

Figure 3-15b. Atmospheric Transmittance vs Wavenumber from Consecutive Records at Various Altitudes for the 2125-2175 cm^{-1} Region

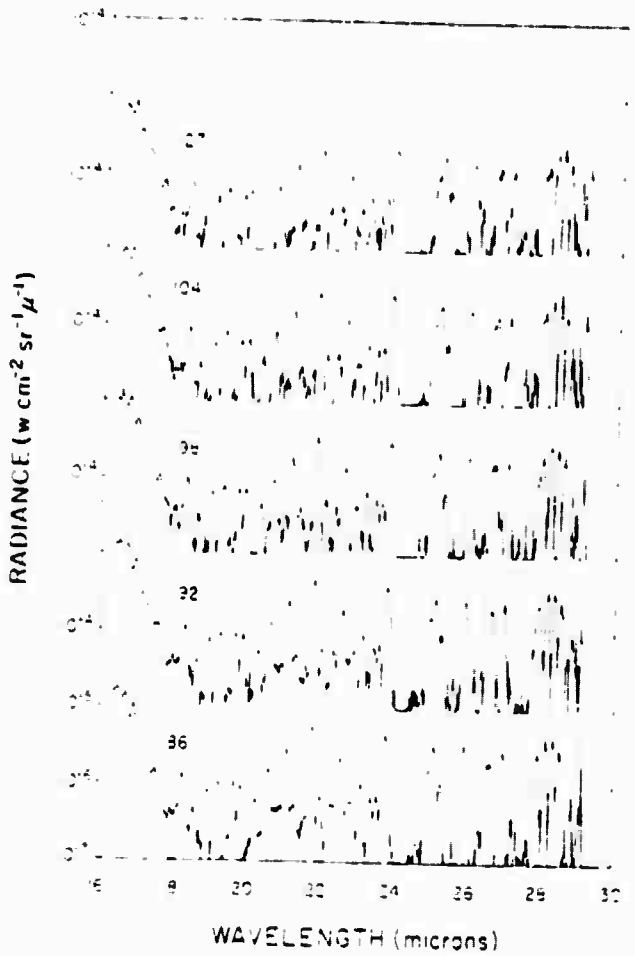

Figure 3-16a. Samples of the Reduced Data Obtained 22 February 1971 at Alamogordo, New Mexico, Showing the Downward Night Emission in the 16-30μ Region as a Function of Altitude. The Zenith Angle Was 45° for All Records. Successive Records are Displaced by Two Decades of the Log Scale

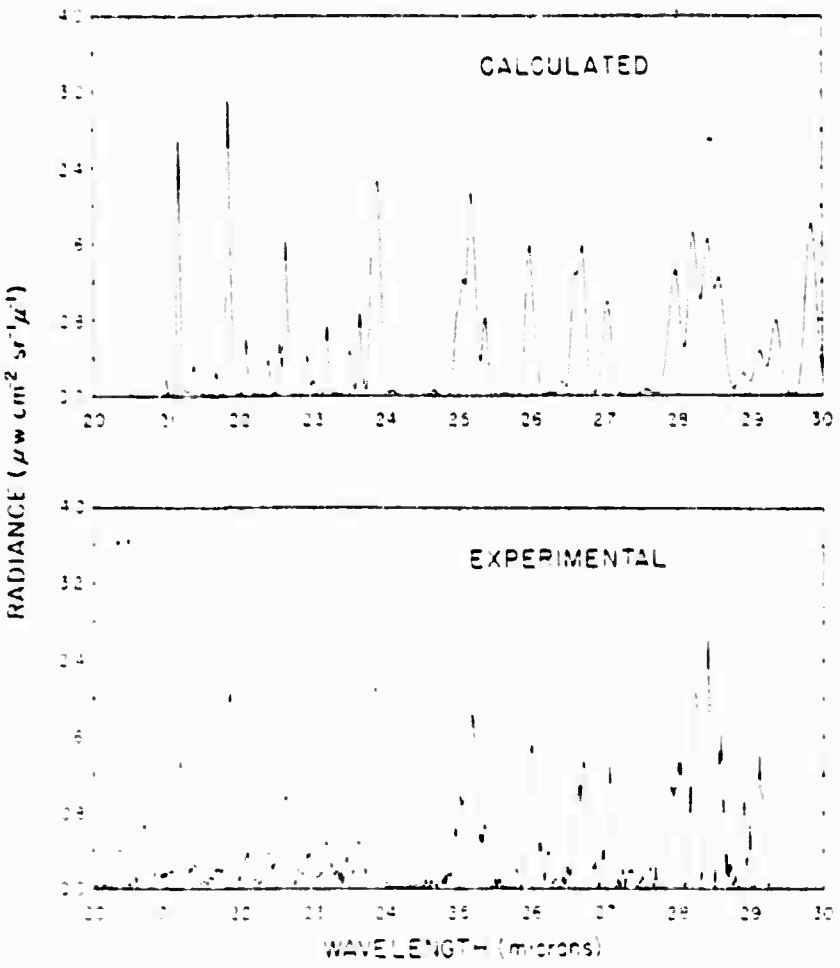

Figure 3-16b. Comparison of Calculated and Measured Emission Spectra in the 20-30μ Region for Record 127 of the February Flight. U(1) is Derived from the 25μ Line Group and Corresponds to a Mixing Ratio of 5.8×10^{-6} gm/gm

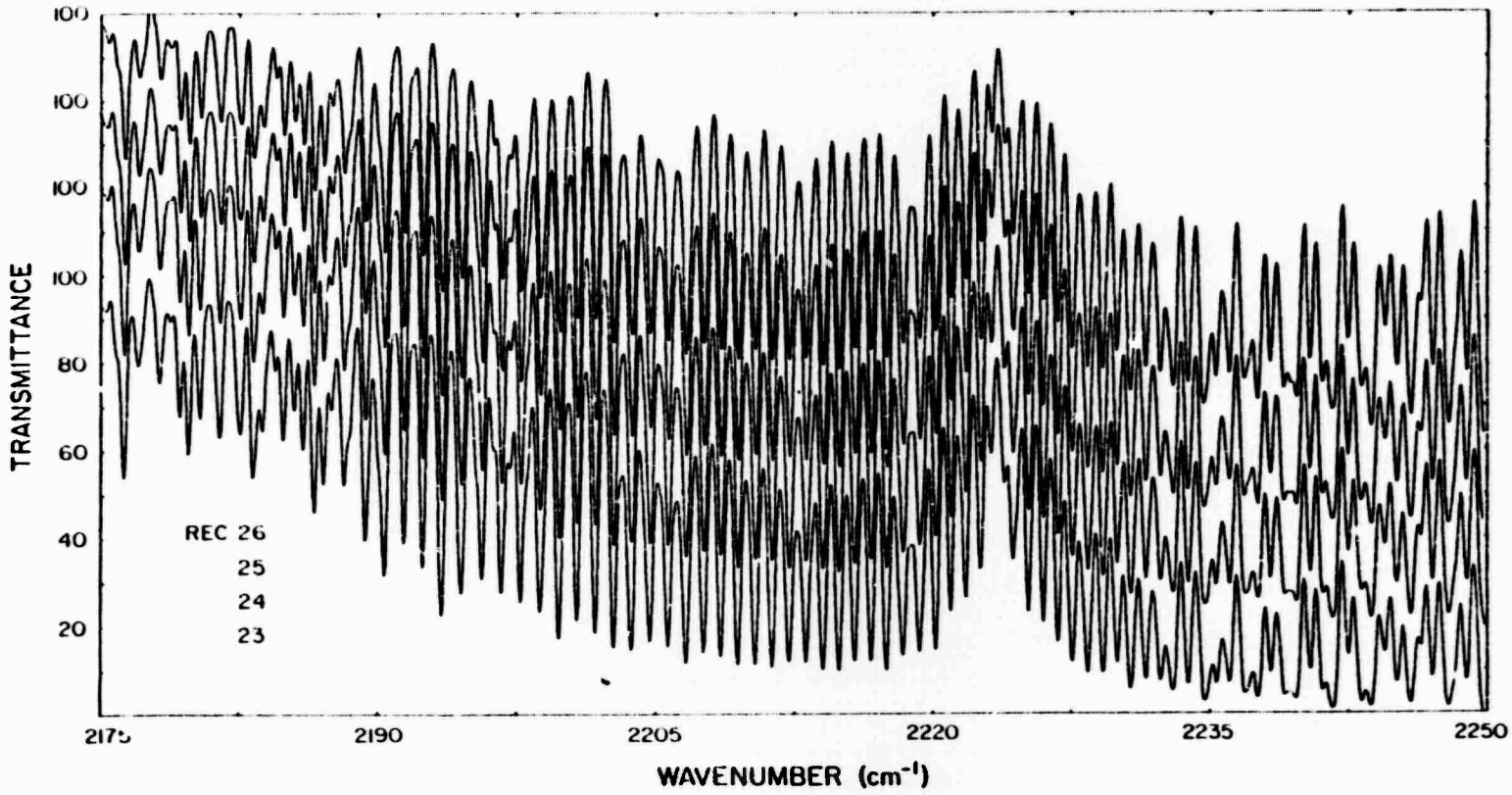

Figure 3-17. Atmospheric Transmittance vs Wavenumber at Various Altitudes for the 2175-2250 cm^{-1} Region, Records 23-26

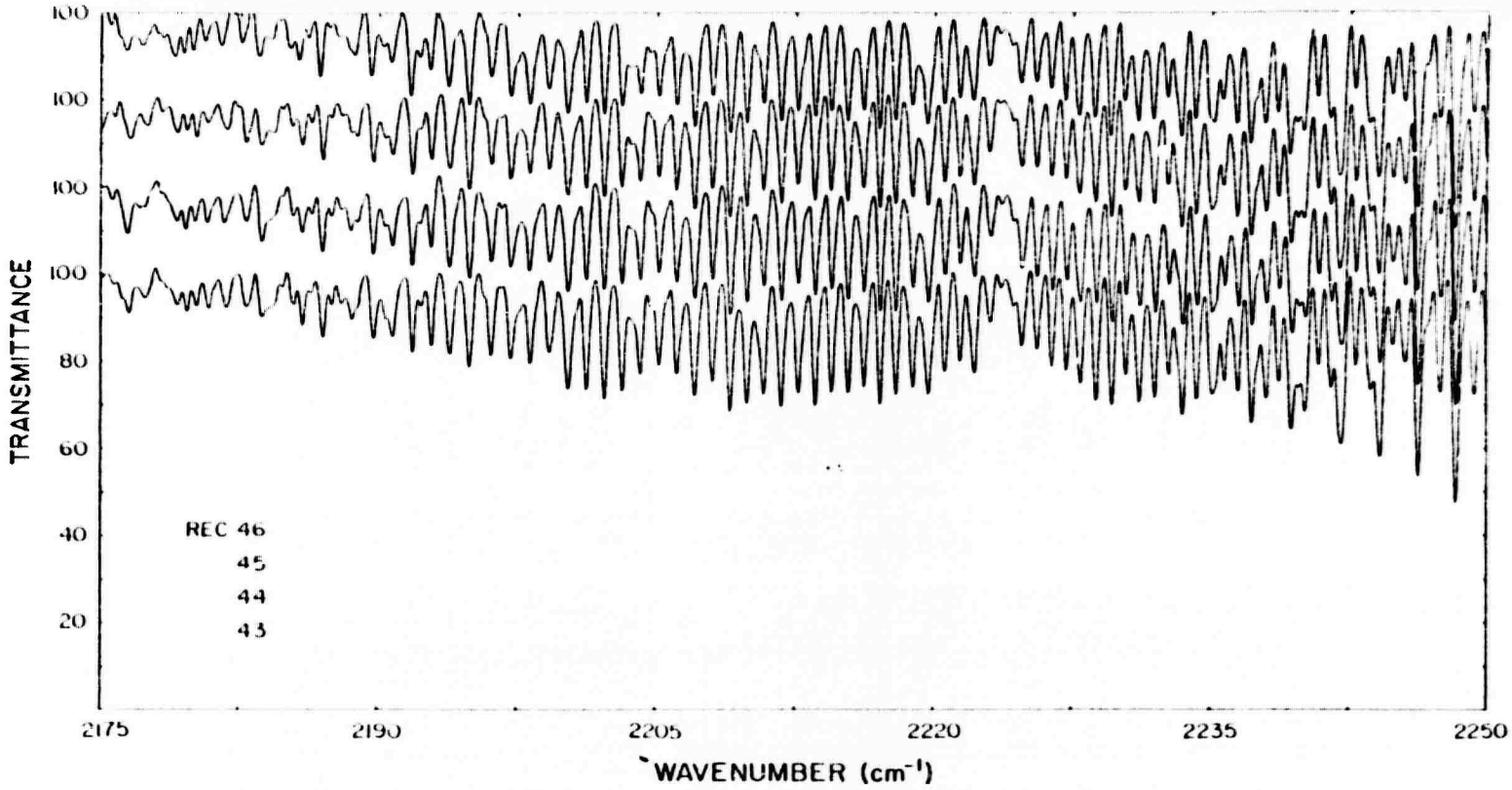

Figure 3-18. Atmospheric Transmittance vs Wavenumber at Various Altitudes for the 2175-2250 cm^{-1} Region, Records 43-46

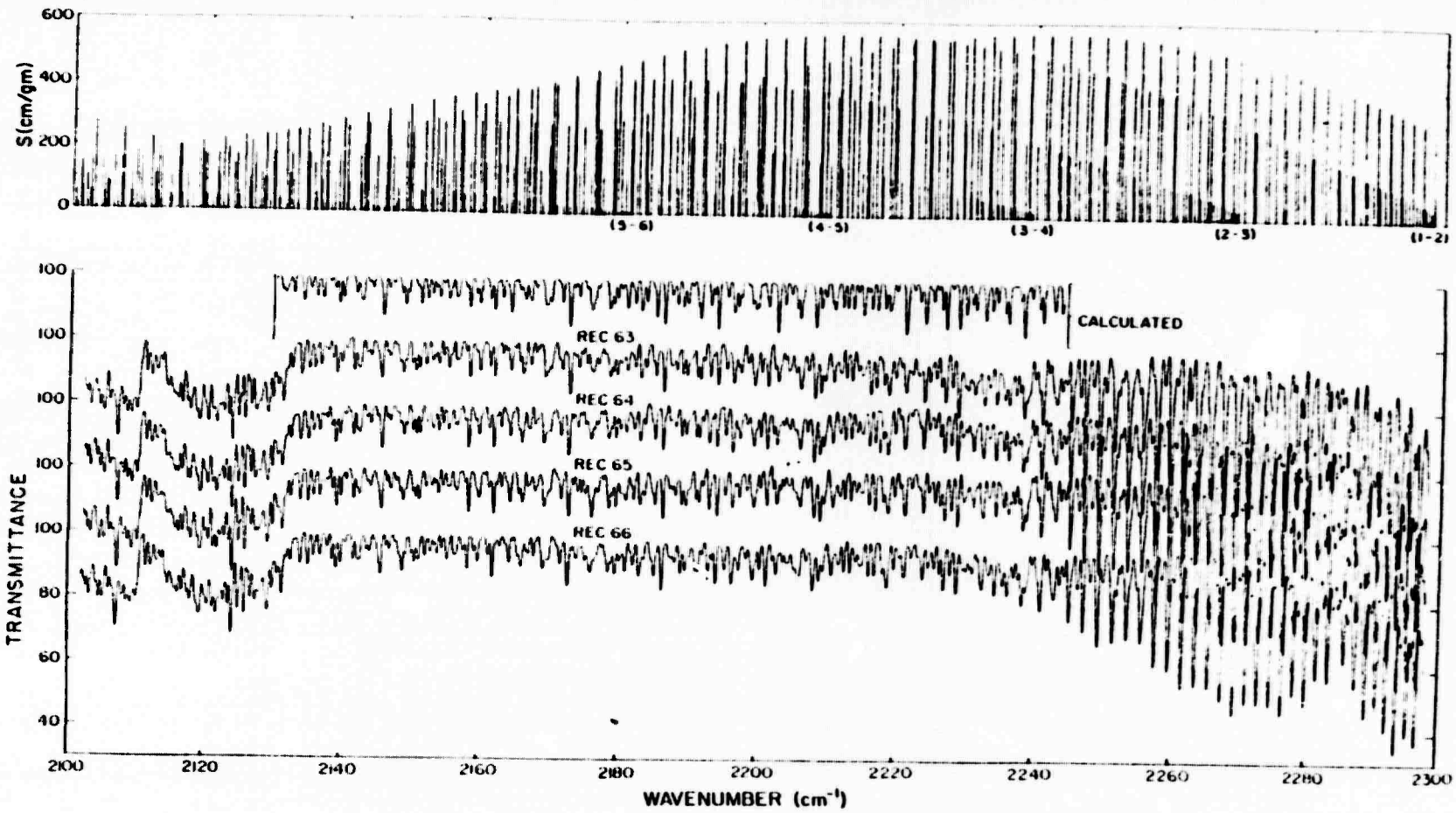

Figure 3-19. Solar Absorption in the CO Fundamental Region, and Its Interpretation as Solar CO at 4500° K

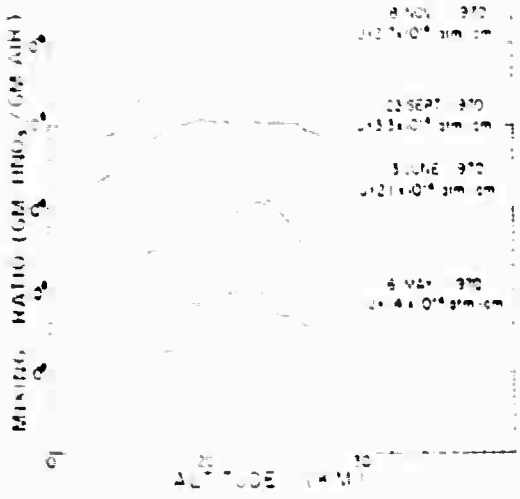

Mixing ratio profiles and total gas amounts for HNO_3.

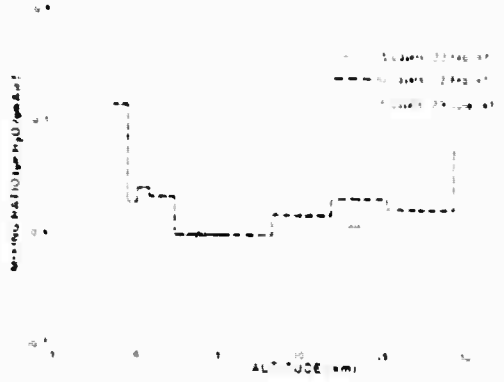

Mixing ratio of water vapor as derived from a 15-layer (solid line) and a 10-layer (broken line) calculation using the 25μ line group for the 22 February 1971 balloon flight. The slash near 14 km indicates the boundary between two layers with similar mixing ratio. The mixing ratio derived from a 15-layer calculation using the 25μ line group for the 29 June 1971 balloon flight is shown by the dotted line

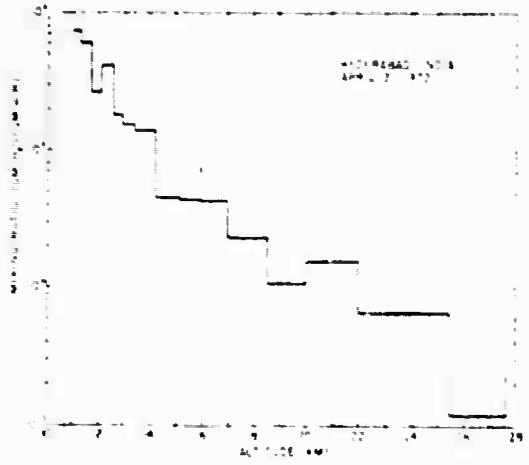

Mixing-ratio profile of H_2O as derived from a 16-layer calculation from the emission of the 25μ line group for the 21 April 1972 balloon flight made from Hyderabad, India.

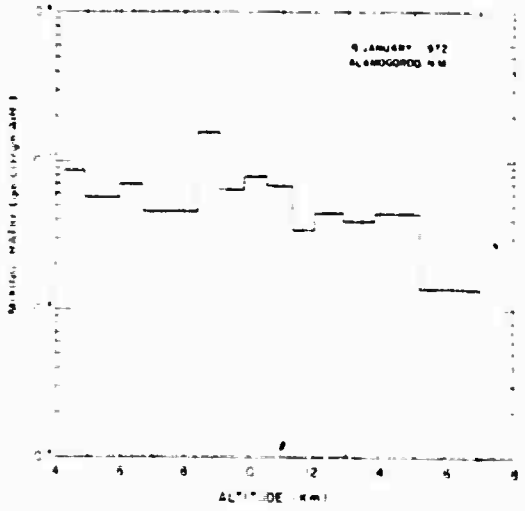

Mixing ratio of CO as derived from a 15-layer calculation using the R(2) and R(3) lines.

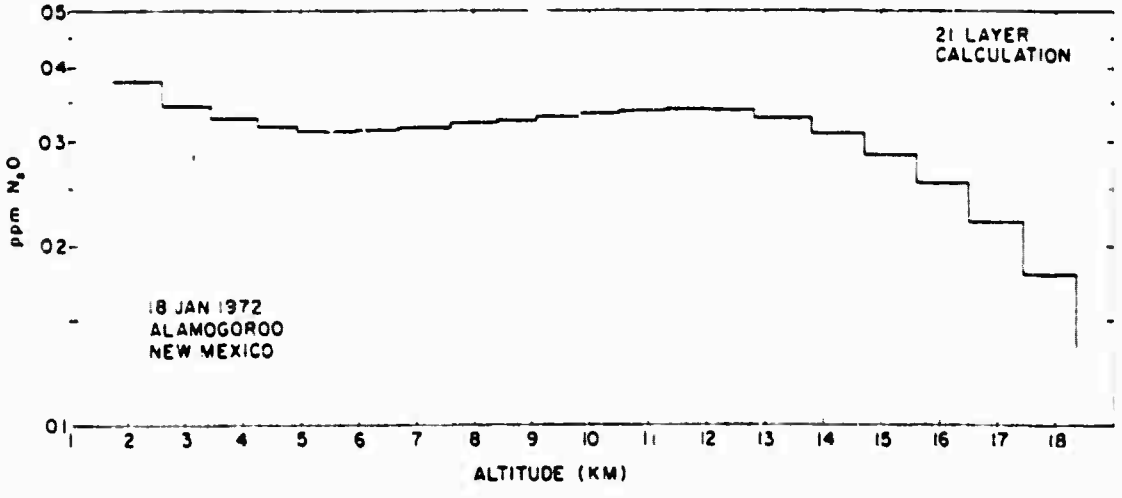

Mixing ratio of N_2O vs altitude as derived from a 21-layer calculation

Figure 3-20. Concentrations of Atmospheric Pollutants, Both Measured and Computed, vs Altitude

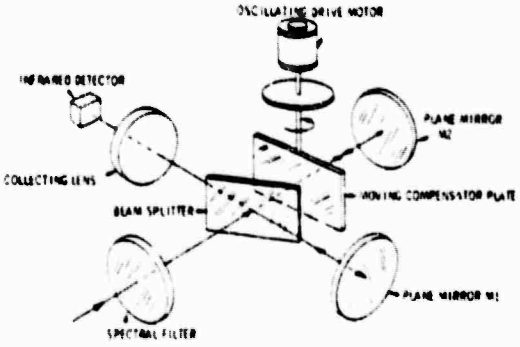

Figure 3-21a. COPE Correlation and Interferometer

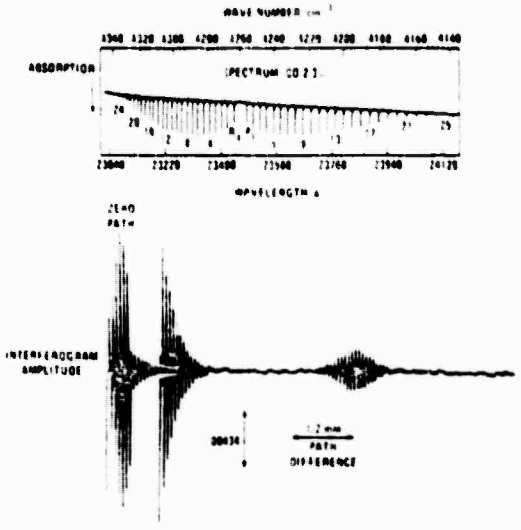

Figure 3-21b. Interferogram and Spectrum of CO

Table 3-5. Spectra Used for Interferogram

(cm^{-1})	Gas	Optical Thickness (atm-cm)
5156 - 4900	CO_2	250
	NH_3	0.036, 0.36
5048 - 4792	CO_2	250
	NH_3	0.0036*
4538 - 4282	CH_4	5.4
	CO	0.36
	NH_3	0.0036*, 0.036, 0.36
	NO_2	0.014*
	N_2O	0.9
4358 - 4102	CH_4	5.4
	CO	0.36
	NO_2	0.014*
3778 - 3522	CO	0.36
	CO_2	250
	NH_3	0.0036*
	NO	0.016*
	N_2O	0.9
3578 - 3322	CO_2	250
	NH_3	0.0036*
	NO_2	1.08*
	N_2O	0.9
3416 - 3160	NH_3	0.036
	N_2O	0.9
3116 - 2860	CH_4	5.4
	NO_2	0.014, 0.14
	N_2O	0.9
	C_2H_6	0.00182, 0.00288, 0.00405, 0.01120, 0.0205, 0.102, 0.507
	C_2H_4	0.0206, 0.0615, 0.1850
3038 - 2782	CH_4	5.4
3800 - 2700	C_2H_6	0.013, 1.3, 13, 99
	C_2H_4	99.8
3600 - 2700	C_2H_4	0.013, 1.3
	C_2H_4O	0.026, 0.13, 45.4
	$C_2H_6O_2$	0.013, 0.59
	$\alpha C_{10}H_{16}$	0.012, 0.5
	$\beta C_{10}H_{16}$	0.012, 0.36
2668 - 2412	CH_4	5.4
	N_2O	0.9
	SO_2	0.072
2598 - 2342	SO_2	0.072
2286 - 2030	CO	0.36
	CO_2	250
	N_2O	0.9
2018 - 1762	CO_2	250
	NH_3	0.0036*, 0.036
	NO	0.004, 0.016
1810 - 1554	NH_3	0.0036
	NO_2	0.014
1506 - 1250	CH_4	5.4
	NO_2	0.014*
	N_2O	0.9
	SO_2	0.0036

*No significant absorption.

- From each such combination spectrum, an interferogram was generated for various atmospheres with and without the trace gas of interest.

The estimated detection sensitivities are listed in Table 3-6. Interferograms for various gases, generated by computer as described above, are shown in Figure 3-22. The abscissa is the path difference caused by motion of the compensator plate.

3.2.8 Experiment No. 7 [Ref. 3-16]

The most famous of the experiments on passive sensing of the lower troposphere from satellite altitudes is that of the Nimbus satellite 4, (NASA), a joint project of Oxford and Heriot-Watt Universities. This satellite, in a polar orbit between 80°N and 80°S, carries a radiometer which measures thermal emission from the 15 micron band of atmospheric CO_2. Emission is spectrally selected in six different radiometric channels corresponding to observation of six different atmospheric layers 2 mb thick. This method depends on the fact that the CO_2 at lower altitudes is progressively warmer, so that its molecules populate higher vibrational levels. Data are sent routinely from the satellite to Washington, D.C., and from there to Oxford University, where they are processed online by computer. Profiles of temperature vs altitude and bs pressure are derived from the six radiances of each observation, down to ground level, for latitude bands 4° wide centered at 4° intervals between 80°N and 80°S. The atmospheric concentration of CO_2 is 3.3×10^{-4} by volume. For one of the six channels, the resolution is one cm^{-1} in band width and about 5 km in altitude.

Table 3-6. Estimated Detection Sensitivities Relative to CO (Assuming Source Intensity to be Independent of Wavelength)

Species	Filter Center Frequency (cm)	(μm)	Delay Range (mm)	Sensitivities Relative to CO = 0.04 atm-cm
CH_4	4280	(2.39)	5.5 - 6.4	5
			All other	2
CO	4280	(2.39)	2.3 - 3.5 5.6 - 6.3 7.4 - 9.4	1
CO_2	4835	(2.07)	5.0 - 6.0	2
			6.0 - 8.0	125
			All other	1250
H_2O	3465	(2.89)	All	1250
NH_3	4500	(2.22)	2.6 - 4.0	5
			6.3 - 7.5	10
N_2O	3465	(2.89)	3.0 - 3.6	5
			8.5 - 9.7	0.5
NO*	1900	(5.26)	2.8 - 3.7	0.2
			5.8 - 7.0	0.08
			9.0 - 9.5	0.08
NO_2*	1630	(6.13)	0.5 - 4.0	0.06
			All other	0.08
SO_2*	1370	(7.30)	~ 2.0	0.03
			2.5 - 4.0	0.2
			4.5 - 5.7	0.2
			8.0 - 9.5	0.3
C_2H_4*	2988	(3.35)	1.0 - 4.0	0.5
			4.5 - 5.5	0.2
			6.0 - 8.5	0.5
C_2H_6	2988	(3.35)	1.0 - 4.0	0.02
			5.0 - 7.5	0.008
			7.5 - 9.2	0.02

*Detector with a $D^* \approx 3 \times 10^{10}$ cm $Hz^{1/2}$ W^{-1}; all other species assume detector with a $D^* \approx 10^{11}$ cm $Hz^{1/2}$ W^{-1}.

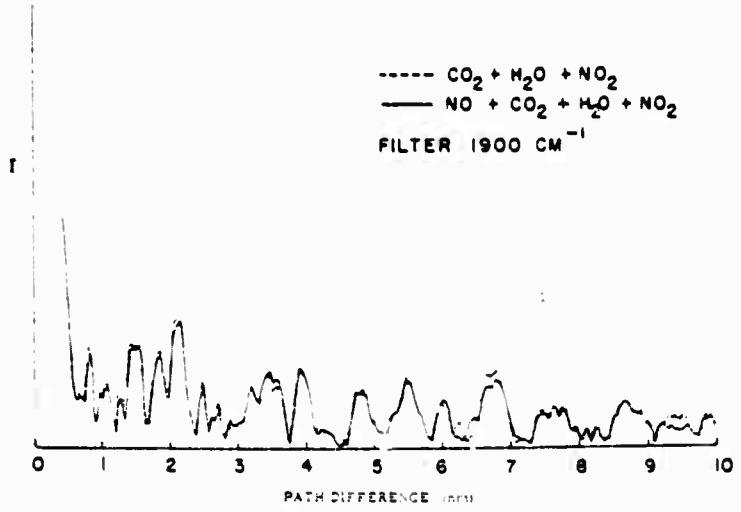

Figure 3-22a. CO Effect on Interferogram

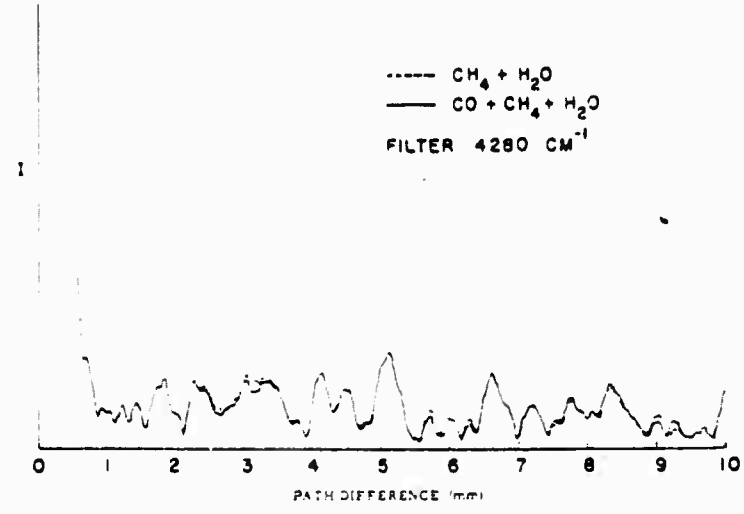

Figure 3-22b. NO Effect on Interferogram

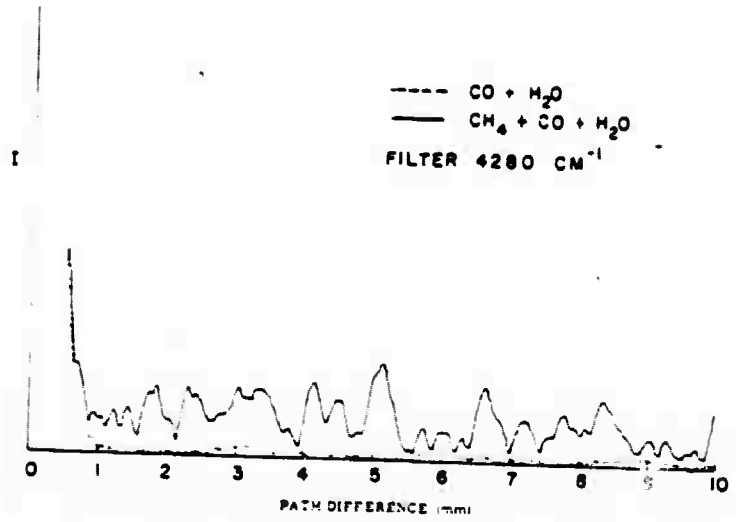

Figure 3-22c. Methane Effect on Interferogram

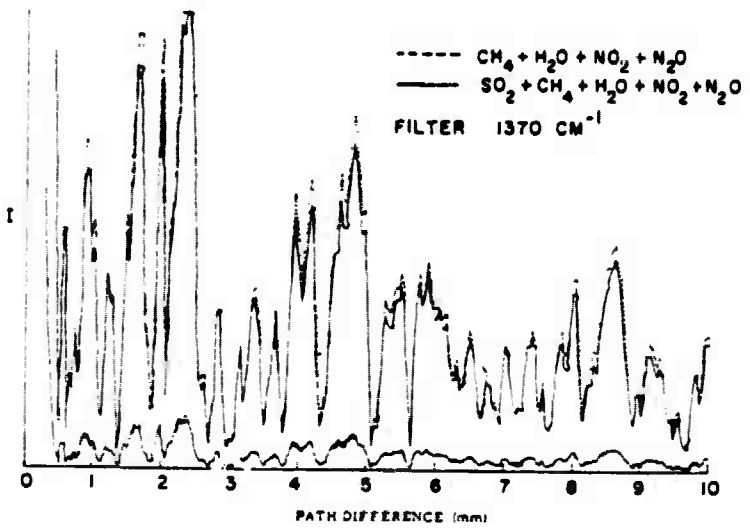

Figure 3-22d. SO_2 Effect on Interferogram

Figure 3-23 shows the weighting functions applied to the radiances measured in each of the six radiometric channels, and Figure 3-24 shows the temperatures evaluated for each of the four channels at the four highest altitudes, and how the averages of those temperatures are distributed globally for one particular day. The temperatures evaluated for upper atmospheric levels are routinely published in the quarterly Nimbus reports (Global Stratospheric Analyses, Oxford University, Atmospheric Physics Department), whereas those for ground levels are evaluated on-line by the computer but not published. The value of this experiment is that it has been reduced to a routine assessment of the vertical temperature profiles of the atmosphere all over the world, daily and hourly, with satellite-borne equipment. These temperature profiles will be useful in evaluating concentrations of gaseous pollutants in the lower troposphere, detected from other satellite-borne equipment (see Figure 3-25) [Ref. 3-16e].

3.2.9 Experiment No. 8 [Ref. 3-17]

Measurement of rotational emissions from interstellar molecules using ground-based radiotelescopes with diameters of, e.g., 10 meters. These radiations, typically in the region of 1 to 100 kilomegacycles, may be attenuated by as much as 100 decibels in traversing the earth's atmosphere. The molecular species which had been observed up to 1973 are listed in Table 3-7 together with the rotational radio frequencies which characterize them. The interstellar clouds which contain these molecules move both toward and away from the solar system, therefore the Doppler broadening of the rotational emission lines is large. Rotational spectra observed for several interstellar molecular species are shown in Figure 3-26. The clouds are usually optically thick so that the brightness temperature equals the excitation temperature of about $4^{\circ}K$ to $45^{\circ}K$. The emissions come from column densities of 10^{12} to 10^{16} molecules per cm^2. Reversing the geometry, a

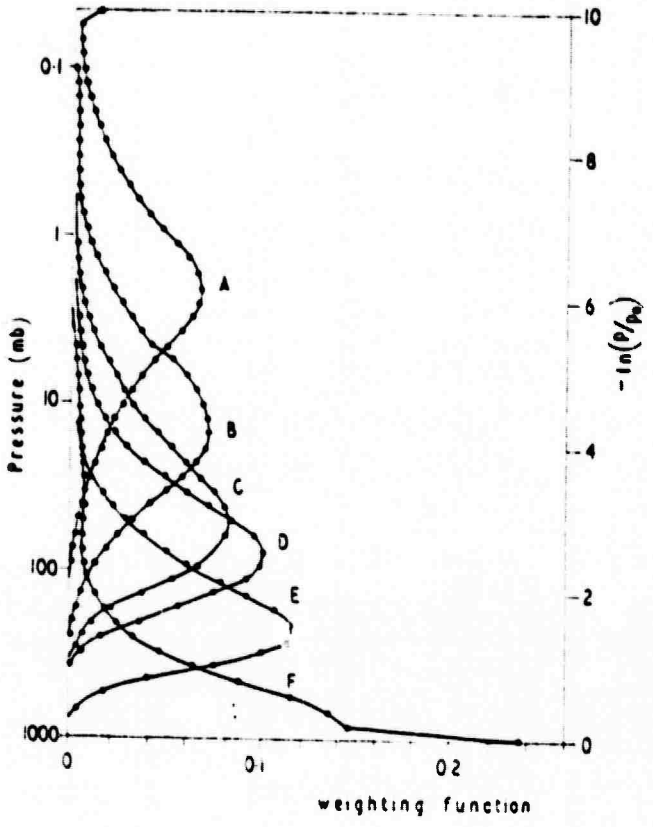

Figure 3-23a. Weighting Functions of the Nimbus IV SCR

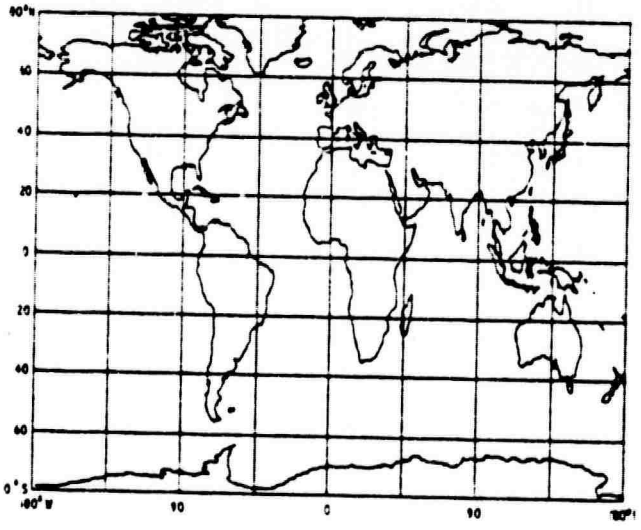

Figure 3-23b. Orbit Plot Overlay

A NOVEMBER - 6 DECEMBER

LAT	MEAN TEMPERATURE (K) A	B	C	D	STANDARD DEV. (K) A	B	C	D
80N	238.3	213.8	208.3	208.2	2.5	1.5	1.6	1.7
70N	236.7	214.1	209.4	209.8	1.8	1.2	1.5	1.5
60N	236.4	217.2	212.5	212.5	1.3	2.1	2.0	1.8
50N	239.3	221.7	217.1	215.9	1.8	1.3	1.1	1.0
40N	245.8	229.1	218.8	215.7	1.7	1.5	0.8	0.8
30N	253.8	234.5	221.6	218.7	1.4	0.9	0.5	0.6
20N	260.3	238.3	221.6	221.2	0.8	0.5	0.4	0.8
10N	262.2	240.9	221.3	222.1	0.7	0.4	0.5	0.7
0	261.1	241.1	221.2	222.1	0.7	0.5	0.7	0.7
10S	262.9	241.1	221.3	222.1	0.8	0.4	0.6	0.6
20S	261.1	241.6	222.0	221.1	0.7	0.6	0.6	0.7
30S	264.6	242.7	223.6	224.2	0.8	0.6	0.5	0.5
40S	266.9	246.2	225.6	228.4	1.1	1.1	0.6	0.6
50S	265.0	246.2	228.2	228.0	2.3	1.7	0.9	0.9
60S	267.1	249.5	232.7	229.1	2.0	1.7	1.0	0.9
70S	263.2	251.2	234.5	232.4	2.2	0.7	0.6	1.0
80S	271.4	255.7	238.1	233.5	1.8	0.8	1.2	2.2

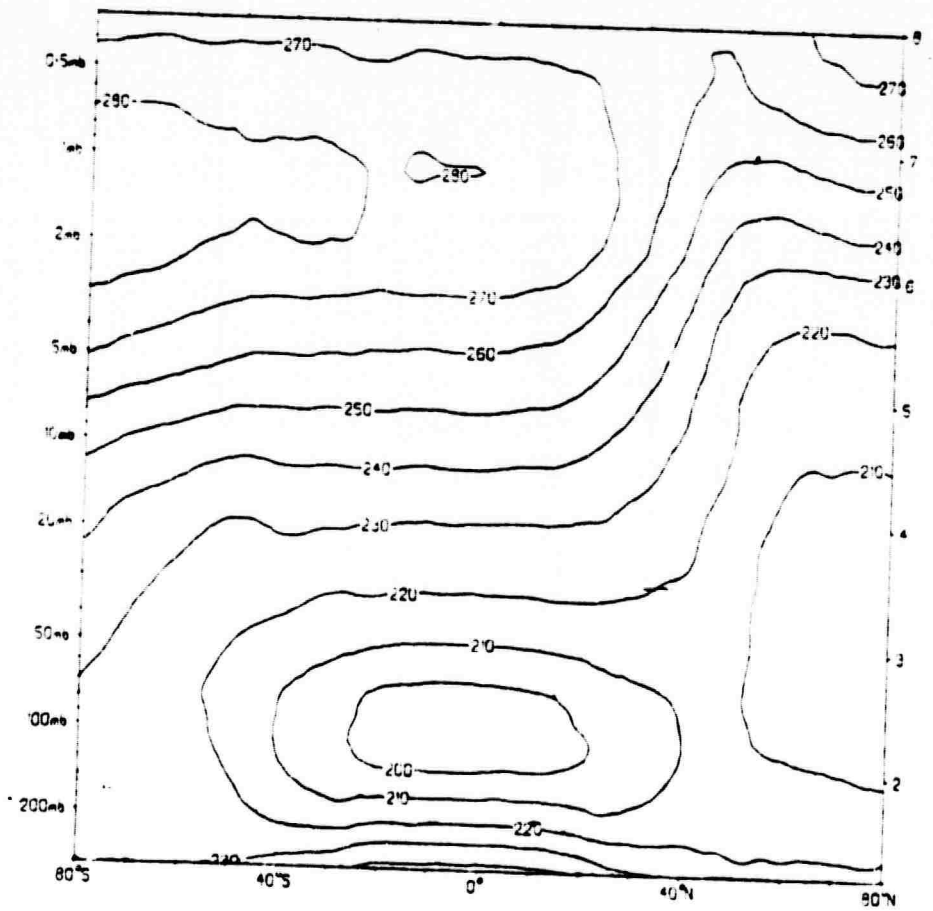

MEAN MERIDIONAL TEMPERATURE °K

DAY 326 1971

Figure 3-24. Typical Temperature vs Altitude and Latitude Plots Deduced from Nimbus Measurements

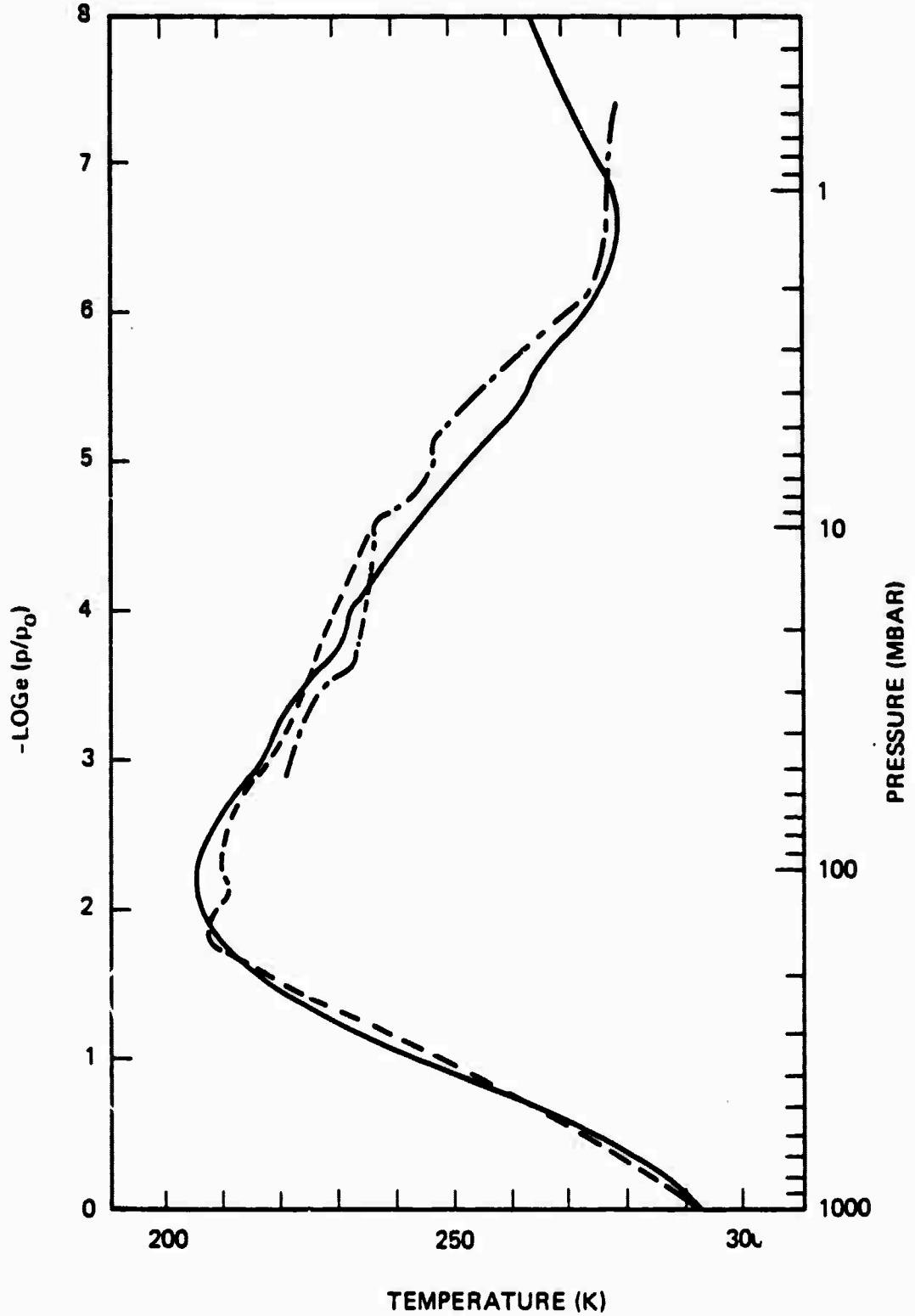

Figure 3-25. Comparison between Temperature Profile Deduced from the Radiances (Full Lines) over Wallops Island June 17, 1970, at 1644 Z Radiosonde from Wallops Island June 17, 1970, at 0000 Z, and rocketsonde from Wallops Island June 17, 1970, at 1630 Z

Table 3-7. Molecules Observed in the Interstellar Medium

Molecule	Frequency of discovery line (GHz)	Discovery transition	Isotopic species observed	Number of different radio transitions observed in all isotopic species	Approximate density* in molecular clouds (cm^{-3})
H_2		No radio lines, ultraviolet only in tenuous clouds; abundance in dense clouds deduced from CO observation and excitation			10^{+4}
CH^+	Optical only	—	$C^{13}H^+$	—	Not observed in H_2 clouds
CH	Optical only	—	—	—	Not observed in H_2 clouds
CN	Optical and 113.492	$J = 1 \rightarrow 0$	—	1	10^{-4}
OH	1.665	$J = 3/2$ Λ doubling	$O^{18}H$	10	10^{-2}
CO	115.271	$J = 1 \rightarrow 0$	$C^{13}O$; CO^{18}	3	1
CS	146.969	$J = 3 \rightarrow 2$	CS^{34}; $C^{13}S$	7	10^{-3}
SiO	130.268	$J = 3 \rightarrow 2$	—	1	(10^{-5})
H_2O	22.235	$J_{K_1K_1} = 6_{16} \rightarrow 5_{23}$	—	1	?
HCN	86.339	$J = 1 \rightarrow 0$	$HC^{13}N$; HCN^{15} DCN	6	maser only 10^{-3}
H_2S	168.762	$J_{K_1K_1} = 1_{10} \rightarrow 1_{01}$	—	1	10^{-4}
OCS	109.463	$J = 9 \rightarrow 8$	—	4	(10^{-4})
NH_3	23.694	$J_K = 1_1$ Inversion doublet	—	7	10^{-2}
H_2CO	4.830	$J_{K_1K_1} = 1_{11} \rightarrow 1_{10}$	$H_2C^{13}O$; H_2CO^{18}	10	10^{-4}
H_2CS	3.139	$J_{K_1K_1} = 2_{12} \rightarrow 2_{11}$	—	1	10^{-5}
HNCO	87.925	$J_{K_1K_1} = 4_{04} \rightarrow 3_{03}$	—	3	(10^{-4})
HCOOH	1.639 (possible)	$J_{K_1K_1} = 1_{01} \rightarrow 1_{11}$	—	1	—
HC_3N	9.098	$J = 1 \rightarrow 0$	—	3	(10^{-4})
CH_3OH	0.834	$J_{K_1K_1} = 1_{11} \rightarrow 1_{10}$	—	9	10^{-3}
CH_3CN	110.383	$J_K = 6 \rightarrow 5$	—	5	(10^{-4})
NH_2HCO	4.619	$J_{K_1K_1} = 2_{11} \rightarrow 2_{12}$	—	1	$(>10^{-5})$
CH_3C_2H	85.457	$J_K = 5_0 \rightarrow 4_0$	—	1	(10^{-4})
CH_3HCO	1.065	$J_{K_1K_1} = 1_{10} \rightarrow 1_{11}$	—	1	$(>10^{-5})$

*The densities are normalized to a typical molecular cloud with a hydrogen density of 10^4 cm^{-3}; values are arrived at from published column densities and estimates of optical depth effects; brackets indicate molecules observed only in Sgr B or A, near the Galactic center.

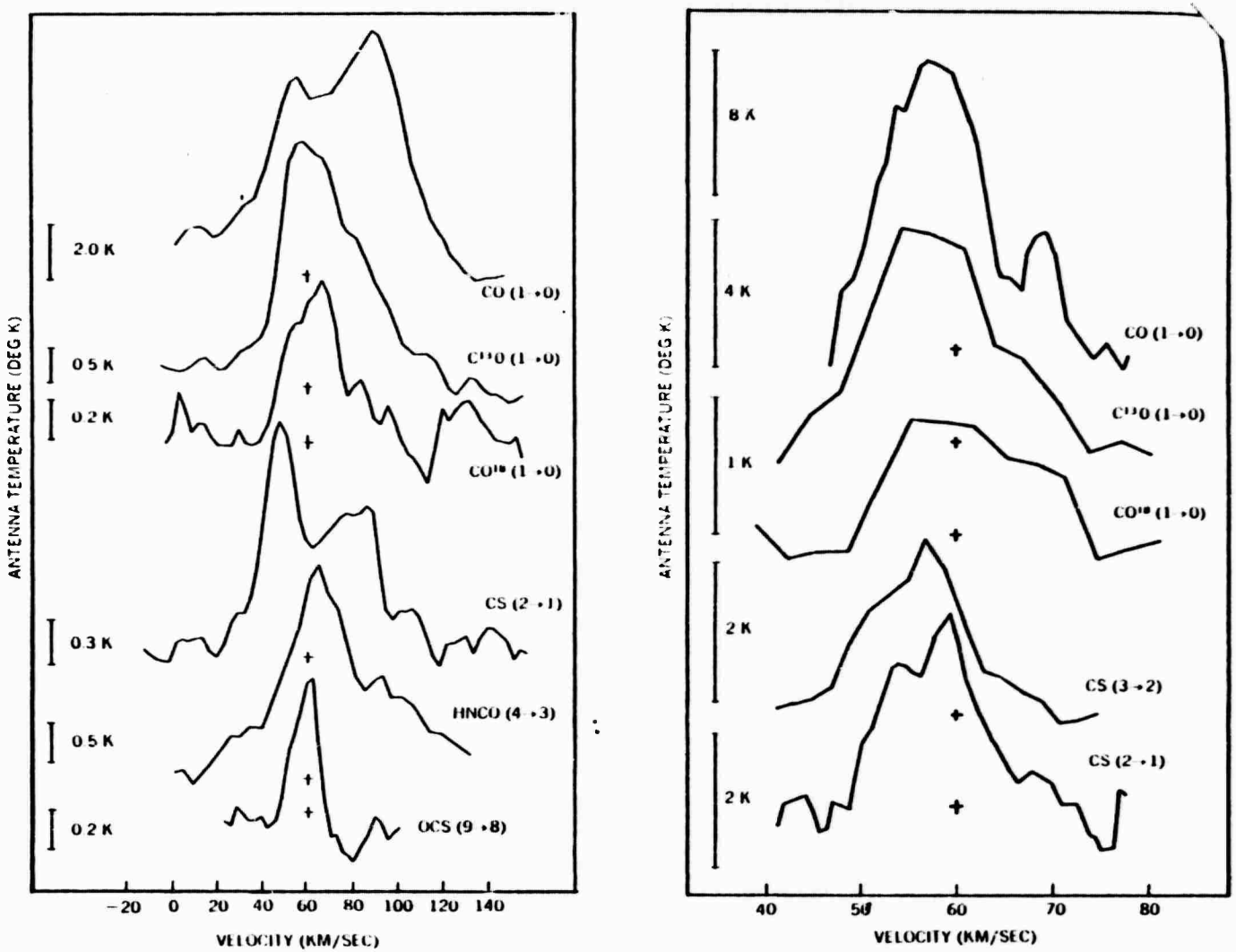

Figure 3-26a. Millimeter Spectral Lines Observed for Several Molecular Transitions in the Direction of SgrB (Left) and W51 Clouds. Intensity (Expressed as Ta) is Shown as a Function of Velocity Relative to the Mean Motion of Stars Near the Sun. Crosses Are at 60 km/sec and 0 Ta for Each Line

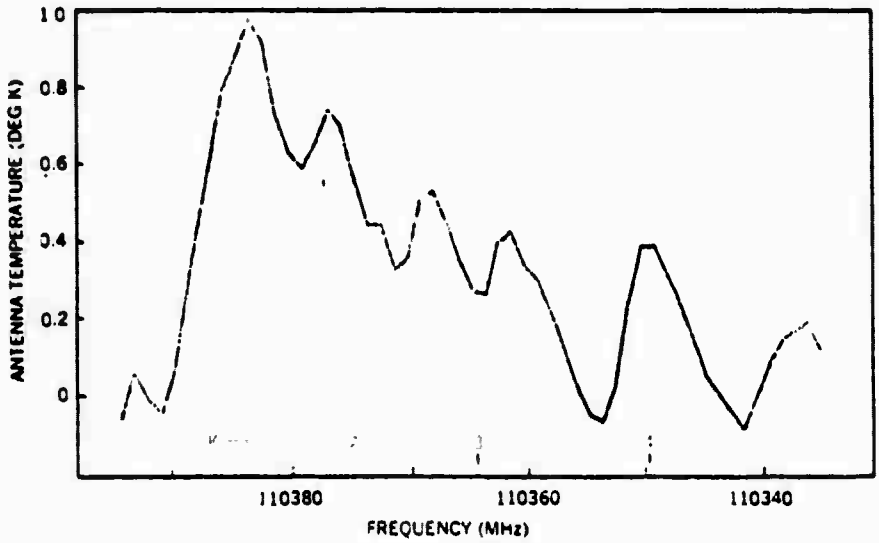

Figure 3-26b. Methyl Cyanide Emission from Sgr B2 (OH) in the $J = 6_K \rightarrow 5_K$ Transition. Five Lines, from K = 0-4, Contribute to the Profile. Relative Intensities of the Lines Indicate a Boltzmann Temperature of About 150°K for the K-Level Population. The K Levels Do Not Mix Radiatively. This Temperature Indicates the Kinetic Temperature. Observations Only 1 Arc Min from This Position Show Much Lower Excitation Temperatures

10-meter radio dish carried above the atmosphere looking down at trace gases in the lowest 50th of the atmosphere may be able to detect them at concentrations of perhaps a part per billion in emission against a cold surface. Instead of Doppler broadening, the rotational lines will be broadened by collisions.

3.2.10 Experiment No. 9 [Ref. 3-18]

A balloon-borne grating spectrometer with a spectral resolution of 0.35 cm^{-1} was used to observe the solar spectrum in the region 4.76 to 5.5 microns. (Thus in principle this instrument could be pointed down to observe similar phenomena against the glitter image of the sun in the surface reflection of oceans, lakes, rivers and ponds.) Absorption lines and bands of solar CO, telluric H_2O, CO_2, and N_2O, as well as NO were observed to a limit of 1 to 3 ppb. The detector was a liquid helium cooled GE:Cu solid-state crystal. Samples of the observed absorption spectra are shown in Figure 3-27.

3.2.11 Experiment No. 10 [Ref. 3-19]

An infrared heterodyne radiometer with a spectral resolution of 0.04 cm^{-1} was used for remote detection in the laboratory at room temperature. Each gas was observed remotely in air at 1 atm. Sensitivities as low as a few parts per billion were achieved. The detected radiation from SO_2, CO_2, O_3, NH_3, and CH_4 was mixed with the output of a local oscillator which was a CO_2 laser, at 10.6 microns. A CO laser at about 5.2 microns was used as the local oscillator for remote detection of NO in stack gases from stationary power sources. The local laser radiation and the radiation to be detected are combined by a beam splitter and then focussed onto the detector which acts as a mixer. The amplifier-and-filter system that receives the

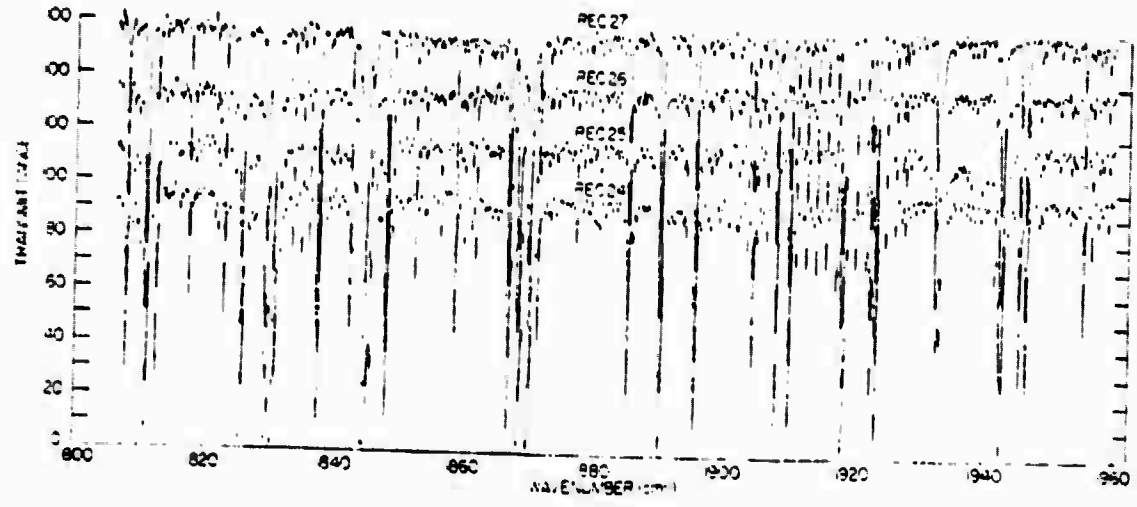

a. For the region 1800-1960 cm^{-1}

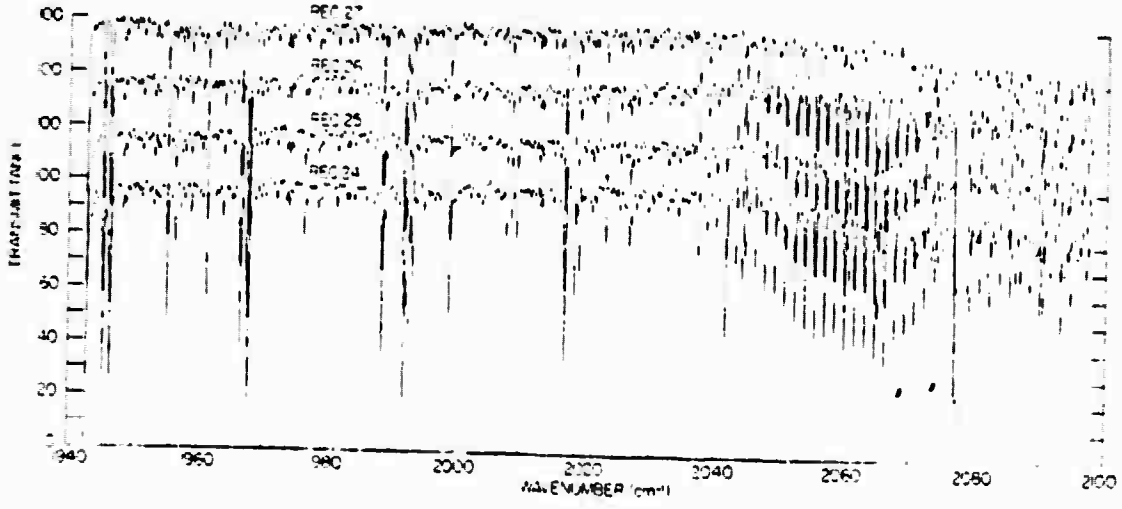

b. For the region 1940-2100 cm^{-1}

Figure 3-27. Observed Spectral Transmittance at Various Altitudes and Solar Zenith Angles. Rec 24 at 8.5 km and 60.37°; Rec 25 at 9.1 km and 60.78°; Rec 26 at 9.8 km and 61.20°; Rec 27 at 10.5 km and 61.57°

output of the mixer is sensitive to the beam frequencies above and below the local laser frequency. Each laser could be tuned over a large number of rotational frequencies by adjusting a grating at one end of the laser cavity. The mixing detector was a high-speed germanium photo-conductor doped with copper. The sensitivities achieved for detection of various pollutants are shown in Table 3-8. Using these sensitivities, the authors computed that the minimum detectable concentration of 0_3 would be 2 ppb under an inversion layer at a 1-km altitude, and that a downward-looking heterodyne radiometer in a space craft could monitor absorption lines of various gases by their absorption lines in the earth's 300°K blackbody spectrum. An analysis of the potential degrading effects of air turbulence indicates that, for radiometers operating above 5 microns, the collecting aperture at the satellite can be made as large as a 1-meter diameter.

3.2.12 Experiment No. 11 [Ref. 3-20]

An infrared heterodyne spectrometer using semi-tuneable semiconductor diode lasers was used at about 8.5 microns to measure laboratory spectral profiles of N_2O and to measure thermal emission from Mars and the Moon from the ground. These measurements were made using a 30-inch telescope to concentrate the infrared emissions. The collected infrared emissions are mixed with the output of a local source, namely the semiconductor diode laser emission, and the mixed signal is detected at the difference frequency, called the intermediate frequency. The limiting spectral resolution is set by the spread in the local semiconductor diode laser frequency, which can be less than 100 kilocycles/sec. Thus spectral resolutions exceeding $1/10^8$ are possible. This high potential resolution makes possible assessment of atomic and molecular species in remote sources at low densities and low temperatures. Figure 3-28 shows laboratory measurements of the N_2O absorption line, and ground-based measurements of Mars and the

Table 3-8. Experimental Sensitivities to Pollutant Gases. The Gases Were at 298 K, Except for NO, Which Was at 390°K. The Band Designations I and II Refer to the Upper and Lower of the Two Mixed ($10^0$0, $02^0$0) States

GAS	SENSITIVITY (atm cm)	LASER LINE	WAVELENGTH (μm)
NITRIC OXIDE	10^{-2}	$^{12}C^{16}O$: 7-6, P(15)	5.19
SULFUR DIOXIDE	10^{-2}	$^{12}C^{18}O_2$: $00^0$1-II, R(40)	9.02
OZONE	2×10^{-4}	$^{12}C^{18}O_2$: $00^0$1-II, P(40)	9.50
	2×10^{-4}	$^{12}C^{16}O_2$: $00^0$1-II, P(14)	9.50
ETHYLENE	5×10^{-5}	$^{12}C^{16}O_2$: $00^0$1-I, P(14)	10.53
AMMONIA	10^{-4}	$^{12}C^{16}O_2$: $00^0$1-I, P(32)	10.72

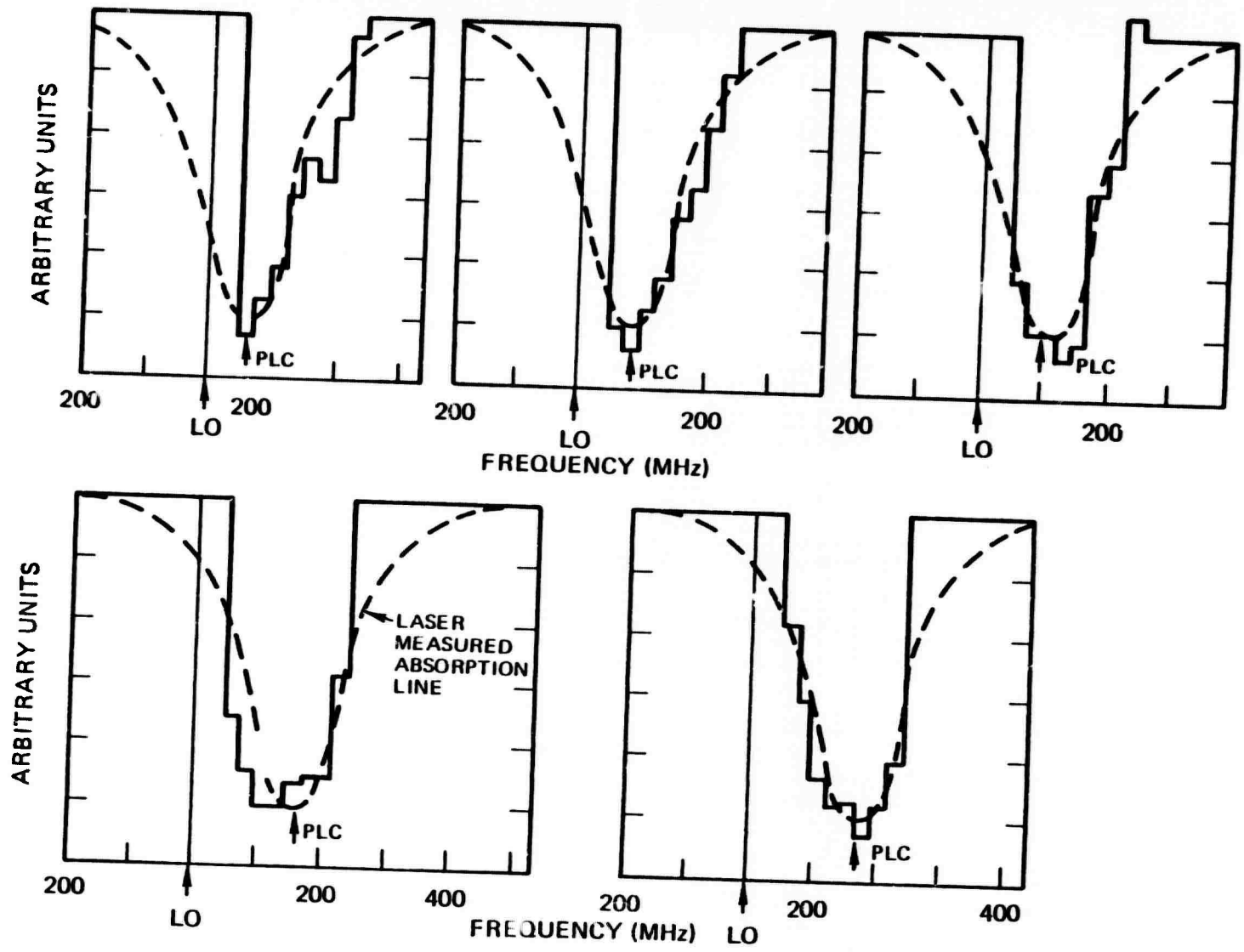

Figure 3-28a. Heterodyne Detection of N_2O Absorption. Absorption Line Profile Measured in the Direct Detection Mode

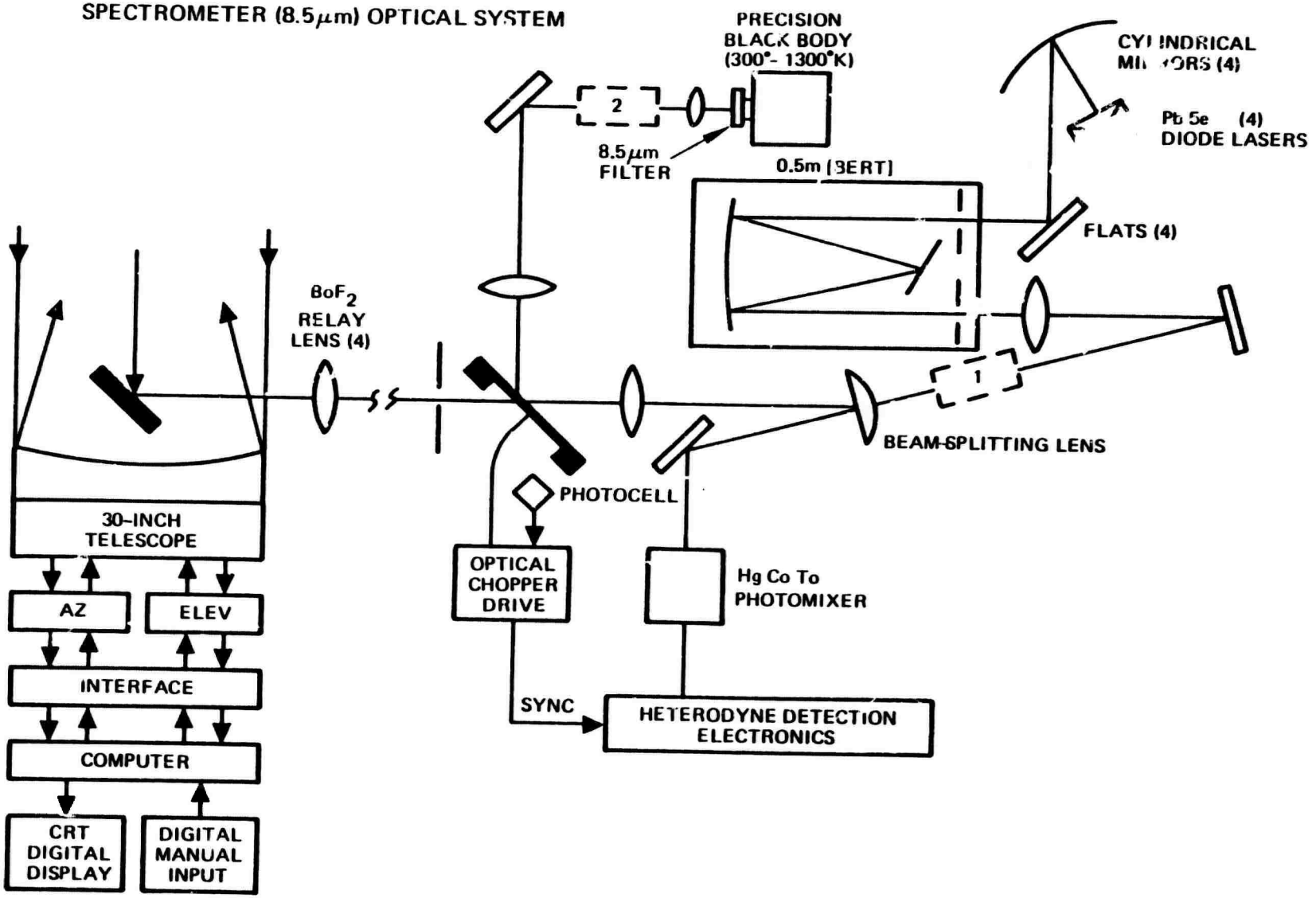

Figure 3-28b. Spectrometer (8.5 μm) Optical System

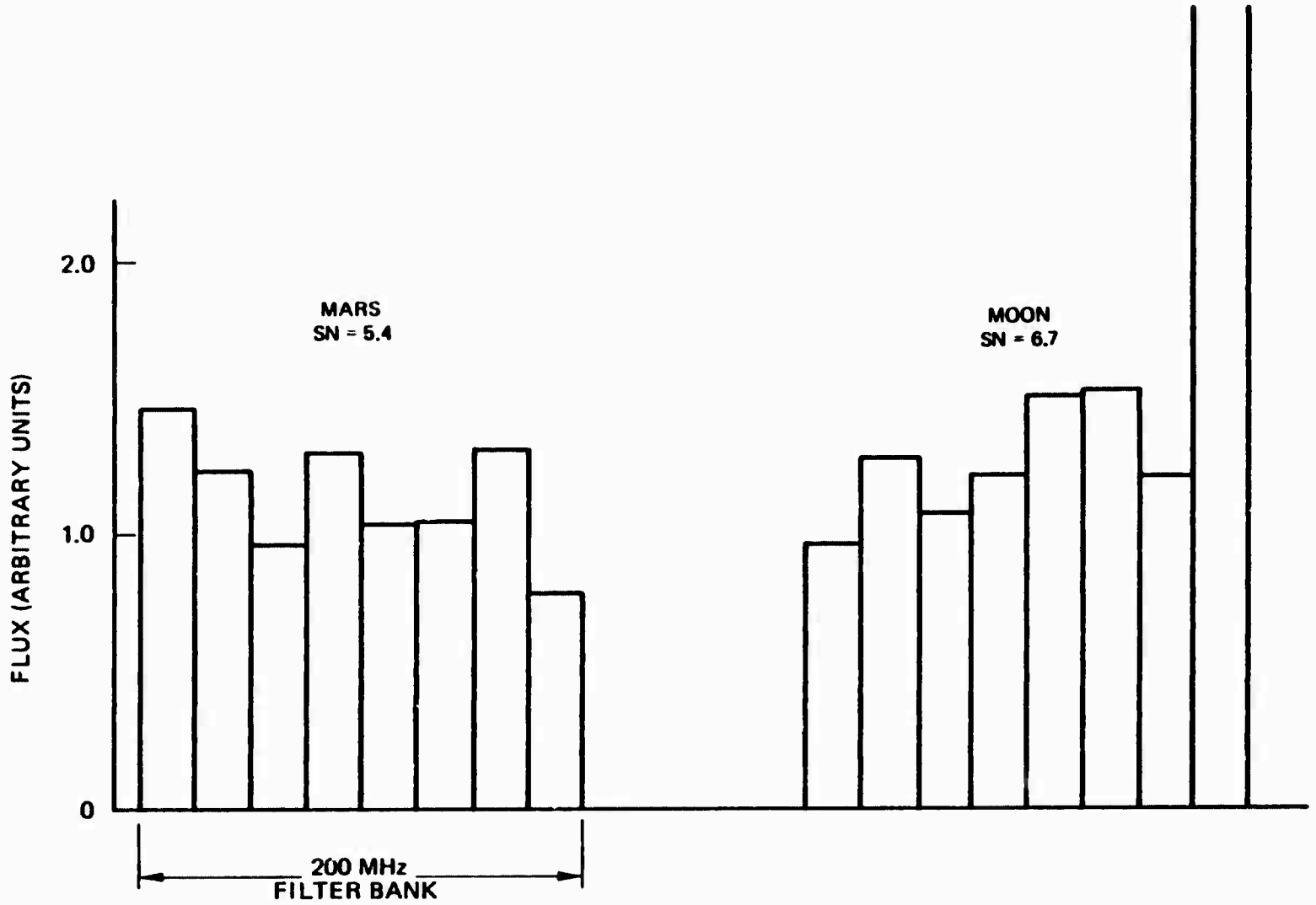

Figure 3-28c. Heterodyne Signals at 8.5 μm from the Moon and Mars. The Signal in Each Channel is Represented by a Bar with a Height Proportional to the Net Flux Received from the Source

Moon at 8.5 microns. Diode lasers emitting at 5-34 microns are commercially available from Arthur D. Little, Inc., having continuous tuning over 30 kilomegacycles at 8.5 microns. The quantum efficiency of the photodiode detector was between 2 and 6.5 percent. Hence, considerable improvement in detection efficiency is possible and should be limited only by quantum noise in the diode. This experiment used a PbSe semiconductor diode laser, and a HgCdTe photodiode as a photomixer and an 8-channel filter bank as receiver. The signal from the source was fed into the photomixer alternately with a calibration signal from a blackbody using a vibrating chopper.

3.2.13 Experiment No. 12 [Ref. 3-21]

Experiments pioneered by Alistair Gebbie at the National Physical Laboratory on millimeter wave detection of pollutant gases used a Cassegrain telescope mirror, that was small enough to fit in a suitcase and which focussed radiation onto a Michelson interferometer. The detector was a bolometer at room temperature. Resolutions of about 0.2 cm^{-1} were obtained. The interferometric record was put through a Fourier transform to obtain the spectrum of amplitude against frequency. Since then, these experiments have been much improved using InSb bolometers cooled to liquid helium temperatures. Spectra have been recorded from 300 to 3000 microns with a sensitivity as low as 0.067 cm^{-1}. The instrument has been used for sideways viewing of atmospheric emission at airplane altitudes in a Comet and in a Corcorde 002, and presumably in a down-looking geometry would detect absorption lines of the atmospheric pollutants against the radiation of the earth's surface, and against that in the solar glitter from the surfaces of bodies of water. Observed spectra are shown in Figure 3-29, and listed in Table 3-9. Experimentally measured mixing ratios are shown in Table 3-10. Signal-to-noise ratios of 50:1 have been achieved.

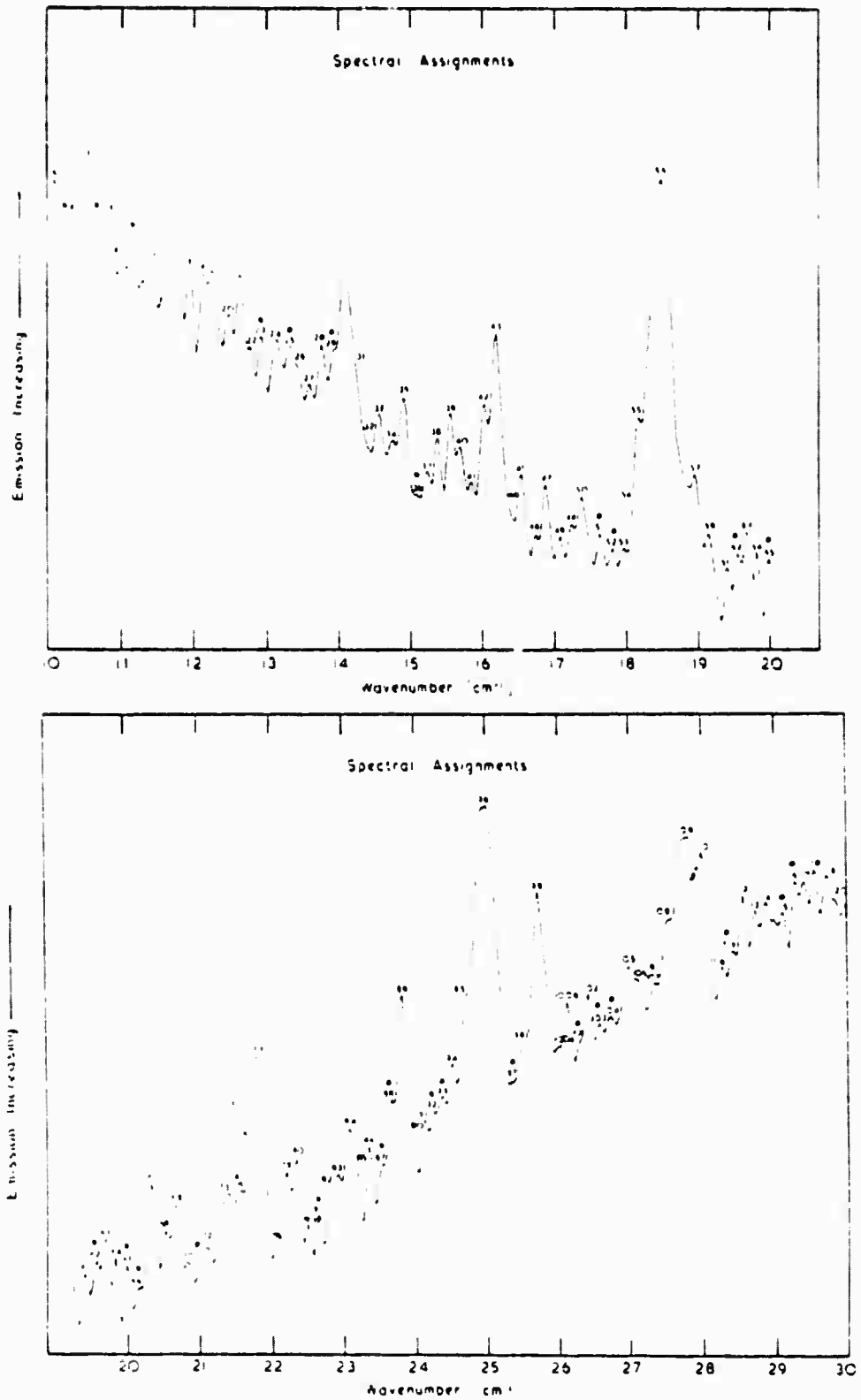

Figure 3-29. The Average of Two Spectra at a Resolution of 0.067 cm^{-2}

Table 3-9. Partial List of Spectral Line Assignments

Line Number	Measured Wavenumber (cm^{-1})	Predicted Wavenumber (cm^{-1})	Species
7	10.181	10.25	HNO_3
10	10.650	10.65	HNO_3
		10.72	N_2O
12	11.064	11.08	HNO_3
23	12.963	12.96	HNO_3
25	13.200	13.14	HNO_3
29	14.104 (s)	13.94	HNO_3
36	15.094	15.06	N_2O
51	17.593	17.58	N_2O
52	17.770 (s)	17.75	HNO_3
62	19.566	19.566	SO_2
65	19.988	20.00	N_2O
66	20.172	20.26	NO_2
		20.26	HNO_3
71	20.944	21.01	NO_2
81	22.578	22.59	N_2O
		22.62	HNO_3
83	22.96 (s)	22.89	NO_2
87	23.53 (s)	23.45	N_2O
88	23.71 (s)	23.67	HNO_3
92	24.262	24.18	NO_2
		24.26	N_2O
93	24.375	24.45	HNO_3
97	25.381	25.45	NO_2
		25.48	SO_2
101	26.287	26.14	HNO_3
103	26.609	26.54	HNO_3
104	26.766	26.73	NO_2
		26.76	N_2O
107	27.325	27.39	HNO_3
		27.339	O_3 (weak)
111b	28.47	28.44	NO
		28.50	SO_2
113	29.119	29.05	HNO_3
116	29.280	29.28	N_2O
		29.29	NO_2

Table 3-10. Experimentally Measured Mixing Ratios

Run Identifier (Date/number)	V_{HNO_3}	V_{H_2O}	V_{N_2O}	V_{NO_2}	V_{O_3}	Flight Altitude (h)		Tropopause Altitude (h_t)		$h - h_t$	Approximate Latitude and Longitude	
	$\times 10^9$	$\times 10^6$	$\times 10^9$	$\times 10^9$	$\times 10^6$	(kft)	(mb)	(kft)	(mb)	(kft)		
20/5.1	2.0	3.93	240	23	4.9	48	140	38	230	10	48N	08W
9/6.2+3	3.1	5.30	300	21	4.6	50	120	52	105	-2	01N	104E
11/6.1+2	3.4	6.60	275	22	4.6	48	125	50	115	-2	05N	110E
11/6.3+4	2.8	6.22	270	20	4.8	51.5	110	50	115	1.5	10N	115E
14/6.1+2	3.2	6.55	325	28	4.6	47	145	52 to 55	85 to 105	-5 to -8	35N	140E
15/6.2	2.9	5.70	270	26	5.5	44.5	155	52.5	100	-8	30N	135E
15/6.5	2.7	6.80	365	23	5.1	48	130	53	95	-5	18N	121E
20/6.1+2	3.2	5.90	265	24	4.8	45	150	37.5	230	7.5	35S	151E
20/6.3+4	3.0	3.60	190	23	3.7	49	120	37.5	230	11.5	35S	151E
20/6.6+7	1.9	2.55	215	18	4.8	47.5	130	37	235	10.5	37S	149E
20/6.8	2.7	3.60	215	16	3.7	40	195	37	235	3	40S	145E
22/6.2	2.1	3.15	210	18	4.9	49	125	39.5	200	9.5	40S	145E
22/6.3	3.0	5.62	350	22	5.4	40	195	39.5	200	0.5	40S	145E
23/6.1+2	2.5	2.49	240	23	4.0	52	105	37	235	15	30S	140E
23/6.3+4	2.7	10.2	390	(a)	5.9	40	190	52.5	100	-12.5	20S	133E
23/6.12+13	2.5	9.21	250	24	3.9	43	145	54	90	-7	12S	125E
23/6.14+15	3.2	8.75	245	25	4.9	52	105	52.5	100	-0.5	05S	115E
24/6.3	1.9	12.9	270	30	3.7	44	155	(b)			01N	104E
28/6.1+2	3.5	16.1	250	22	3.4	35	260	52.5	100	-17.5	20N	70E

Notes: (a) Tropopause too high
(b) No meteorological data available

3.2.14 Experiment No. 13 [Ref. 3-22 & 3-23]

The balloon-borne, 1/2-meter grating spectrometer with a liquid helium cooled Ge:Cu photodetector was used to obtain absorption spectra against the setting sun as a source. Spectral absorptions were observed which have been assigned to CF_2Cl_2 at 921 and 923 cm^{-1}, and to $CF\ Cl_3$ at 847 cm^{-1}. These spectral features occur in a window of the atmosphere between minor absorptions of HNO_3 and CO_2. The measured spectra are shown in Figure 3-30. By comparison with the absorption coefficients measured in the laboratory for these gases, mixing volumes of 5×10^{-11} and 2×10^{-11} were estimated respectively for the abundance of these two pollutants. Presumably in a down-looking geometry, concentrations of these gases in the lower troposphere could be measured to equivalent limits by measuring their absorptions of the continuous spectra of ground-based electrical lighting and the sun glitter.

3.2.15 Conclusions

We may conclude this section by assuming that it is assured that any gaseous pollutant which has rotational vibronic and/or electronic signatures in spectral windows of the atmosphere may be sensed remotely by the corresponding reflectance of sunlight if its concentration exceeds 0.02 ppm over a path of 1 km. There is a possibility to lower this threshold by combining spectroscopes simultaneously observing several bands characteristic of a given pollutant. This technology has been demonstrated up to a 30-km altitude (and perhaps has already been demonstrated up to a 30-km altitude and is already in use on satellites)*. The

*See, for example, titles announced for the International Conference on Environmental Sensing and Assessment to be held September 14-19, 1975, in Las Vegas, Nevada, co-sponsored by the World Health Organization, the U.S. Environmental Protection Agency, and the University of Nevada.

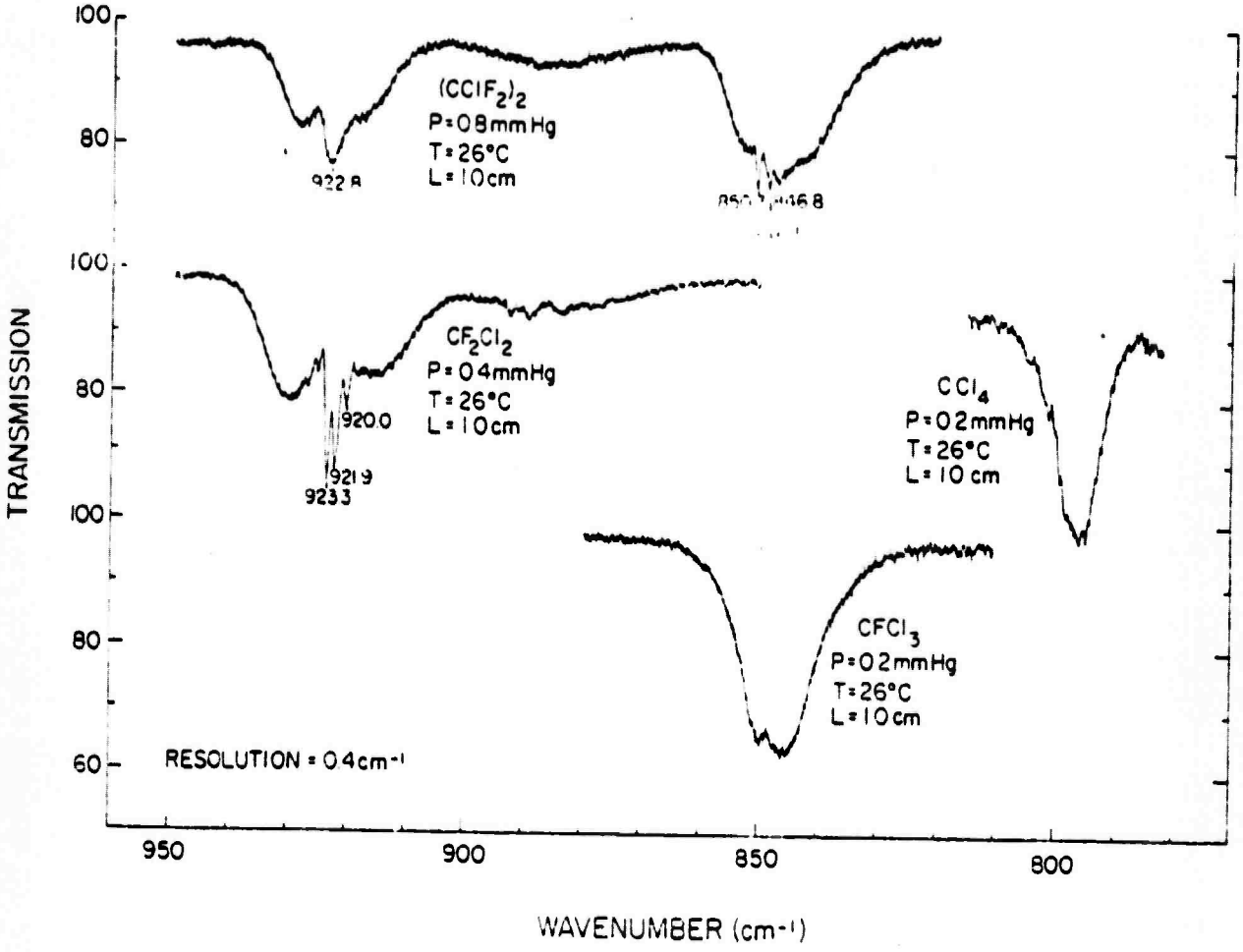

Laboratory absorption spectra of selected halogenated hydrocarbons in the 780-950 cm^{-1} region.

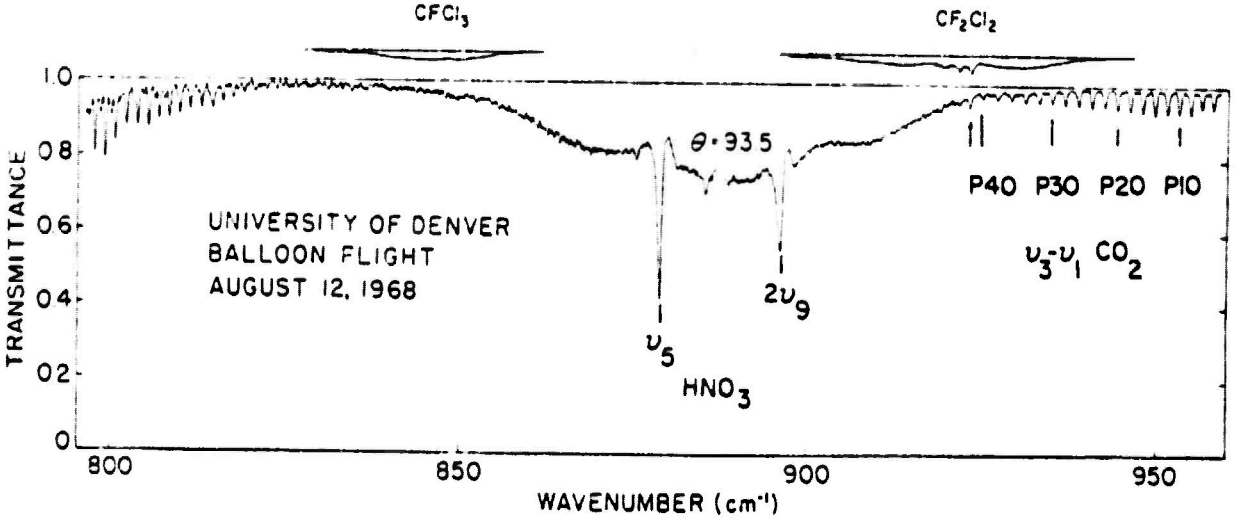

Solar spectrum observed at a height of 30.5 km and a zenith angle of 93.5°. The height of the tangent path is 18.4 km and the optical path is 6.0 air masses. The approximate height of the tropopause is 14 km. The volume mixing ratio for CF_2Cl_2 is 5×10^{-11} v/v and for $CFCl_3$ is 2×10^{-11} v/v.

Figure 3-30. Spectrum Observed at Various Altitudes

sensitivity may be increased also by finding more sensitive microwave and infrared detectors and more powerful reference lasers for heterodyning.

Consider the molecule, for example,

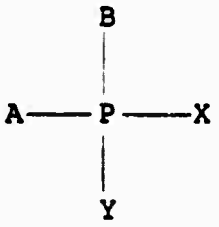

where A, B, X, and Y are ligand groups such as O, OH, F, S, SH, Cl, CN, CO, NH_2, C_nH_{2n+1}, OR, and R where R is a hydrocarbon ligand, etc. To determine the presence of this molecule in the low troposphere from satellite altitudes, one could construct masks in the spectrograph to fit the vibration spectra of two or more of these ligands, and construct two or more masks for vibration spectra of the bonds between P and the ligand groups. In this way, assessment of a particular polyatomic molecule could be obtained, at concentrations of down to 0.02 ppm. Heterodyning technologies where several characteristic molecular frequencies are combined with several reference laser frequencies have been proven as workable possibilities. It seems possible that the minimum concentration of assessment can be lowered.

Furthermore, the reflectance technique is practical for assay of oils on surfaces of waters and of pollutants in waters and for assay on the surface of the earth such as slag piles, mine tailings, ore piles, and the like.

3.3 EXCITATION OF VISIBLE AND INFRARED EMISSION AND ABSORPTION BY GROUND-BASED SOURCES SUCH AS FIRE, LIGHTNING, ARTIFICIAL ELECTRIC LIGHT, AND SUN GLITTER ON OCEANS, LAKES, RIVERS AND HARBORS

Ground-based sources which are capable of causing emission and absorption of electronic- and near-infrared transitions offer a gratuitous methodology of remote assessment of tropospheric gases, as follows:

Forest fires and urban fires including flare-offs of gases from oil wells and refineries can excite atomic and molecular emissions which are lines and bands in the visible and infrared, and can produce a visible infrared continuum against which absorption bands of gaseous molecules and their ligands may be observed. The same is true of concentrations of electric lights, such as those that characterize cities, highways, and airports at night. Some kinds of artificial lights emit lines (Ne, Na, Hg, etc.) as well as continua, but usually these lines are no hindrance (such lines are a common phenomenon in photographic exposures with astronomical telescopes, the radiation being scattered into the telescope by the atmosphere).

The sun glitter, by specular reflection on bodies of water, is a well-known phenomenon in the astronauts' photographs of the surface of the earth. See, for example, Specular Reflections of the Sun, This Island Earth, NASA SP-250 (1970), Washington, D.C., pp. 42-45, 49, 52, 54, 57 and 58; Earth Photographs from Gemini III, IV and V, NASA-SP-129, Washington, D.C. (1967), pp. 33, 34, 45 and 216.

The glittering spot enlarges as the wind waves enlarge. The spot is almost as bright as the sun and reflects all wavelengths able to come through the windows of the atmosphere. Thus,

measurements made with a spectrograph having its slit pointed at the glitter (or at the source of artificial light) and extending beyond the image of the source will show the spectrum of the source at the center of the photographic plate, overlain by absorption bands of pollutants, while the images of the extensions of the slit into the dark regions on each side of the light source might show the spectrum of emission lines and bands of excited atomic and molecular pollutant species. See Figure 3-31.

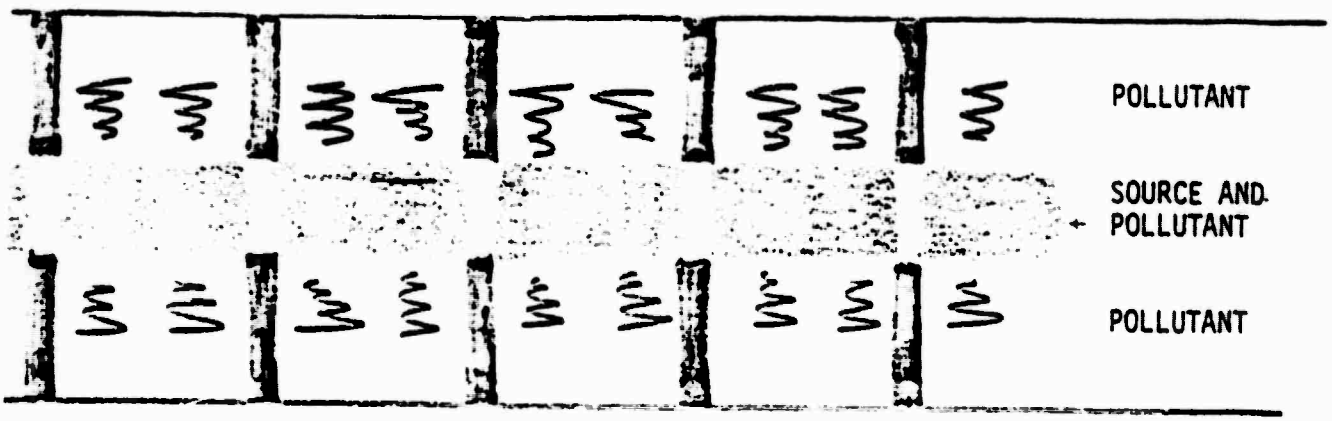

Figure 3-31. Spectra Observed with Spectograph Slit Laid Across Sun's Glitter into Regions of Little Reflection from Earth's Surface

If the source is the sun's glitter, there will also be Frauenhofer absorption lines. These are well known and therefore can be corrected.* An orbiting satellite will have frequent opportunities to measure spectra excited by the sun glitter. The sensitivity of detection can be enormously increased by replacing photographic flim with photomultipliers. Only about 3 photons

*Actually, in the solar light reflected from the ground, the Frauenhofer absorption lines are to a large extent filled in by Raman scattering [Ref. 3-23].

are needed to produce a count in a photomultiplier whereas sufficient blackening of film to produce a line (compared with random black spots in the film) requires a much larger photon flux.

3.4 EXCITATION BY TROPOSPHERIC LIGHTNING

3.4.1 Experiment No. 14 [Ref. 3-24]

A slitless spectrograph has been used in Tucson since 1960 to study the spectra of lightning flashes. Being slitless, the image of the stroke is depicted on the film in a wide range of wavelengths. Also, absorption bands appear in the continuum light of the stroke. The spectrograph has an aperture of 8 cm, a focal length of 61 cm, and a dispersion of 25 Å/mm. Spectra have been obtained in the near ultraviolet, visible, and infrared, from 4000 Å to 9500 Å. Photographs have been made using a fixed film holder so that integrated spectra are obtained for several strokes, and using a rotating drum for study of single strokes. Emission lines and absorption bands observed are listed in Table 3-11. Reproductions of some of the infrared spectral features are shown in Figures 3-32 and 3-33. In emission, lines were obtained only from neutral atoms such as nitrogen, oxygen, argon, carbon, and hydrogen. No molecular bands were observed in emission, but O_2 and H_2O bands were observed in absorption of the continuum light of the stroke. The emission lines of the neutral atoms come even from levels close to the ionization potential. Multiple discrete lines of OI are emitted from upper excitation levels above the ionization potential of OI.

3.4.2 Experiment No. 15 [Ref. 3-25]

A larger slitless spectrograph, focal length 122 cm, aperture 20 cm, and dispersion 12 Å/mm gave new information, for example, absorption bands of water vapor near the center of H alpha and

Table 3-11. Lines Identified in the Slitless Spectrum of Lightning from 6563 to 8820 A

λ	Source	Multiplet No. & UEP(eV)	Remarks
6562.8	H	(1) 12.0	v. broad
6610.6	N II	(31) 23.4	sharp
6645.0	N I	(20) 13.6	diffuse
6653.4	N I	(20) 13.6	diffuse
6723.1	N I	(31) 13.6	diffuse
6726.4	O I	(2) 10.9	diffuse; 2 lines within 0.2 A
6868	O_2		absorption band
7156.8	O I	(38) 14.4	single line. UEP is 0.8 eV above ionization potential of O I. See also O I (34), (35), (37), (55).
7423.6	N I	(3) 11.9	
7442.3	N I	(3) 11.9	
7468.3	N I	(3) 11.9	blends with O I (55).
7476	O I	(55) 15.7	central λ for 6 lines within 9.3 A
7503.7	Ar I	(8) 13.4	
7593	O_2		absorption band
7723.8	Ar I	(1) 13.1	
7772.0	O I	(1) 10.7	usually show
7774.2	O I	(1) 10.7	as a close
7775.4	O I	(1) 10.7	pair.
7939.5	O I	(35) 14.0	
7943.2	O I	(35) 14.0	blend of 6 components resolved
7947.2	O I	(35) 14.0	as two lines in spectrum.
7947.6	O I	(35) 14.0	
7950.8	O I	(35) 14.0	blend of 6 components resolved
7952.2	O I	(35) 14.0	as two lines in spectrum
8014.8	Ar I	(1) 13.0	
8103.7	Ar I	(3) 13.0	
8115.3	Ar I	(1) 13.0	
8184.8	N I	(2) 11.8	
8188.0	N I	(2) 11.8	
8200.3	N I	(2) 11.3	
8210.6	N I	(2) 11.8	
8216.3	N I	(2) 11.8	
8223.1	N I	(2) 11.8	Blends with O I (34)
8228	O I	(34) 14.0	Central λ for 7 Lines within 13.5 A
8242.3	N I	(2) 11.8	
8264.5	Ar I	(8) 13.3	
8408.2	Ar I	(8) 13.2	
8424.6	Ar I	(3) 13.0	
8446.6	O I	(4) 10.9	Central λ for 3 Lines within 0.4 A
8521.4	Ar I	(8) 13.2	
8567.7	N I	(8) 12.1	
8594.0	N I	(8) 12.1	Completely resolved multiplet
8629.2	N I	(8) 12.1	with no blends
8655.9	N I	(8) 12.1	
8680.2	N I	(1) 11.7	
8683.4	N I	(1) 11.7	
8686.1	N I	(1) 11.7	
8703.2	N I	(1) 11.7	
8711.7	N I	(1) 11.7	
8718.8	N I	(1) 11.7	
8728.9	N I	(1) 11.7	
8747.4	N I	(1) 11.7	
8820.4	O I	(37) 14.1	Single line

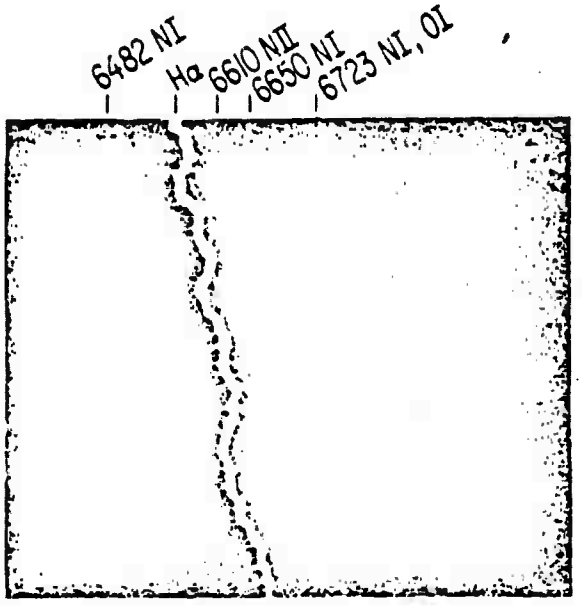

Figure 3-32a. Region of H-alpha--Enlargement of a Negative from 0.6 meter Spectrograph

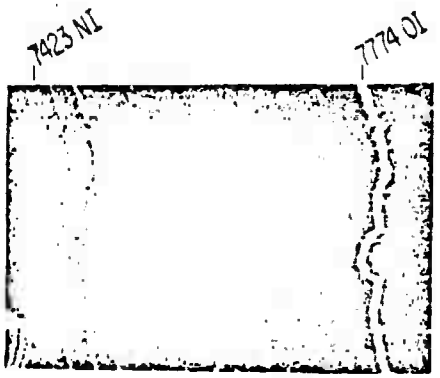

Figure 3-32b. Region of 7423 A to 7774 A-- Broadened NI and OI Lines

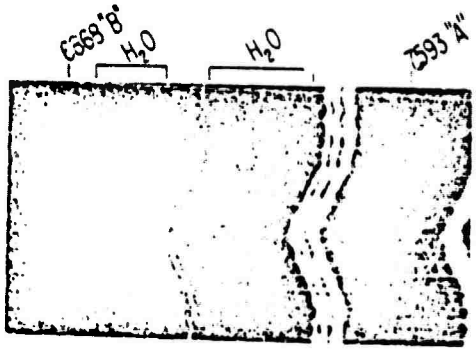

Figure 3-32c. Absorption Bands Due to O_2 in Air-Path

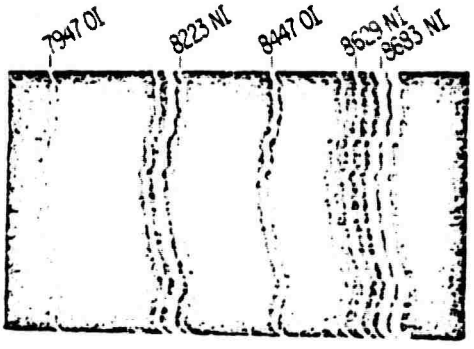

Figure 3-32d. NI and OI Multiplets, from 7947 A to Region of 8683 A

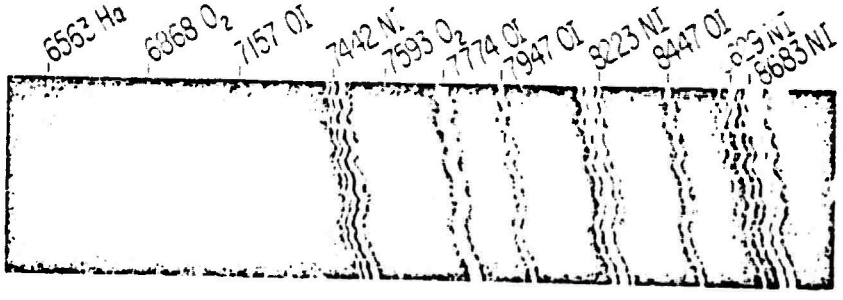

Figure 3-32e. A Slitless Spectrum of Lightning in Near Infrared

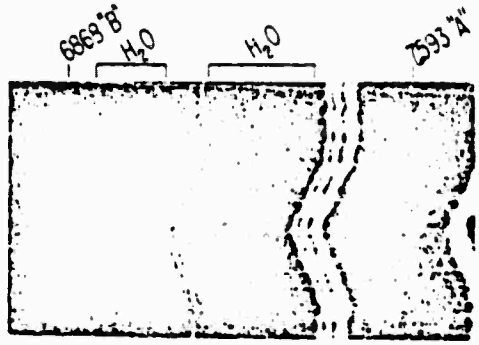

Figure 3-33a. Absorption Bands Due to O_2 in Air Path

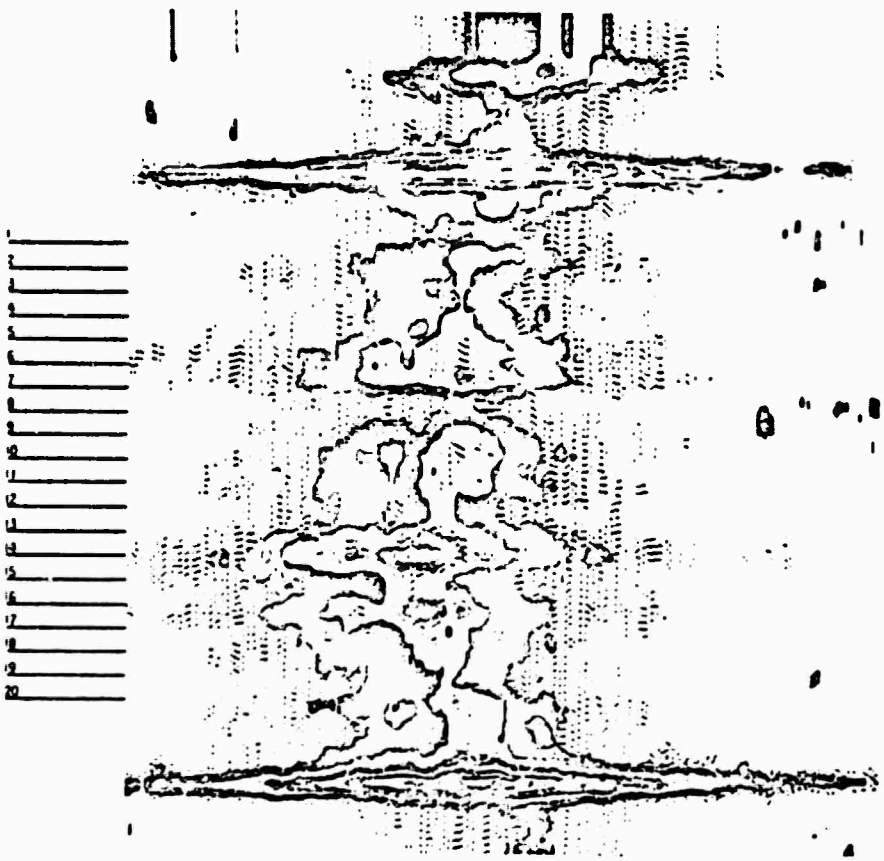

Figure 3-33b. Isodensity Tracing of H-Alpha

in its wings, and more absorption bands between the absorption bands of O_2 at 6868 and 7593 A. The emission lines are broadened by Stark effect in the strong electric fields of the strokes so that theoretical dispersions are not obtained. Comparison of relative intensities of emission lines of multiplets allows the temperature of the lightning strokes to be determined as 24,000 to 300,000°K. Salvane is developing the use of a slitless spectrograph at 3000 to 3300 A [3-24].

3.4.3 Experiment No. 16 [Ref. 3-26]

Orville uses a slitless spectrograph with a moving high speed streak camera. The focal length is 20 cm, and the dispersion is 72 Å/mm The writing rate of 0.12 nm/μsec produces a 4-μsec time resolution. In this way, it is observed that singly ionized NII emissions emit first within 10 μsec followed by an emission of a continuum, which in turn is followed by neutral emission of O, C, N and especially H as shown by the streak spectra in Figure 3-34. The stroke temperature vs time is found to decay from ~36,000°K with a half-life of about 20 μsec. The electron densities are ~$10^{18}/cm^3$ in the first 5 μsec decreasing to $10^{17}/cm^3$ at 25 μsec. Electron densities may be much higher at times less than ~5 μsec. Pressures in the stroke at 5 sec are about 10 times atmospheric, and densities are correspondingly increased about a factor of 10 (see Figure 3-34). (N.B., although NIII emissions are predicted, they had not yet been observed in Experiment 16.)

3.4.4 Summary

One notes that neutral emission lines of argon are excited in lightning strokes. Argon is present to about 1 percent by volume in air. Whe metal reprocessing plants for nuclear fuels are

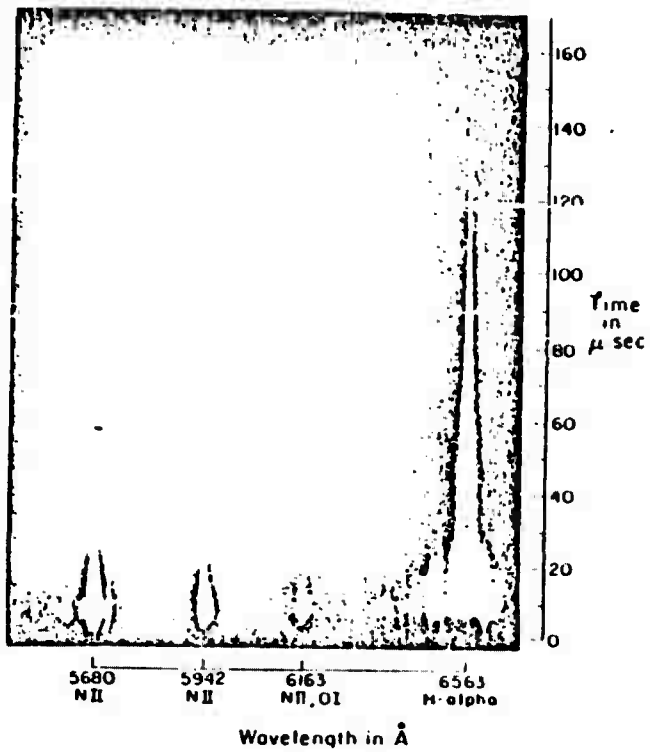

Figure 3-34a. High-Speed, Time-Resolved Spectrum of a Lightning Stroke (b) the Same Negative Used in (a) Has Been Printed with Less Exposure to Show the Persistence of Several Lines

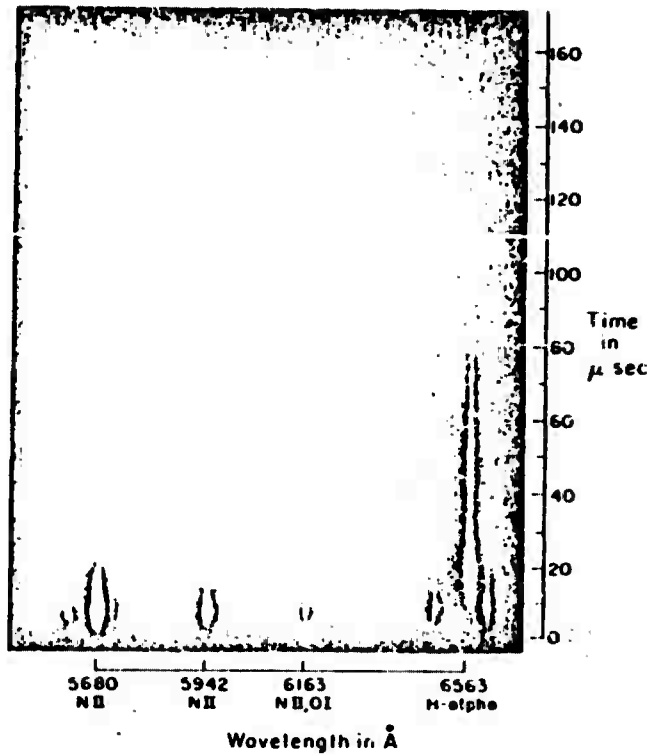

Figure 3-34b. High-Speed, Time-Resolved Spectrum of a Lightning Stroke (a) A 10-m Section of a Lightning Return Stroke Has Been Isolated and the Spectral Emissions Streaked in Time. The Time Resolution is 5 Sec. Singly Ionized Atoms Emit First, Followed by the Continuum Radiation, which in Turn is Followed by the Neutral Emissions (H-Alpha)

active, their stack gases contain several percent of krypton, xenon, bromine and iodine. In principle, lightning storms far downwind of the stacks might excite observable emission of the neutral and singly ionized states of these atoms and hence allow their presence to be detected by remote assessment in the visible and near infrared. Measurements on atmospheric spectra stimulated by lightning should be carried out near industrial centers in order to determine if interesting pollutants may be assessed remotely this way.

REFERENCES TO SECTION 3

3-1. W. Heitler, The Quantum Theory of Radiation, Third Edition, Oxford at the Clarendon Press, 1954, p. 36.

3-2. H. A. Kramers and W. Heisenberg, Zs. f. Phys., 31, 1925, p. 681.

3-3. Jeppeson Company, 8025 East 40th Avenue, Denver, Colorado 80207, telephone 303/320-6070.

3-4. "An Eye on the Enemy Over the Horizon," New Scientist, November 1974, pp. 420-423, and Appendix A.

3-5. J. M. Hendrick and M. I. Skolnick, Proceedings IEEE, June 1974, pp. 664.

3-6. C. E. Grosch, M. J. Henich, H. A. Montes, and E. S. Posmentier, Summary Report, Atmospheric Propagation Studies, September 1969; and H. A. Montes, Summary Report, Atmospheric Propagation Studies, Teledyne Isotopes, Westwood, New Jersey, IWL-7556-175, September 1970.

3-7. J. E. Sones, Observation of Traveling Ionospheric Disturbances by the Doppler Technique with Spaced Transmitters, ESSA Technical Report ERL-142-SDL-11.

3-8. The Radio Amateur's Handbook, American Radio Relay League, West Hartford, Connecticut, 1958.

3-9. A. R. Barringer and J. P. Schock, Proc. Symposium on Remote Sensing of the Environment, 1966, pp. 779-791; A. J. Moffat and A. R. Barringer, "Remote Detection of SO_2 and NO_2," Proc. Symposium on Remote Sensing of the Environment, Vol. I, 1969, pp. 379-413.

3-10. A. R. Barringer, B. C. Newbury, and A. J. Moffat, "Remote Detection of SO_2 and NO_2," Proc. Symposium on Remote Sensing of the Environment, 1968, pp. 123-155.

3-11. R. H. Dye and A. Prostak, Proceedings on Symposium on Remote Sensing of the Environment, Vol. 2, 1971, pp. 843-844.

3-12. R. K. Vincent, Proc. 8th International Symposium on Remote Sensing of the Environment, Willow Run Laboratories, University of Michigan, 1972, pp. 1239-1247.

3-13. Y. I. Rabinovich, G. G. Shechukin and V. V. Melentyev, "The Basic Directions of the Development of Aerial Methods for the Study of Natural Resources of the USSR," Proceedings of the Symposium on Remote Sensing of the Environment, Willow Run Laboratories, University of Michigan, Ann Arbor, Michigan, 1971, pp. 2275-2294.

3-14. D. B. Barker, J. N. Brooks, A. Goldman, D. G. Murcray, F. H. Murcray, W. J. Williams, Second Conference on Climatic Impact Assessment Program (CIAP), U.S. Department of Transportation, Transportations Systems Center, DOT-TSC-OST-73-4, November 1972, pp. 86-98.

3-15. M. H. Bortner, H. W. Goldstein, Third Conference of CIAP, Department of Transportation, February 1974, pp. 117-123.

3-16a. J. T. Houghton, S. D. Smith, "Remote Sounding of Atomspheric Temperature from Satellites, I. Introduction," Proc. Roy. Soc. Lond., A 320, 1970, pp. 32-33.

3-16b. P. G. Abel, P. Ellis, J. T. Houghton, G. Peckham, C. D. Rodgers, S. D. Smith, E. J. Williamson, "Remote Sounding of Atmospheric Temperature from Satellites, II. The Selective Chopper Radiometer for Nimbus D.," Proc. Roy. Soc. Lond., A 320, 1970, pp. 35-55.

3-16c. J. J. Barnett, M. J. Cross, R. S. Harwood, J. T. Houghton, C. G. Morgan, G. E. Peckham, C.D. Rodgers, S. D. Smith, and E. J. Williamson, "The First Year of the Selective Chopper Radiometer on Nimbus 4," Quart. J. R. Met. Soc., 98, 1972, pp. 17-37.

3-16d. C. D. Rodgers, "Remote Sounding of the Atmospheric Temperature Profile in the Presence of Cloud," Quart. J. R. Met. Soc., 96, 1970, pp. 654-666.

3-16e. P. J. Ellis, G. Peckham, S. D. Smith, J. T. Houghton, C. G. Morgan, C. D. Rodgers, E. J. Williamson, "First Results form the Selective Chopper Radiometer on Nimbus 4," Nature, 228, October 10, 1970, pp. 139-143.

3-16f. J. J. Barnett, R. S. Harwood, J. T. Houghton, C. G. Morgan, C. D. Rodgers, E. J. Williamson, G. Peckham and S. D. Smith, "Stratospheric Warming Observed by Nimbus 4," Nature, 230, March 5, 1971, pp. 47-48.

3-16g. R. S. Harwood, "A Traveling Wave in the Southern Hemisphere Stratosphere," submitted to Quart. J. R. Met. Soc., 1972.

3-16h. C. Prabhakara, B. J. Conrath, and R. A. Hanel, J. Atmos. Sci., 27, 1970, pp. 689-697.

3-16i. C. L. Mateer, D. F. Heath, A. J. Krueger, X-651-71-223, Goddard Space Flight Center, Greenbelt, Maryland, June 1971.

3-16j. C. Prabhakara, V. V. Salomonson, B. J. Conrath, J. Sterenka, and L. J. Allison, J. Atm. Sci., 28, 1971, pp. 828-831.

3-16k. G. L. Wick, Science, 172, 1971, pp. 1222-1223.

3-17. P. M Solomon, Physics Today, March 1973, pp. 32-40; also M. Bertojo, M. F. Chui and C. H. Townes, Science, 184, 1974, pp. 619-623.

3-18. A. Goldman, D. G. Murray, F. H. Murcray, J. Van Allen, S. C. Schmidt, W. J. Williams, Third Conference on CIAP, February 1974, pp. 246-253.

3-19. R. T. Menzies and M. S. Shumate, Science, 184, 1974, pp. 570-571.

3-20. M. Mumma, T. Kostiuk, S. Cohen, D. Buhl, and P. C. Von Thuna, Nature, 253, 1975, pp. 514-516.

3-21a. J. E. Harries, N. R. W. Swann, J. E. Beckman, and R. A. R. Ade, "High Resolution Observations of the Submillimeter Stratospheric Emission Spectrum," Nature, 236,1972, p. 159; see also H. A. Gebbie, W. J. Burroughs, J. E. Harries and R. M. Cameron, "Submillimiter Wave Spectroscopy of the Earth's Atmosphere Above 39,000 Feet," Astrophys. J., 154, 1968, p. 405.

3-21b. J. E. Beckman, P. A. R. Ade, J. S. Huizinga, E. I. Robson, D. G. Vickers, J. E. Harries, "Limits to the Sub-millimeter Isotropic Background," Nature, 237, 1972, p. 154.

3-21c. J. E. Harries, W. J. Burroughs, "Measurements of Submillimeter Wavelength Radiation Emitted by the Stratosphere," Quart. J. Roy. Met., 97, 1971, p. 579.

3-21d. J. E. Harries, W. J. Burroughs, "Measurements of Submillimeter Wavelength Radiation Emitted by the Stratosphere, Using Fourier Transform Techniques," NPL Division Report DES 7, 1971.

3-21e. W. J. Burroughs, J. E. Harries, "Observations of Millimeter Wave Solar Radiation at Sea Level," Infrared Phys., 11, 1971, p. 99.

3-21f. J. E. Harries, "Measurements of H-O-N Compounds in the Stratosphere from Concorde 002," NPL Division Report DES 16, 1972.

3-21g. W. J. Burroughs, J. E. Harries, "Direct Method of Measuring Stratosphere Water Vapour Mixing Ratios," Nature, 227, 1970, p. 824.

3-21h. N. W. B. Stone, "Spectroscopy of Some Gases in the Far Infrared Using a Michelson Interferometer," Ph.D. Thesis, University of London, 1964.

3-21i. J. M. Dowling, "Investigations in the Far Infrared with a Lamellar Grating Interferometer," Air Force Report SSD-TR-67-30, 1967.

3-21j. E. D. Palik, N. K. Rao, "Pure Rotational Spectra of CO, NO, and N_2O Between 100 and 600 Microns," J. Chem. Phys., 25, 1956, p. 1174.

3-21k. J. E. Harries, W. J. Burroughs, and G. Duxbury, "The Pure Rotation Spectrum of HNO_3," Nature, Phys. Sci., 232, 1971, p. 171.

3-21l. E. K. Gora, "The Pure Rotation Spectrum of Ozone," J. Mol. Spec., 3, 1959, p. 78, and private communication.

3-21m. G. R. Bird. G. R. Hunt, H. A. Gebbie, and N. W. B. Stone, "The Far Infrared Pure Rotational Spectrum of Nitrogen Dioxide (NO_2)," J. Mol. Spec., 33, 1970, p. 244.

3-22. D. G. Murcray, F. S. Bonomo, J. N. Brooks, A. Goldman, F. H. Murcray, and W. H. Williams, Geophysical Research Letters, 2 1975, pp. 109-112; also D. G. Murcray, F. H. Murcray, W. J. Williams, T. G. Kyle, and A. Goldman, Appl. Optics, 8, 1969, pp. 2519-2536.

3-23. D. G. Murcray, A. Goldman, F. H. Murcray, W. J. Williams, J. N. Brooks and D. B. Barker, "Vertical Distribution of Minor Atmospheric Constituents as Derived from Air-Borne Measurements of Atmospheric Emission and Absorption in Infrared Spectra," Proc. of Second Conference on CIAP, U.S. Department of Transportation, November 1972, pp. 86-98; also, D. G. Murcray, A. Goldman, W. J. Williams, F. H. Murcray, J. Van Allen and S. C. Schmidt, "Observations of the Solar Spectrum in the 1800-2100 cm^{-1} Region and the Search for NO Lines," Proc. Third Conference on CIAP, U.S. Department of Transportation, February 1974, pp. 246-253.

3-24. L. E. Salvane, "Planetary Electrodynamics," Proc. Int'l Conference on Universal Aspects of Atmospheric Electricity, 4th Symposium, Tokyo, Japan, 1968, pp. 449-466, Ed. Coronetti, Gordon and Breach, 1969.

3-25. L. E. Salvane, loc. cit.

3-26. R. E. Orville, "Planetary Electrodynamics," Proc. Int'l Conference on Universal Aspects of Atmospheric Electricity, 4th Symposium, Tokyo, Japan, 1968, Ed. Coronetti, Gordon and Breach, 1969.

SECTION 4. METHODS OF ASSESSMENT BY ACTIVE METHODS: SUCCESSFUL EXPERIMENTS

4.1 ACTIVE PROBING AT AIRPLANE AND SATELLITE ALTITUDES

There have been several active measuring devices used at airplane and satellites altitudes. The importance of many of the following experiments lies in the fact that the surface of the earth has routinely been being probed by artificial electromagnetic radiations produced at satellite altitudes and beamed at the ground. Experiments 1 through 4 assess quantities other than gases.

4.1.1 Experiment No. 1

Skylab carries a 13.9-GHz radiometer/scatterometer and a 13.9-GHz radar altimeter ($\lambda \sim 2$ cm) plus its transmitter. All satellites use data transmission capabilities; e.g., ERTS A and B use 20 Megacycle data transmission [4-1].

4.1.2 Experiment No. 2

An active microwave radar at 16.5 GHz, sidelooking, and two scatterometers at 400 MHz and 13.3 GHz, borne on a Lockheed NP-3A-Orion [4-1].

4.1.3 Experiment No. 3

An active 13.3-GHz microwave scatterometer borne on a Lockheed Hercules (NC-130B) [4-1].

4.1.4 Experiment No. 4

An active radar altimeter borne on an RB-57A. These latter experiments have been tested over the U.S., Gulf of Mexico, Caribbean, Atlantic, Mexico, Brazil, Argentina, and Peru [4-1].

4.1.5 Experiment No. 5

The polar orbiting Alouette satellites, which have been in orbit since 1965 have been regularly irradiating the earth's atmosphere with pulses of 0.2 to 14.5 Mc, at 300 W [4-2], see Subsection 3.1.

4.1.6 Experiment No. 6

A neon laser (5401 Å ± 0.01 Å) was airborne on a Turbo-Commander aircraft flying at ~500 ft above Lake Ontario. Peak pulse power of the laser was 30 kV, at pulsewidth 3 nsec, at 100 pulses/sec. Time of flight of return of the laser pulse reflected back to the aircraft was measured to determine the depth of the layer of water which was scattering the laser light. In clear water, this laser light probes to a depth of 120 ft, whereas in turbid water, the effective depth may be reduced to about 30 ft. The time of return by reflection from the bottom can be measured if the water is not too deep. Signal-to-noise ratios of 100 were obtained at an ~1-km altitude [4-3].

4.1.7 Experiment No. 7

Routine irradiation of Eastern Europe, Russia, China and India by over-the-horizon, Doppler-shifted ionosonde transmission at about 20 Mc, see Appendix A, at about a 300-kW power. The transmitters are tunable to optimize reception.

4.1.8 Experiment No. 8

Routine irradiation of world countries by amateur radio transmitters, communication satellite transmitters, navigational and aircraft transmitters, airplane and fixed radars, submarine to shore transmitters, The Voice of America, microwave transmitters, ICBM radars, communications satellites, etc.

4.1.9 Experiment No. 9

A very large (geographically and energetically) Doppler-shifted backscatter experiment was conducted at Jicamarca, near Lima, Peru, [4-4], for many years by the Bureau of Standards at Boulder, Colorado. The frequencies used were ~40 and ~80 Mc, at powers of several hundred kilowatts. The purpose was to study movements of plasma layers of the ionosphere. Lima is at about zero degrees magnetic latitude, so the reflected electromagnetic signal comes directly back down to the laboratory.

4.1.10 Experiment No. 10

R. M. Schotland [4-5,4-6] has measured water vapor concentration up to a 2.1-km altitude using a ground-based pulsed ruby laser beam scattering backward. The laser wavelength was tunable through the range 6934-6950 Å, delivering 0.5 J pulses of a 40-nsec duration, at a rate of one every 7 sec. The beam divergence was about 5 mrad. The lines of water responsible for enhanced backscatter are shown in Figure 4-1. The detector was a photomultiplier. The bandwidth was 2 megacycles. The optical efficiency was 0.4. The signal-to-noise ratio was 10 at 7 km, filter of 4 Å half width mounted in front of the 14 stage with a photomultiplier. Presumably the signal-to-noise ratio can be improved by better thermal control of the ruby laser, the filter, and the photomultiplier, and with a laser capable of more power per pulse. The laser used in this experiment had a spectral width ~0.1 Å and a power level greater than 10^7 watts in a pulse of ~100 nsec. The radiance background for the 7000 Å region is given as 2×10^{-13} watt/cm^2/sterad/Å for night and 2×10^{-7} watt/cm^2/sterad/Å for day. The signal-to-noise ratios for levels up to 5 km are quoted as ~25 at night and ~20 in the day. The signal-to-noise ratio is expected to improve as $n^{1/2}$ where n is the number of pulses.

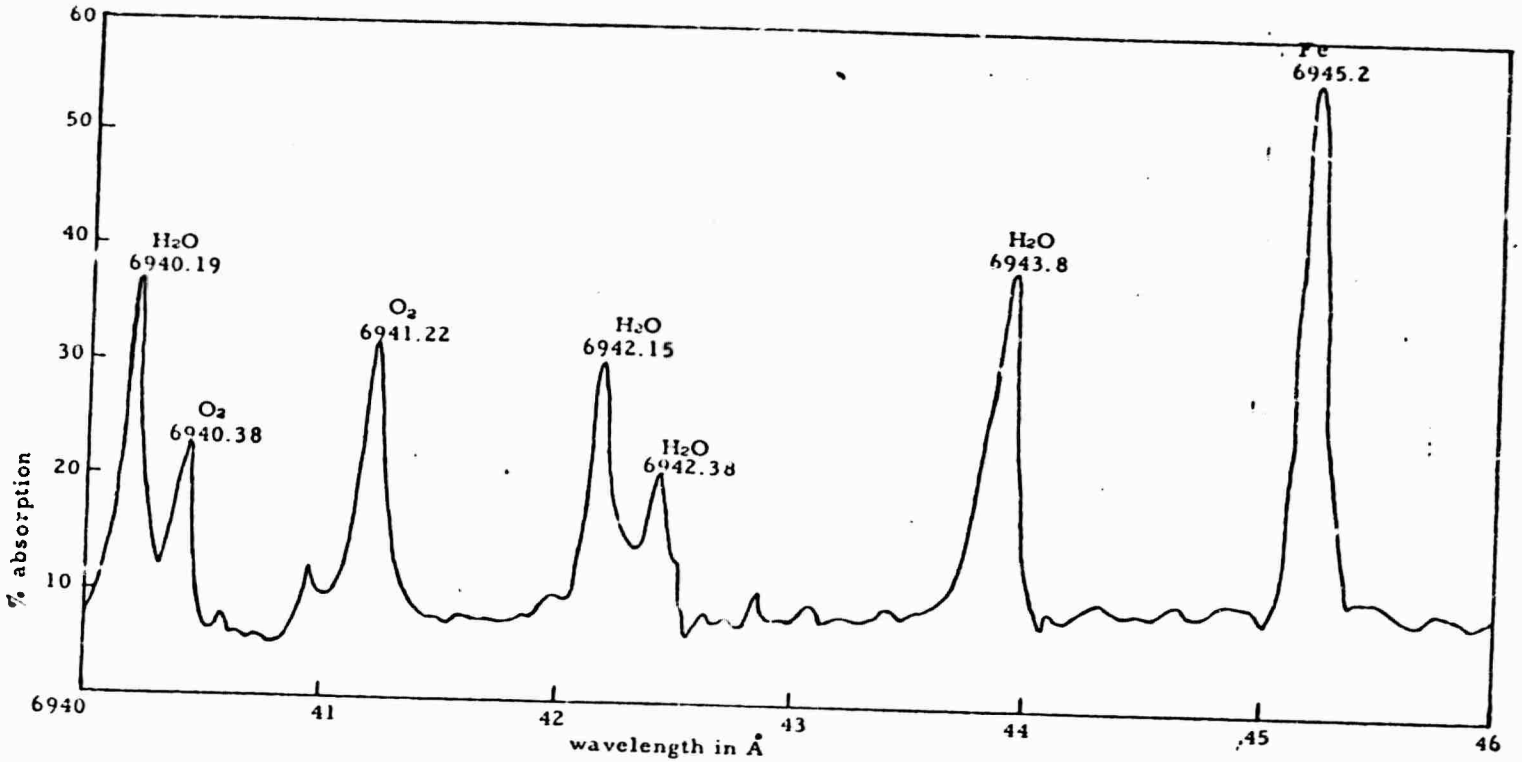

Figure 4-1. Major Atmospheric Absorption Lines from 6940 Å to 6946 Å

4.1.11 Experiment No. 11

A pulsed N_2/Ne tunable dye laser 100-kw peak power for detection of various kinds of chlorophyl in water down to about 20 meters depth has been investigated in the laboratory and on aircraft. The capability seems able to measure chlorophyl down to concentrations of ppb. Laser excitation spectra for various kinds of algae range from 4200 Å to 6750 Å, while their fluorescent spectra range from 5800 to 6850 Å. About 2 percent of the energy in the laser pulse is reflected from the surface of the water. With Ne, the laser frequency is 5401 Å. With N_2, and with a dye cell attached, the laser is tunable from 4000 to 7000 Å. The pulse width is 5 to 10 nsec, and the repetition rate is 100 to 1000 pps. The fluorescence spectra of the various kinds of algae were measured using a grating and photomultiplier. The time for emission of fluorescence was found to be about 8 nsec, with quantum yields of about 1 percent. The signal-to-noise ratio was about 100 at a 1-km altitude for the airplane. A schematic of the time of flight vs pulse height is shown in Figure 4-2, and some fluorescent spectra for various algae species are shown in Figures 4-3 and 4-4 [Ref. 4-7].

4.1.12 Experiment No. 12

The hydroxyl radical (OH) resonance fluorescence in air has been detected by reflection of tunable laser radiation near 2828 Å in the ultraviolet. Concentrations determined in this way ranged from about 10^8 hydroxyl radicals per cm^3 in the daytime to about 10^6 per cm^3 at night. The hydroxyl transitions causing the fluorescence were those for $2\pi \leftarrow\rightarrow {}^2\Sigma$. The laser light was derived from the second harmonic of a dye laser consisting of rhodamine dissolved in methanol. The repetition rate was one per 10 sec, at about a 0.5-μsec pulse width, 6 mJ per pulse, and about a 0.4-cm^{-1} spectral width.

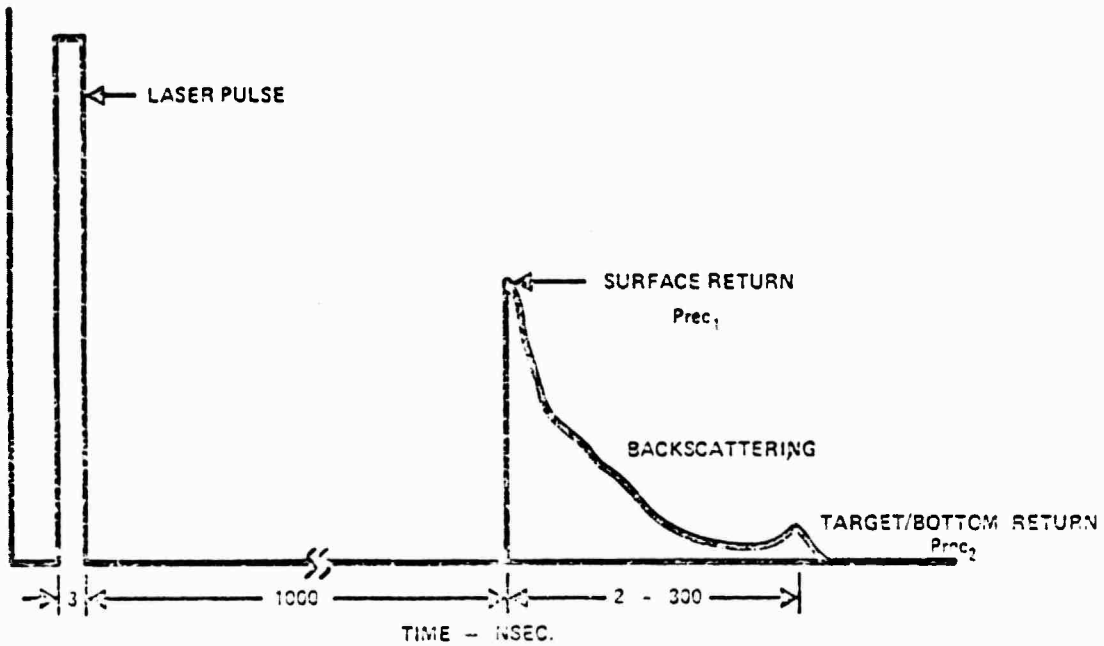

Figure 4-2. Schematic Timing Diagram Showing Laser Pulse and Various Return Signals

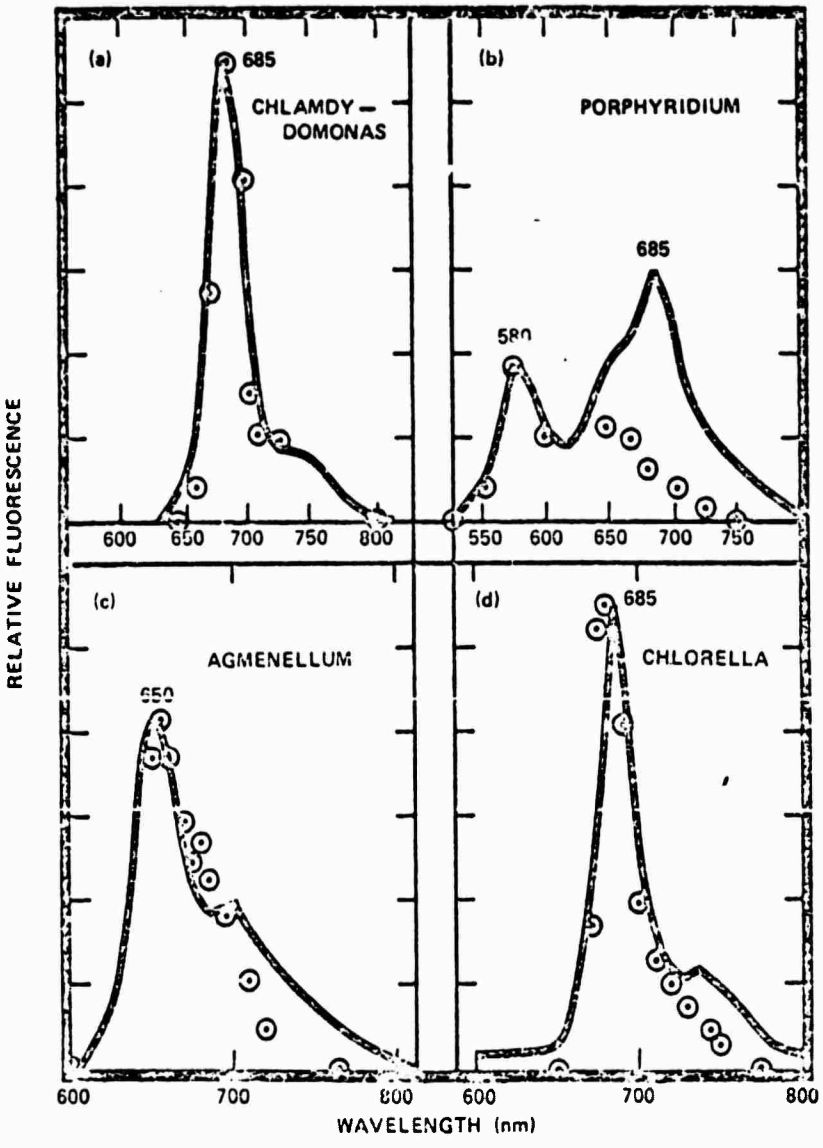

Figure 4-3. Fluorescent Spectra of Various Species of Algae (Circles are Laser-Generated Data, While the Solid Lines Were Obtained from the SPF)

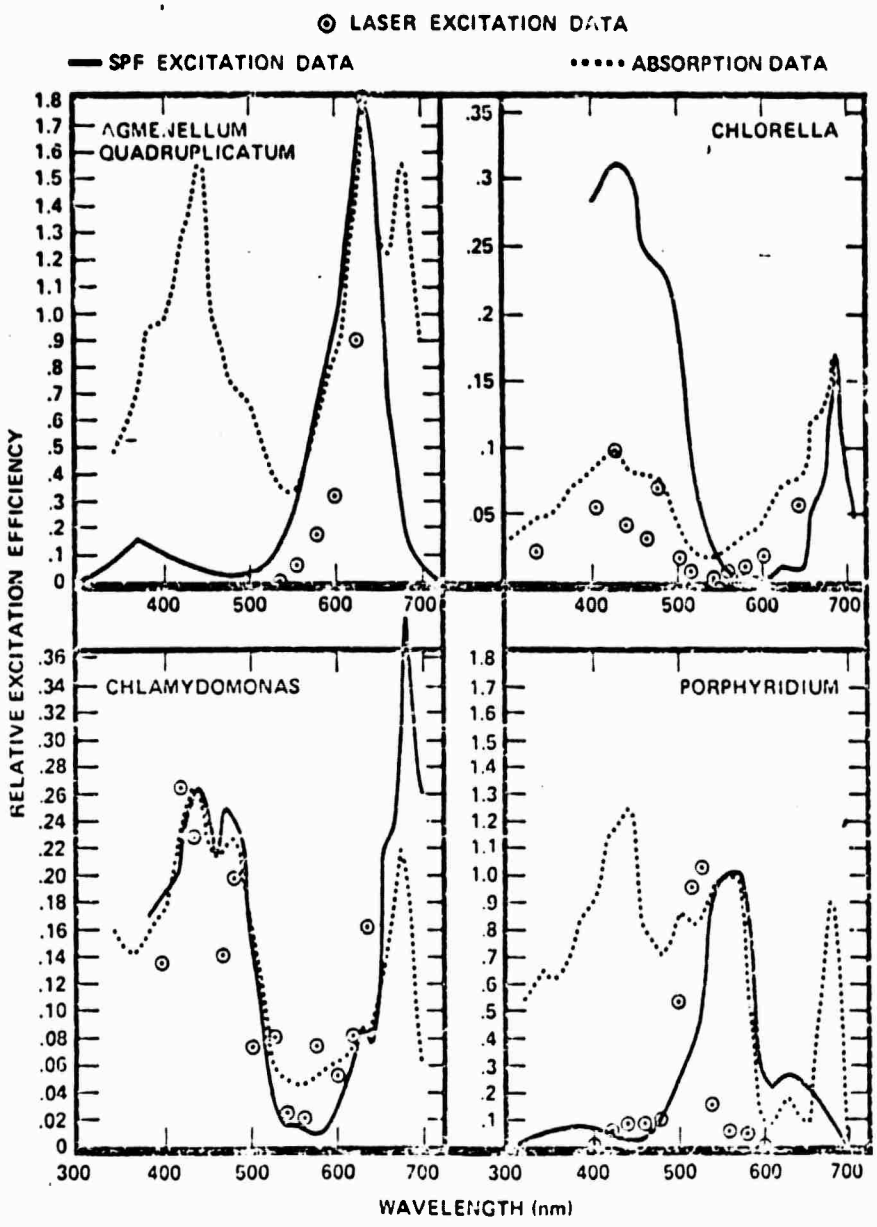

Figure 4-4. Excitation and Absorption Spectra for Various Algae Species

Fine tuning of the laser was accomplished using a grating for end reflector in the laser together with a Fabry-Perot etalon. The observed fluorescently reflected spectra are shown in Figure 4-5. The power of the fluorescent signal was found to depend linearly on the power of the laser pulse [4-8].

4.1.13 Experiment No. 13

Gibson and Thomas [4-9] made measurements with a ground-based laser, wavelengths variable between 2970 and 3080 Å, between ground level and about 20 km. The transmitter consisted of a flash-lamp-pumped dye laser, tuned with Fabry-Perot etalons, frequency doubled by an ammonium dihydrogen phosphate (ADP) crystal oriented for critical phase matching. The receiver used a one-meter mirror with filters and a photomultiplier. The data represent firings on five nights with between 100 and 1000 firings per night, and are consistent with returns expected for Rayleigh scattering for a standard atmosphere. The parameters of the UV laser were about 3000 Å tunable wavelength, at 0.2 nm beamwidth, 1 pulse/sec, 0.2 mJ per pulse, 5 msec pulse width. The differences in attenuation between two different wavelengths, namely 3080 and 3035 Å, were interpreted as caused by ozone, from which interpretation of a measure of the ozone concentration vs height was obtained. Improvements on the technology and methodology are anticipated.

4.1.14 Experiment No. 14

Raman backscatter from the real atmosphere has been accomplished by various people [4-10]. For example, D. Leonard observed Raman backscatter from atmospheric nitrogen, using a pulsed nitrogen laser at 3341 Å. The Raman frequency shift for nitrogen is 2340 cm^{-1}. The Raman return occurs, therefore, at 3625 Å. Leonard also observed the 0_2 Raman vibrational return. The laser was low powered and the range therefore was limited to 1.2 km.

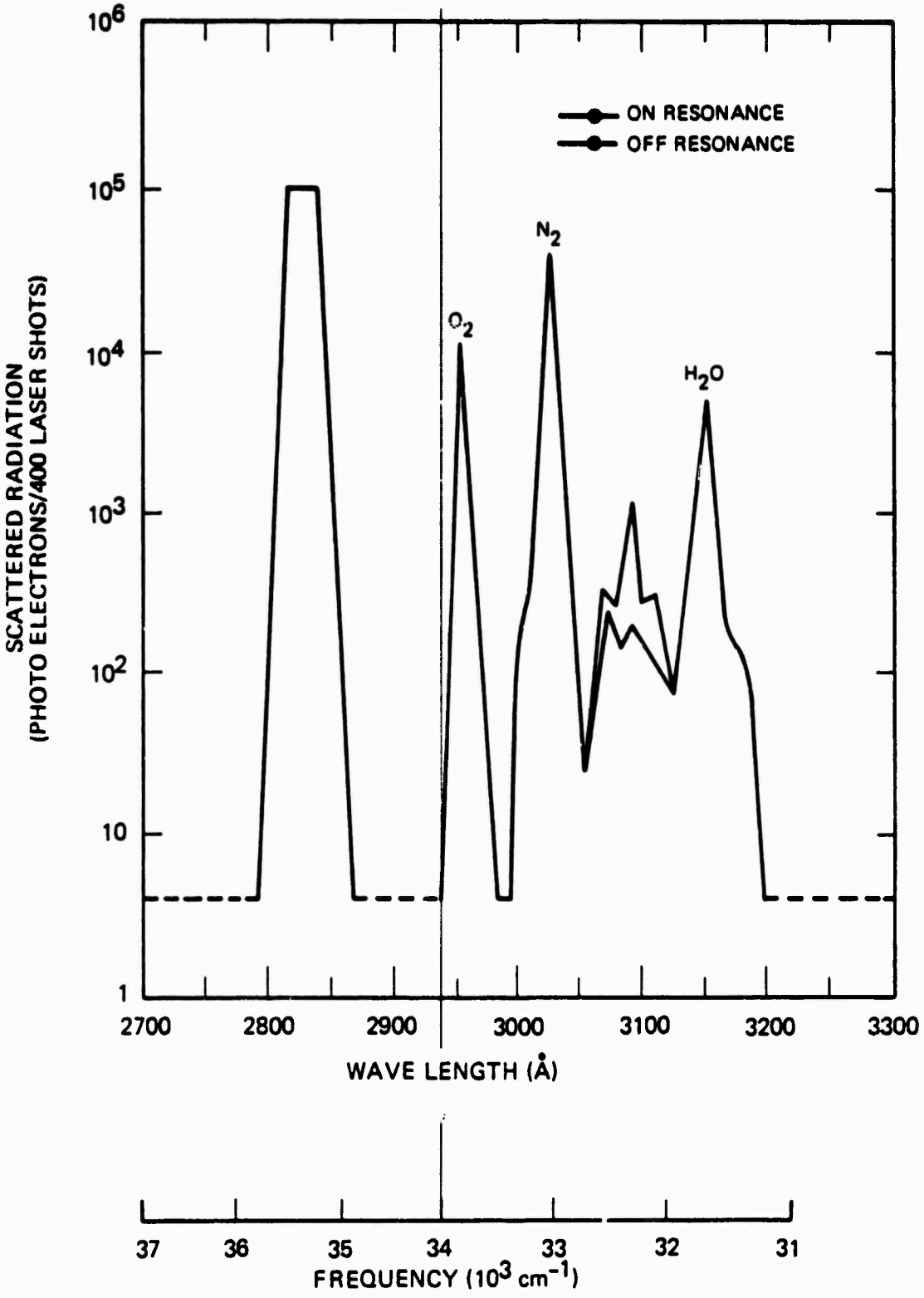

Figure 4-5. Spectrum of the Scattered Light Excited in Air by the Incident Radiation near 2825.8 A. The Peaks at 2956, 3025, and 3151 A Are Due, Respectively, to the Spontaneous Raman Scattering of Oxygen, Nitrogen, and Water in Air

4.1.15 Experiment No. 15

J. Cooney [4-11] detected the nitrogen Raman backscatter from the real atmosphere using a pulsed ruby laser at 6943 Å. Melfi et al. [4-12] used a frequency-doubled ruby laser to detect Raman backscatter of water vapor to altitudes of 1.5 km. Aerosol backscatter does not show up in the Raman return because the Raman backscatter is caused by gases only, so neither clouds nor other particulates interfere with observations.

4.1.16 Experiment No. 16

Detection of SO_2, CO, and CO_2 in stack gases has been proven by Kobayasi and Iraba [4-13], using a ruby laser and a monochromator to select the Raman backscattered light.

Preliminary results of Schwiesow [4-14 & 4-15] indicate that the cross section for Raman scattering from the CH stretching bond in organic molecules may be 20 times that of N_2, large enough to allow detection of organic pollutant films on water surfaces. See, also, Gross and Hyatt [4-16].

4.1.17 Experiment No. 17

The feasibility of measuring water temperatures to depths of 30 m by remote observation of Raman backscatter has been demonstrated in the laboratory by Chang and Young [4-17], using a dye laser (AVCO C950) of 0.3-watt average power and a monochromator at 4590 Å and a photomultiplier. The Raman-shifted spectrum of the OH bond returns at 3911 Å corresponding to $\Delta\nu = 3450\ cm^{-1}$. The polarization of the backscatter line is temperature dependent as are the intensities at different wavelengths. About 10^6 photoelectrons can be collected in 20 sec using a laser of 0.3-watt average power carried on a helicopter flying at a 50-m altitude

using a single photomultiplier. At a 100-mile altitude, they would be decreased by $\sim 10^8$. In order to receive 10 photons in 20 sec, the number of photomultipliers could be increased so that the area of their windows went up by a factor of 1000 or the laser power could be increased or both. For example, the average depth of the ocean thermocline should be measurable from satellite altitudes by Raman backscatter according to the present analysis.

4.2 SAFETY ASPECTS OF LASER PROBE FROM A SATELLITE

Consider safety aspects of visible laser light, $\lambda \sim 6000$ Å. We choose a visible wavelength because visible and ultraviolet light are more dangerous than infrared. The eye is essentially opaque to radiation longer than 14,000 Å (because it is made chiefly of water) so that such light is not focused on the retina whereas visible is. We take the square divergence of the laser beam to be 10^{-5}, as follows:

> The theoretical square divergence is $(D/\lambda R)^2$ where D is the aperture ($\sim$10 cm), λ is the wavelength ($\sim 10^{-4}$), and R is the distance ($\sim 10^{7}$).

In practice, the square divergence appears to be smaller, about 4×10^{-7} for a laser at 3000 Å [4-18] equivalent to $\sim 10^{-6}$ at 6000 Å. Suppose we consider a satellite-borne experiment which carries a laser of 1-watt power, making 1 pulse per sec, equivalent to 3×10^{18} photons emitted per sec, on an aperture of ~ 1 cm^2. We assume a target of polluting gases at 10 ppm in an atmospheric ground layer of a 10^3-m thickness, equivalent to 3×10^{19} atoms/cm^2. The electric dipole scattering cross section is 7×10^{-25} cm^2/electron. The number of photons scattered resonantly is therefore $(3 \times 10^{18})(3 \times 10^{19})(7 \times 10^{-25})$/sec = 6×10^{13}/sec per electron.

In returning to the satellite, the photons are diminished by $1/4\ R^2\ \ 10^{-15}/cm^2$ so that there are 0.06 photons received per cm^2 per sec, or 6 photons received in 100 sec for molecular targets containing one electron. Suppose there are six identical bonds in the target (e.g., six bonds of CH with two electrons per bond), then the number of photons received at the satellite is increased by 12 times, etc.

The wattage of a 1-watt laser received on the ground is less than 10^{-6} watt/cm^2 or for example, 1 joule per 30 nanosec focussed on the retina. This is a million times smaller than the level of corneal irradiation presently judged to be safe, namely 1 watt/cm^2 in the visible [4-19].

We have used the cross section for elastic scattering in the above analysis. The magnitude of the cross section for Raman scattering can be made to approach that for elastic scattering if the laser frequency is chosen to approach a resonant frequency of the molecule to be detected.

If one were to use laser probes at satellite altitudes, it would be reasonable to direct the laser beam pointed downward along the line connecting the satellite with the sun (on the day side of the earth) because humans and animals do not look at the sun and hence would not receive laser radiation in their eyes.

A photomultiplier gives a positive count with as few as three visible photons. Hence, these signals are detectable. We have taken no account of the effects of atmospheric turbulence (twinkling). Some measured Raman cross sections are shown in Table 4-1 [4-17].

Table 4-1. Raman-Scattering Cross Section

COMPOUNDS	$[C_6H_6(l)]_{4880A}$	$[CS_2(l)]_{4880A}$	$[H_2O(l)]_{4565A}$	$[H_2O(g)]_{4565A}$
$\nu(cm^{-1})$	992	655	3130 - 3700	3652
$\Delta\nu(cm^{-1})$	2.3	1.4	~350	14.2
n	1.49	1.61	1.33	
$\sigma(cm^2/sr\text{-}prt\text{-}cm^{-1})$	$1.05 \cdot 10^{-29}$	$1.93 \cdot 10^{-29}$		
$\sigma(cm^2/sr\text{-}prt)$	$2.42 \cdot 10^{-29}$	$2.70 \cdot 10^{-29}$	$0.91 \cdot 10^{-29}$	$0.21 \cdot 10^{-29}$

4.3 RECENT DEVELOPMENTS IN LASER TECHNOLOGY

A summary of progress in several kinds of lasers, their wavelengths, efficiencies, and powers is shown in Tables 4-2 thru 4-5. Mirror sizes needed for efficient communications between the earth and satellites in low earth orbit and in geo-synchronous orbit are shown in Table 4-6. For detection, fewer laser photons are needed than for communications, so the mirror sizes can be smaller.

4.4 PRESENT CAPABILITIES OF BOLOMETRIC SENSORS AND THEORETICAL LIMITS TO SENSITIVITIES

Present and projected radiometric sensitivities and theoretical limits to sensitivities are shown in Figures 4-6 and 4-7 [4-20].

Table 4-2. Characteristics of High-Intensity Lasers [4-21]

Laser Medium	Wave-length	Efficiency (%)	Peak power (W)	Pulse duration	Laboratory
Nd : glass	1.06 μm	0·2	7×10^{11}	1·5 ns	Battelle, Columbus, USA
			4×10^{12}	230 ps	Lawrence Livermore, USA
			10^{12}	1 ns	KMS Fusion Inc. USA
			2×10^{12}	500 ps	Univ. Rochester USA
			5×10^{11}	2 ns	Lebedev, Moscow, USSR
CO_2	10·6 μm	3–5	5×10^{11}	1 ns	Los Alamos, USA
Iodine	1·31 μm	0·5	10^{11}	700 ps	Max-Planck-Inst. Garching, Germany
Hydrogen fluoride	2·7 μm	180 (electrical) 5 (chemical)	10^{11}	35 ns	Los Alamos and Sandia, USA
Dye	605 nm	$<10^{-3}$	3×10^{8}	3 ps	Imperial College London
Xenon	173 nm	>2	4×10^{8}	20 ns	Los Alamos and Maxwell Labs, Inc. USA

6050 Å

1730 Å

Table 4-3. Operating Characteristics of Double-Pulsed Metallic Vapor Lasers [4-22]

Operating Parameters	Lasant				
	Manganese Chloride	Lead Chloride	Copper Chloride	Copper Iodide	Copper Formate
Buffer gas	He at 1-2 torr	He at 1-2 torr	He and Ar at 1-20 torr	He at 1-2 torr	He at 1-2 torr
Time delay,[a] sec	150	150	100	100	100
Temperature, C	680	500	400	575	135
Laser energy density, J/cm^3	1.3	4	35	11	— —
Laser peak power density, w/cm^3	33	160	1700	500	— —
Wavelength, A	5341	7229	5107	5107	5107

[a] 1-in.-diam. tubes.

T-2 IMPORTANT IR LASERS

Laser	Wavelength, m	$h\nu$ ev	$T_s = h\nu/k$	Absorbing gas	E_{diss}, ev
CO_2	10.6	0.11	1300	SF_6	3.13
CO	4.7	0.26	3000	CO	11.1
HCl	3.5	0.35	4100	HCl	4.4
HF	2.8	0.44	5100	HF	5.9

Table 4-4. Blue-Green Laser State-of-the-Art

Laser	Mechanism	λ	Average Power	Per Pulse Energy	Repetition Rate	Efficiency	Problems
Nd YAG Doubled	CD*A frequency doubler	.53μ	10 watts			~ 1%	Heating of frequency doubling material destroys phase metal limited upscaling.
3 Wave Up-conversion	C_s metal vapor non-linear frequency mixing	.457μ	Has not been demonstrated in laboratory but is expected to be generated in next few months			~1%	50% conversion using 9.6μ photon and 2 visible photons demonstrated.
Copper Vapor		.5106μ	10 watts	3 millijoules	3000 pps	~ 1%	High gain low impedance power supply maintaining E/P
Flashlamp Pumped Dye	flowing gas flash-lamp	tunable	40 watts	.4 joule	100 pps	~.3%	Pulses too long for range gating; lamp lifetime a problem for high rep rate applications.
Laser Pumped Dye N_2		tunable	.5 watt	5 millijoules	100 pps	$< 10^{-3}$	Efficiencies could be increased to order of 1% but will be difficult to increase pulse energy to 100 millijoule level.
Nd 3rd Harmonic	C_s metal vapor non-linear frequency tripler						10% conversion from Nd wavelength already demonstrated; 50-100% conversion appears practical.
Excimer	Ar - N_2 or others						Have demonstrated 1-1/2% efficiency on Excimer laser at 3500Å; need to develop different pumping method.
Recombination	He - N_2 transfer laser						Demonstrated 1-1/2% efficiency at 4278Å; new pumping mechanism required.
Excimer							Have to find Excimer or Excimer laser operating in band; new pumping mechanism required.
Recombination	He - N_2 transfer	4278Å				1-1/2%	Have demonstrated 1-1/2% efficiency at 4278Å; new pumping mechanism required.

Table 4-5. Blue-Green Laser Potential

Laser	Near Term (1-3 Years					Far Term (5 or More Years)				
	λ	Average Power	Energy per Pulse	PRF	Effleiency	λ	Average Power	Energy per Pulse	PRF	Efficiency
Nd YAG Doubled	.53μ	2 watts	5 millijoules	400 pps	~ 1%	.53	10-20 watts	10-20 millijoules	1000 pps	~1%
3 Wave Up-conversion	.457μ	500 watts	.1 joule	5000 pps	~ 1%					
Copper Vapor	.5106μ	150 watts	50 millijoules	3000 pps	1%	5106	500 watts	100 millijoules	5000 pps	2%
Flamp Pumped Dye	tunable	1-200 watts	.5 joule	400 pps	~ .5%	tunable	500-1000 watts	1-2 joules	500 pps	~ 1%
Laser Pumped Dye N_2	tunable	15 watts	5 millijoules	3000 pps	~ .5%.	tunable	150 watts	50 millijoules	3000 pps	~1%
Nd 3rd Harmonic	tunable	500 watts	.1 joule	5000 pps	~ 1%					~1%
Excimer	0.35μ	10 watts		3000pps	5%					10-20%
Recombination					5%					10-20%
Excimer					5%					10-20%
Recombination					5%					10-20%

Table 4-6. Laser Transmitter and Receiver Sizes. For Low Earth Orbit (160 km), and Geostationary Orbit (36,000 km) and CO_2 (10.6 μm), CO (5 μm), and Hypothetical Visible Laser (0.5 μm). No Atmospheric Absorption.

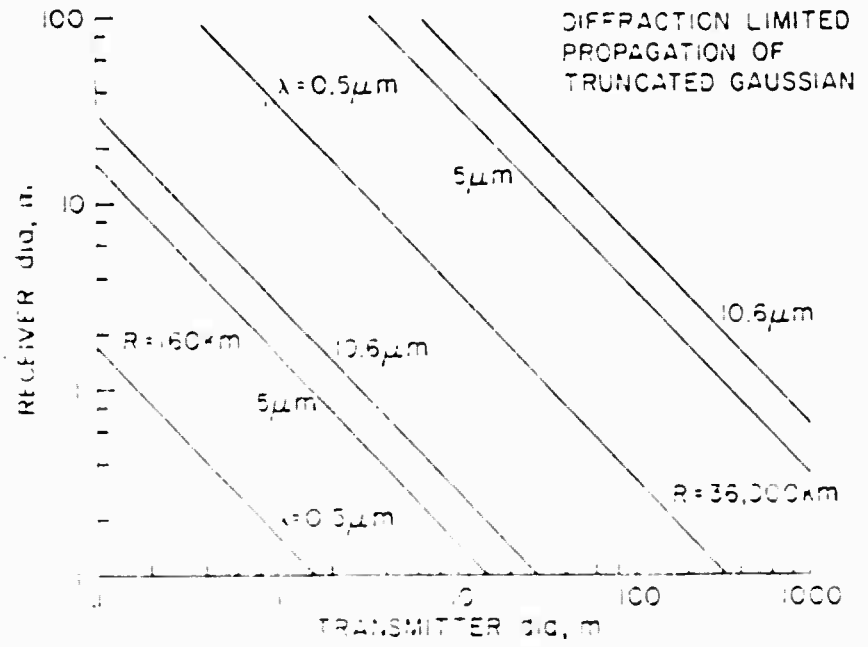

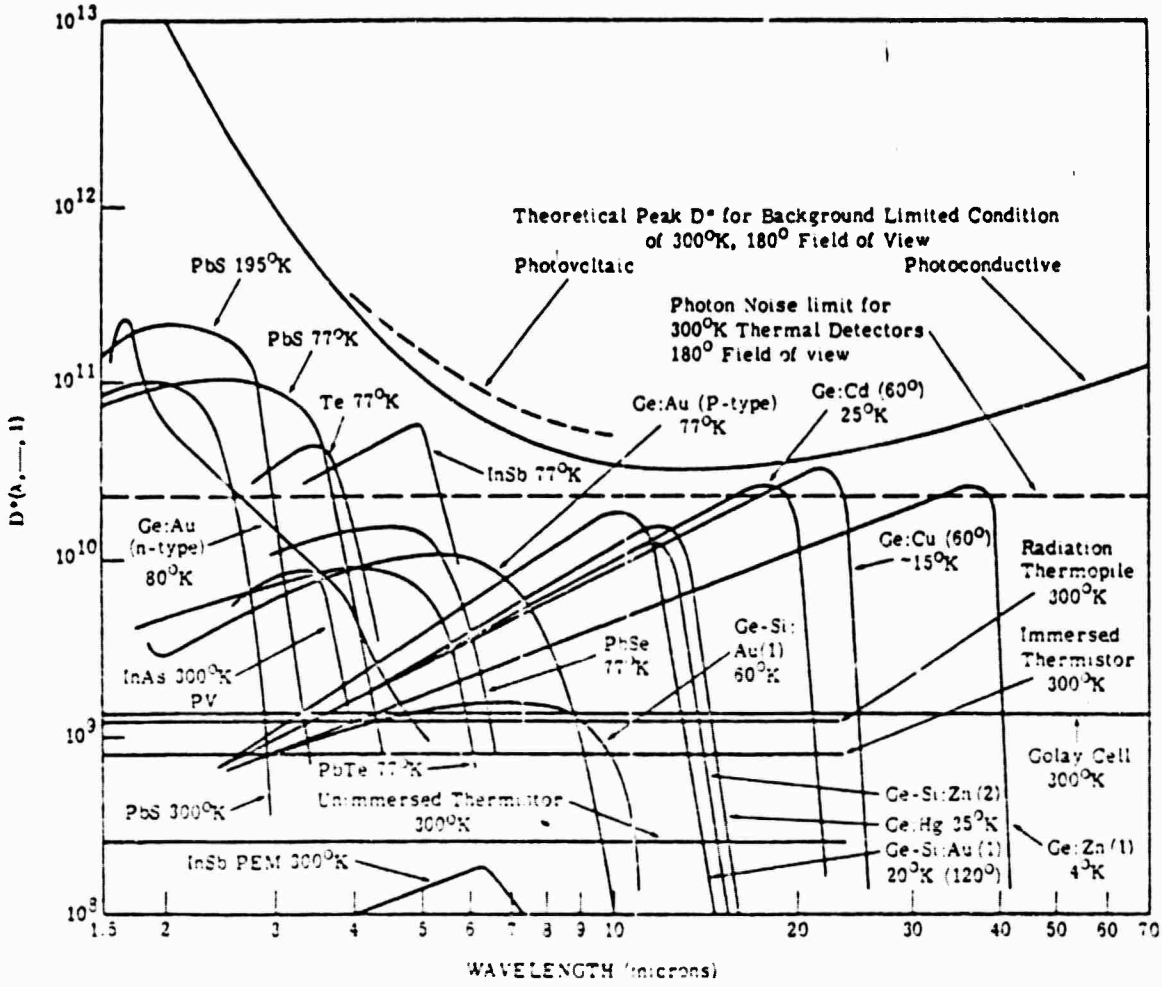

Figure 4-6. Characteristic Responses of Various Infrared Detectors

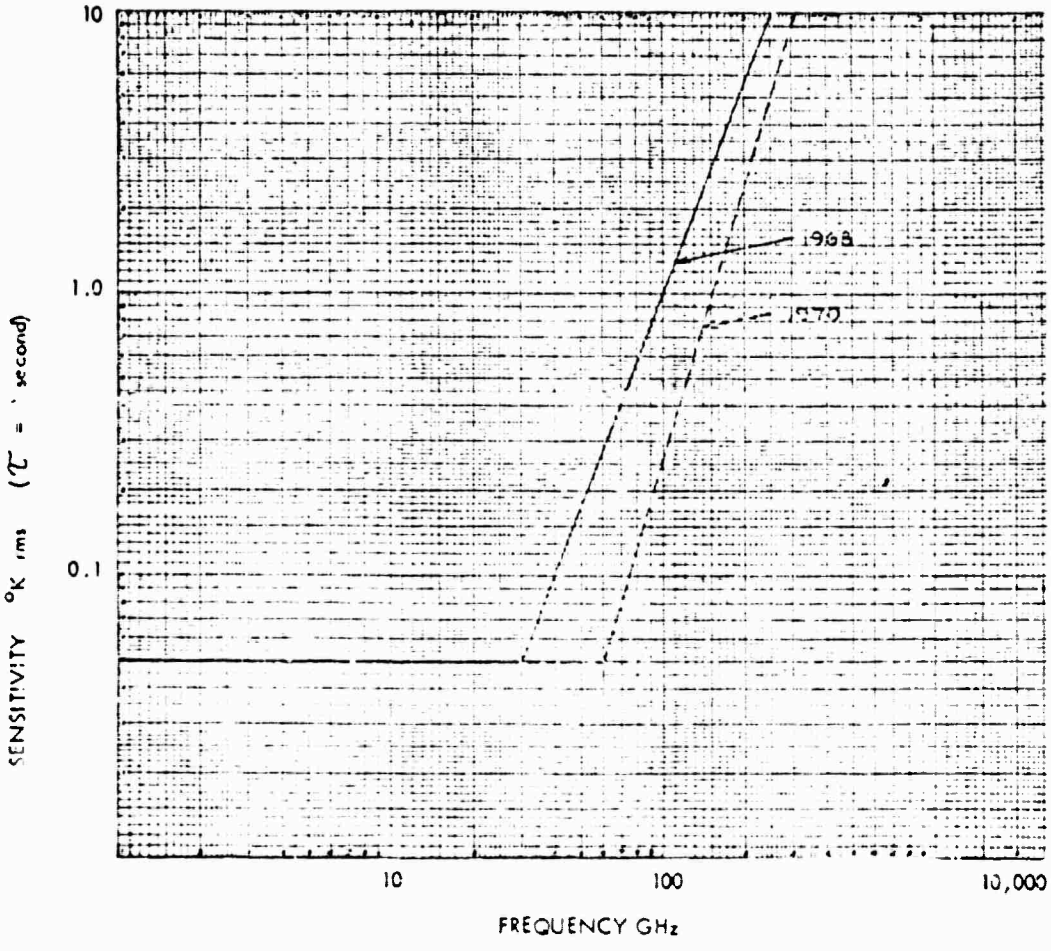

Figure 4-7. Present and Projected Radiometric Sensitivities

REFERENCES TO SECTION 4

4-1. Earth Resources Survey System, Vol. I, U.S. G.P.O., NASA, Washington, D.C., 1972, pp. 133-136.

4-2. G. Herzberg, Infrared and Raman Spectra, Van Nostrand-Reinhold Co., 1945; also Spectra of Diatomic Molecules, Van Nostrand-Reinhold Co., 1950; also Electronic Spectra of Polyatomic Molecules, Van Nostrand-Reinhold Co., 1966.

4-3. G. D. Hickman, J. E. Hogg, A. R. Spadew, and M. Flescher, Proc. International Symposium on Remote Sensing of the Environment, Vol. 2, 1969, pp. 1061-1074.

4-4. R. F. Woodman, Space Sci. Res., 12, 1972, pp. 969-974.

4-5. R. M. Schotland, Proc. Symp. Remote Sensing of Environment, 1964, pp. 215-223; also Proc. Remote Sensing of Environment, University of Michigan, Ann Arbor, Michigan, 1966, pp. 273-283.

4-6. R. M. Schotland, "The Determination of the Vertical Profile of the Atmospheric Gases by Means of a Ground-Based Optical Radar," Proc. Symposium on Remote Sensing of the Environment, Willow Run Labs, 1964.

4-7. G. D. Hickman, J. E. Hogg, E. J. Friedman, and A. H. Ghovanlou, Proc. Symposium of Remote Sensing of Environment, 8, Part 1, 1972, pp. 617-637.

4-8. C. C. Wang and L. I. Davis, Jr., Phys. Rev. Let., 32, 1974, pp. 349-352.

4-9. A. J. Gibson and L. Thomas, Nature, 256, 1975, pp. 561-563.

4-10. D. Leonard, Nature, 216, 1967, p. 142.

4-11. J. Cooney, ed. R. Zirkind, Proc. Symposium on Electro-Magnetic Sensing by Earth Satellites, Polytechnique Press, Brooklyn, New York, 1965, pp. 1-10.

4-12. S. H. Melfi, J. D. Lawrence, and M. P. McCormick, Appl. Phys. Let., 15, 1969, p. 295.

REFERENCES TO SECTION 4 (Cont.)

4-13. T. Kobayasi and H. Inaba, Proc. IEEE, 58, 1970, pp. 1568-1571.

4-14. R. L. Schwiesow, J. Amer. Inst. Aeronaut & Astronaut, 11, 1973, pp. 87-90.

4-15. R. L. Schwiesow and V. E. Derr, J. Geo. Res., 75, 1970, pp. 1629-1632.

4-16. H. G. Gross and H. A. Hyatt, Proc. 7th Inter. Symposium on Remote Sensing of the Environment, University of Michigan, 1971, pp. 869-888.

4-17. C. H. Chang and L. A. Young, Proc. 8th Inter. Symposium on Remote Sensing of Environment, University of Michigan, October 1972, pp. 1049-1068.

4-18. A. J. Gibson and L. Thomas, Nature, 256, 1975, pp. 561-563.

4-19. F. F. Hall, Jr., Planetary Electrodynamics, pp. 161-225.

4-20. Proc. 8th Inter. Symposium on Remote Sensing of the Environment, 1969, pp. 52-79.

4-21. D. J. Bradley, "High Intensity Lasers," Endeavor, 34, 1975, pp. 90-96.

4-22. K. W. Billman, "Laser Energy Conversion," Astronautics and Aeronautics, July/August 1975, pp. 56-65.

SECTION 5. SUMMARY AND RECOMMENDATIONS

Electromagnetic signatures of gases and of subcomponent ligands in gaseous molecules have been itemized. The methods to compute these signatures have been detailed. Functioning successful technologies to identify these signatures remotely and their related hardware and sensors have been described in the foregoing report.

Recommendations to use this information in ARPA's program for remote assessment of materials are described here.

I. Implement remote assessment of materials of interest to the Department of Defense as follows:

a. Obtain laboratory absorption and emission spectra, including Raman spectra and ESR, for reasonable column densities of materials of interest from the literature or by making such measurements.

b. Computerize and compute composite spectra for various appropriate combinations of atmosphere plus gases of interest plus atmospheric pollutants, (or in the case of liquids, compute composite spectra for water plus liquids of interest plus pollutants. In the case of solids, compute spectra for various kinds of soils plus solids of interest plus pollutants). In this terminology, the material to be assessed is excluded from the term "pollutant."

c. From the computed composite spectra, generate interferograms or other outputs of the various sensors used in presently successful technologies of remote assessment.

d. Decide on the frequency interval in which the substance of interest could be most sensitively detected and by which of the several technologies already successful.

e. Design the equipment for measurement at satellite altitudes for telemetry of the measured information to ground and/or for date reduction.

Operations whose remote assessment may be important to the DOD and whose signatures might be relevant to the above analysis include the following:

a. Explosives manufacturing: for example, gases evolved in the manufacture and storage of aliphatic-fluoro-nitro high-density compounds.

b. Nuclear fuel manufacture, enrichment, and reprocessing; gases evolved are, for example, SF_6, UF_6, HF, organic solvents such as ether, NO_x, Kr, Xe, I_2, Br_2.

c. Manufacture of insecticides, chemical warfare gases and CW components, gases which may be input materials or may be evolved in the manufacture of CW gases and insecticides.

d. Manufacture of propellants, gases which may be input materials or may be evolved in manufacture, e.g., hydrazine and UDMH.

e. Emission of gases used in high-power chemical lasers, e.g., F_2, Cl_2, H_2, Xe, Kr, Ne, A, HF, HCl.

f. Stockpiling of ores, raw materials, waste materials from manufacturing and mining and refining, specifically, rare earth deposits, tungsten ores, asbestos ores, steel mill slag, coal piles, cryolite, platinum and platinum group metal ores.

g. Disposal of liquid effluents from manufacturing and mining and refining, oils, trace chemicals in waste waters.

II. Support research and development on gas, liquid and solid lasers, for high power, better methods of cooling, greater variety of lasing wavelengths, higher repetition rate.

III. Improve bolometer sensors, the sensitivities of which are now far below their theoretical limits.

IV. Analyze technology of heterodyning to evaluate the sensitivities which may be achieved with various kinds of reference frequencies and their sources, and various kinds of sensors and filters.

V. Update the present report on methodology of remote assessment of gases to include unpublished new results, hardware, sensors, and technology successfully demonstrated in the last year, by NASA, CIAP, ESRO-ENDO (European), and Russian researchers. For example, the Proceedings of the Fourth Conference on Climatic Impact Assessment Program is in proof for publication early in 1976; experiments of interest should be abstracted.

VI. Support further study of lightning spectra at optical, microwave and decametric frequencies from ground level and balloon and airplane altitudes, especially in polluted atmospheres, near stack gas emissions, and near metal refineries.

VII. Support study of optical spectra measured in absorption of the sun's glitter and in emission close to the glitter, as the glitter is reflected from oceans, lakes, harbors, rivers and ponds, using airplanes and balloons.

VIII. Support airborne study of optical spectra measured using urban artificial light sources, especially from airports and streets.

IX. Support a search at airplane altitudes for Raman-shifted frequencies of radiations from ground-based transmitters.

APPENDIX A

The following article by Peter Laurie entitled, "An Eye on the Enemy Over the Horizon," taken from the New Scientist, 7 November 1975, has been reprinted in its entirety in this appendix.

Orford Ness, the £22 million experimental over-the-horizon radar station on the Suffolk coast, was shut down two years ago. Is OTH just another expensive military toy? Or is it, in fact, so effective that the U.S. really was ready to intervene in war-torn Cyprus to protect the operational OTH station there?

For those who enjoy dabbling in defense mysteries, over-the-horizon (OTH) radar is public enough for one to know that it exists, yet little enough has been published about it to make the subject intriguing. The principle is simple enough and is fundamentally the same as microwave radar with which we are all familiar. Instead of using radio waves in the centimetric region, which travel in almost straight lines and limit radar ranges against aircraft to 300 miles or less, one uses waves in the high-frequency band (HF) which are normally used for intercontinental communication. They bounce alternately off the ionosphere and the Earth's surface to give ranges of several thousand miles. A powerful, directional transmitter emits pulses of these waves which are reflected by aircraft targets several thousand miles away and which are then detected in a sensitive directional receiver. This much is obvious and has been for decades; what has not been so obvious is how to make the system work.

There are several snags. The first is to secure good ionospheric reflection without too much absorption. Again, as in communication frequency management, it is necessary to tailor the frequency used to the time of day and the sunspot cycle. Low frequencies are necessary at night to get reflection, and high ones during the day to avoid excessive absorption. In practice, an OTH radar needs a secondary, vertical, sounding radar to test the ionospheric weather, together with an HF receiver to search the band for quiet channels. The best radar frequency is then calculated by a computer and the transmitters and

receivers adjusted accordingly--which, for installations as powerful and complicated as these are, is in itself quite a performance.

The second snag is that signals of interest arrive at the receiver at extremely low vertical angles. Aerials which produce a beam only 2° - 4° above the horizontal are necessarily massive structures whose most important feature is a good conducting ground plane extending some 3 km in the forward direction. This can be, and has been, done on land by laying vast areas of wire mesh, but it is much easier to use the sea, and the majority of OTH are to be found on the coast. Together with a need for low-angle radiation goes the necessity of a narrow beam in the horizontal plane--this improves the signal-to-noise ratio and gives better discrimination between targets. To produce a beam 1° in the HF region, an aerial array about 1.5 km wide is needed.

Already the difficulties seem staggering, but worse is to come. The majority of the returned signals will be from ground and sea: a 50 kW OTH radar at the Appleton Laboratory at Slough, where much of the early theoretical work was done, showed about 1 mV signals on the aerial from ground clutter, while returns from aircraft were predicted as one hundredth of this voltage. Happily, picking these out is not as difficult as it might seem, for if HF radars are imprecise about distance and bearing, they are acceptably accurate when used to detect radial motion through Doppler shifting of the returned echo. At 20 MHz, it is possible to resolve a 1.5-knot difference in target speeds, while ground and sea clutter is easily filtered out.

Ranging is not so good. Since the signal is busy bouncing off the ionosphere for the first 1000 km out from the transmitter or receiver, no echoes can be returned from this region. Range resolution is apt to be 20-40 km and, relative to a known target, an accuracy of 2-4 km can be achieved. This is for signals on the first bounce--that is, out to a distance of 4000 km. Signals that have arrived by two bounces will show worse resolutions.

Bouncing Off the Sky

The real difficulty in making these devices operational, however, has been in understanding the mechanics of the bounce off the ionosphere. This layer is the interface between two fluid layers and is disturbed as the surface of the sea. One can see the lower manifestations of ionospheric waves in the occansional bands of high cloud that look like

breakers. These waves, together with more random swirls and twists, distort the returned echoes like mirrors in a fun-fair. Professor E. D. R. Shearman of Birmingham University, who uses an ingenious aperture synthesis technique to apply OTH radar to the study of sea waves far out in the ocean, likens the result to the "undulating, warped view we see of the bottom of a swimming pool when looking down at it through the rippled water surface" [Spectrum, No. 67, 1969].

What has made OTH radar a useful tool, both for the military and for oceanographic and ionospheric studies, is real-time computer processing of the echoes using the distorted pre-Doppler filtered ground returns as a guide to the state of the ionosphere, so that appropriate corrections can be applied to active targets. (Interestingly enough, the same problem occurs in processing the returns from the huge low-frequency sonars that survey equally vast areas of ocean for submarines, and for the same reason--that is, waves on the sea surface.) One ionospheric disturbance that, it seems, no amount of computer processing can correct is when the ionosphere is punched in by blasts of electrons from the Sun to form aurorae. So OTH radar paths ought really to avoid latitudes higher than 60°.

The first thorough description of an OTH radar with military potential appeared a few months ago (J. L. Hendrick and M. I. Skolnick, Proceedings of IEE, June 1974, p. 664). The paper described the U.S. Navy's Project Madre radar at Chesapeake Bay, Virginia, which can look south to Cape Canaveral to get experience with returns from rockets and their ionized wakes and across the Atlantic to follow commerical aircraft. As long ago as 1961, it was tracking flights out to 4000 km with 50 kW of power. The aerial array consists of a double row of dipoles in 90° corner reflectors, and measures 93 by 43 meters. A large, low-angle HF aerial of some interest was built in Australia at Rockbank, 20 miles NW of Melbourne, in the early 1960s. It consisted of several slow wave structures lying parallel on a bearing of 306° True, each four wavelengths long, including the large ground plane. Altogether, the aerial used some 25 miles of wire. It worked at a fixed frequency near 20 MHz and could be steered by phase shifting the feeds to the different sections to cover Singapore, Calcutta, and the U.K. (J. F. Ward, Nature, 205, p. 1062).

The one great advantage that HF radar has over centimetric radar is that targets of military interest give returns by resonant, rather than optical reflection--since their dimensions are often comparable with a half wavelength (1/2 λ at 20 MHz is 7.5 meters). This means that they re-radiate as

well in the forward direction as backwards to the transmitter. Consequently, OTH radars can be employed in both forward- and back-scatter modes. Thus near targets can be examined by having a receiver near a powerful slewing transmitter, and far targets can be studied by placing another receiver at the far end of a great circle through the area of interest. This makes sense on economic grounds as well, since one transmitter, which tends to be a heavy and expensive item, can cover twice as much ground. A constant satellite link would be needed to coordinate frequency shifts at the receiver and transmitter.

Extrapolating Madre

So far nothing much has been published about the military applications of OTH radar, but we can make some intelligent guesses by extrapolating the Madre results. The basic radar equation says that if the aerial gain, noise conditions, target reflectivity and frequency are constant, the minimum transmitter power needed to produce a usable return varies as the fourth power of the range. One can adapt this to the forward-scatter mode by saying that the transmitter power (P) is equal to $Kd_1^{-2} \times d_2^{-2}$ where the target is a distance d_1 from the transmitter and d_2 from the receiver. Inserting the Madre result that 50 kW successfully illuminated aircraft targets at 3000 km, the constant turns out to be 6.17×10^{-10} when d is in km and P in watts (Figure 1).

The known OTH radar sites are Orford Ness in Suffolk, built by the Americans and operated until recently by joint British and U.S. staff; Cyprus, built by the British and operated by the Americans; and Okinawa which is presumably completely American. Concentrating on the last two for the moment, one sees (Figure 2) that the cover one might expect from a forward-scatter radar in Cyprus (or Okinawa, the pattern being symmetrical) would take in many of the areas in central Asia which must be of interest to British and American intelligence. (As well as detecting aircraft and missiles, OTH also reveals nuclear bursts, which focus or diffuse the radio beam, producing unusually bright or dim echoes from ground about as far away again.) One of the areas "visable" would certainly be Tyuratam, the Soviet Union's main rocket launching station; others would include the Kara Kum desert and the Semipalatinsk regions where the Russians are reported to have tested nuclear weapons, the Sary Shagan ABM development center, the Tarim desert where the Chinese are reported to test missiles, as well as their Lop Nor nuclear proving ground. Lop Nor lies exactly on the great circle joining Cyprus to Okinawa.

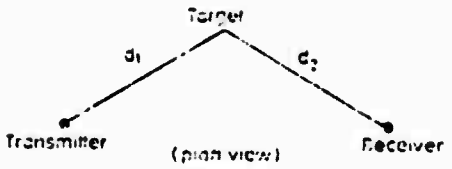

Figure 1. Over-the-Horizon (OTH) Radar Operating in a Forward-Scatter Mode

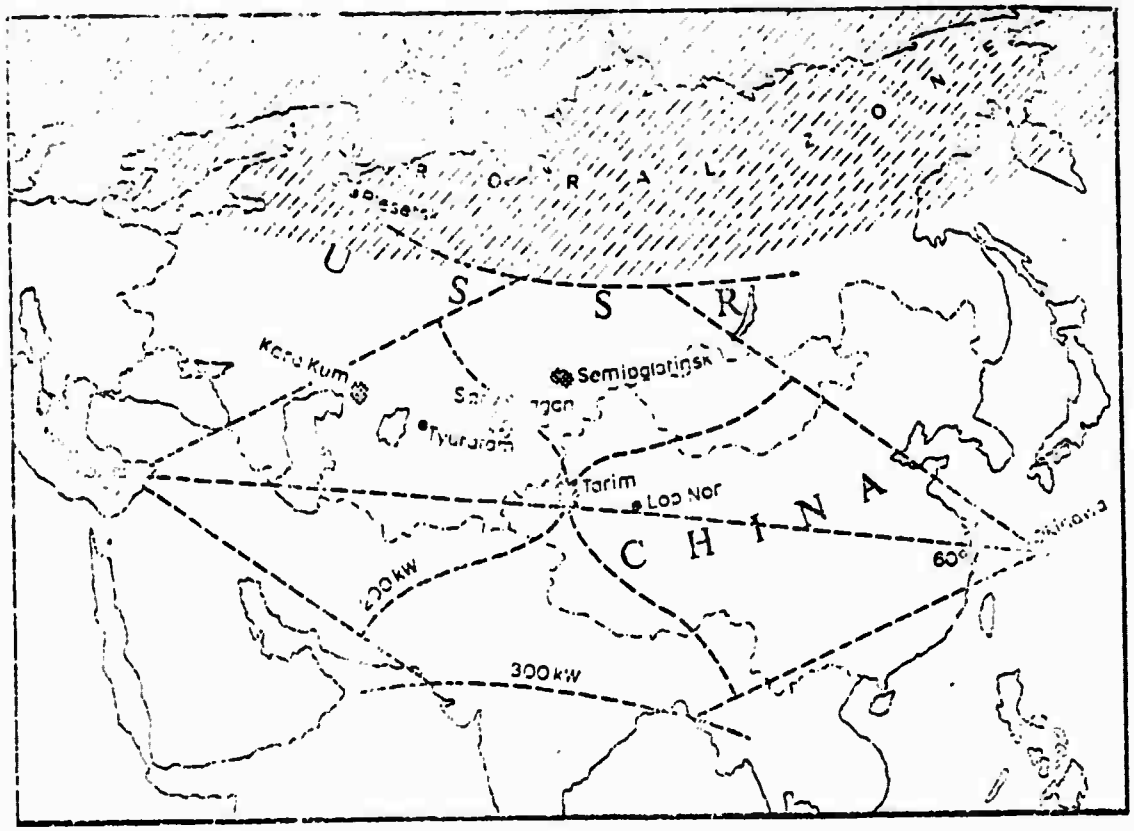

Figure 2. Radar Cover of a Forward-Scatter OTH Transmitter in Cyprus and Receiver in Okinawa (and Vice Versa). Cover Shown for Transmitter Powers of 200 kW and 300 kW

A back-scatter radar in Cyprus running only at 33 kW (many ordinary broadcasting stations run at higher powers than this) would just illuminate Tyuratam, while a transmitter broadcasting with a power of 300 kW would nominally cover the whole areas in Figure 2; in practice about four times as much power would be needed to allow for absorption on the second bounce. (The coverage for 200 kW is shown to illustrate how much more rapidly forward-scatter coverage increases with power than one would expect from the fourth law for back-scatter radars.)

No doubt the victum of OTH intelligence cover would like to take steps to stop it by jamming the receiver. Although a relatively low-powered transmitter in the receiver's beam working at the right frequency would obliterate target returns, to do this operationally might be difficult. It would perhaps be possible to shield a particular site from a particular receiver by putting a jammer between them, but the problem of tracking and imitating the radar frequency would remain. The intruders would any way be able to re-site the receiver, which is not a very expensive item, particularly if it only had to watch in one direction.

Although the Cyprus-Okinawa path gathers in a rich harvest of sites, doubtless the Americans and British would like to watch the other areas--particularly Russia's northern rocket-launching site at Plesetsk, near Archangel, and their northern nuclear testing ground in Novaya Zemblaya. It is significant that Orford Ness lies very close to the great circle through Plesetsk and Okinawa. We were told when it started operating that Orford Ness was for the study of HF propagation in high latitudes through aurorae. One can now see that this was perfectly true, though the Ministry of Defense was careful not to say why they should wish to spend so much to learn about this recondite subject. One must assume that the experiments were a failure, since the station was closed down in 1972 after a year's operation. It may be a coincidence, but Orford Ness lines up with Tyuratam and a point on the north-west Australian coast not far from the U.S. Navy's controversial station at North West Cape for controlling Polaris submarines. It is possible that there is, or was, an OTH receiver there also. Or, again, it may have been intended to work with the Australian Army's low-angle array at Rockbank. But since the path would have been 14,000 km or more and the power demanded at least 1.2 MW, one must assume that the returns were too weak to be useful.

However, the Orford Ness array is of some interest, since it is the only known military site to have been photographed in enough detail to make some guesses about the design (Figure 3).

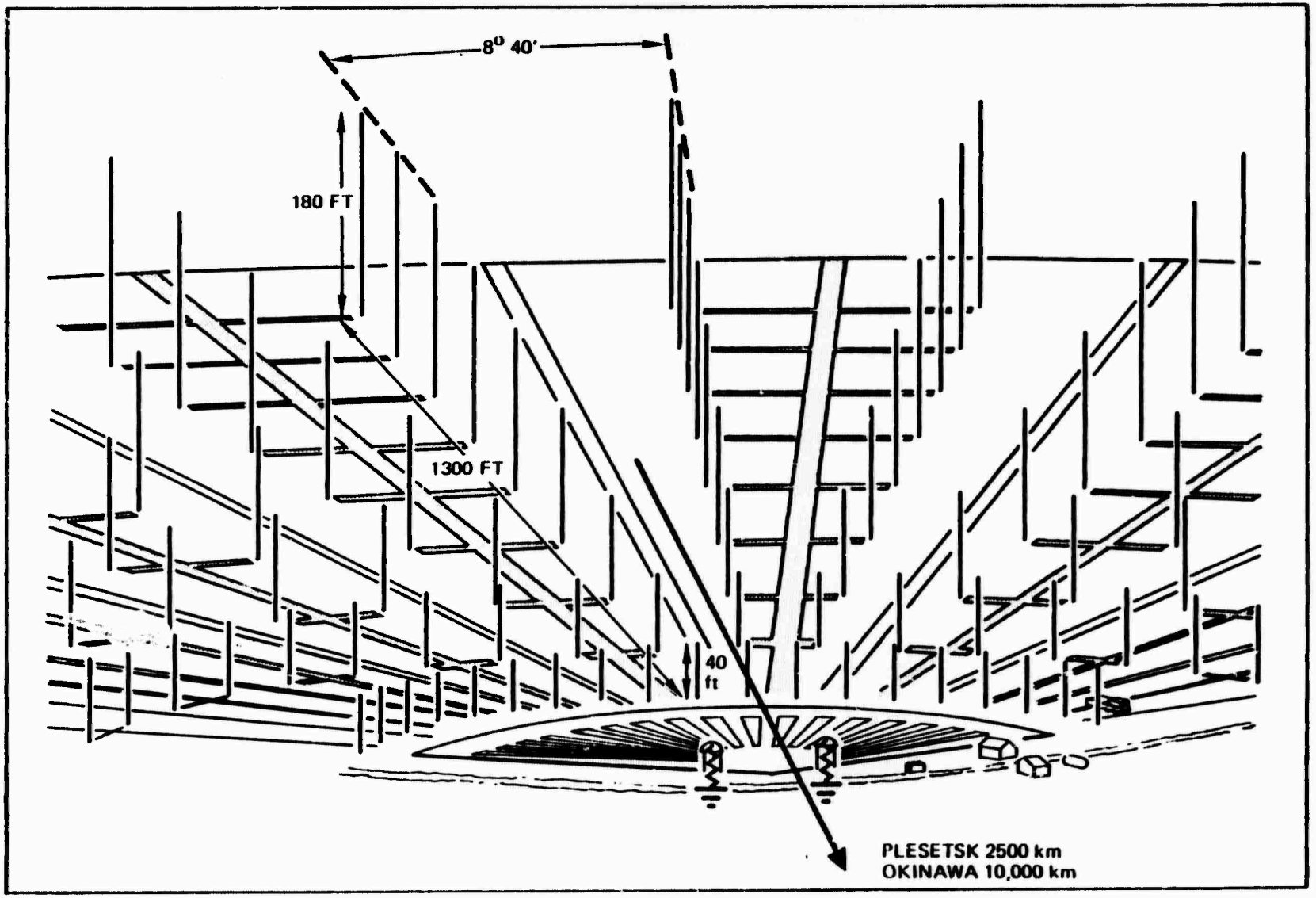

Figure 3. Orford Ness OTH Array on the Suffolk Coast Consists of 150° Fan of 18 Aerials, 8°40' Apart, with an Axis Bearing 60° True. The Great Circle from Orford Ness to Okinawa Passes through the Plesetsk Rocket Range in Northern Russia

It consists of a fan of 18 aerials, 8°41' apart, spread over 150° whose axis bears 60° True. Each aerial consists of a wire about 430 meters long supported on a row of poles: those farthest from the sea are 60 meters high, tapering to 13 meters at the center of the fan. It rather looks as though the aerials were meant to work in pairs to act as a front half of a rhombic array. This gives a nonresonant aerial with high gain and a sharply directional beam. For instance, at 40 MHz the two wires of a V aerial this long need to be at 15° to each other. This would mean selecting wires that straddle the desired heading. The V so formed would need to be terminated in a resistance of about 430 ohms. And presumably this is what the metallic mushrooms are in the foreground (they would certainly have to be massive, for at full power some 500 kW would be dissipated in them). The downward slope towards the sea would presumably aid low-angle propagation. In the horizontal plane, one might expect a beam width of 5°30'. At the lowest frequency of operation, 6 MHz, the beam width would be about 26°. When the transmitter was operating, everyone had to be cleared from the site lest their eyes be cooked.

If this interpretation is correct, Orford Ness is an odd design and one not usually used for transmitters, since so much energy is dissipated in the terminating resistors. However, there may be other economic tradeoffs that are not immediately apparent. For instance, the structure of the masts is reported to be most unusual, being made of concrete or earthenware drain pipes cemented together. No doubt this is to avoid eddy current losses in metal masts, and perhaps the guy wires are formed from terylene. (ICI breifly marketed a synthetic non-stretch rope for staying aerial masts; it was also offered as shrouds for yachts but failed to perform well, and is no longer available.)

Having said all this, which may be of some interest to the radar specialist, what is the layman to make of it all? First, one must deplore the secrecy with which even the existence of OTH radars is surrounded. It is naive to suppose that the Russians and Chinese have not noticed torrents of HF energy pouring across their most secret military installations, especially since the Soviet Union seems to have had an early lead in the technique.. Indeed, anyone anywhere in the world with an ordinary communications receiver could detect emissions from these stations. But it is a good thing that the Super Powers should know as much as possible about each other's capabilities, and it is presumably useful that a small amount of the taxpayers' money should be spent to this end.

What one does not know is whether OTH is worth what it costs (Orford Ness came in at about £22 million) or whether it is another expensive toy for the military; perhaps that is why it is still secret. On the other hand, perhaps it works very well, and that the recent Cyprus troubles are due partly to the British and American determination to hold on to such a useful vantage point. Certainly, when the Turks invaded the island, there was debate whether the Marines should be sent in to hold the OTH radars against our NATO allies.